

THE PHOTOIONIZATION AND DISSOCIATION OF MOLECULES

by

DANNY, SHIU HUNG, MAK

B.Sc. McGill University, 1960
M.Sc., University of British Columbia, 1962.

A THESIS SUBMITTED IN PARTIAL FULFILMENT OF
THE REQUIREMENTS FOR THE DEGREE OF
DOCTOR OF PHILOSOPHY
in the Department
of
Chemistry

We accept this thesis as conforming to the
required standard

THE UNIVERSITY OF BRITISH COLUMBIA

April, 1966.

In presenting this thesis in partial fulfilment of the requirements for an advanced degree at the University of British Columbia, I agree that the Library shall make it freely available for reference and study. I further agree that permission for extensive copying of this thesis for scholarly purposes may be granted by the Head of my Department or by his representatives. It is understood that copying or publication of this thesis for financial gain shall not be allowed without my written permission.

Department of CHEMISTRY

The University of British Columbia
Vancouver 8, Canada

Date April, 1966

The University of British Columbia

FACULTY OF GRADUATE STUDIES

PROGRAMME OF THE
FINAL ORAL EXAMINATION
FOR THE DEGREE OF
DOCTOR OF PHILOSOPHY

of

DANNY SHUI HUNG MAK

B.Sc., McGill University, 1960
M.Sc., The University of British Columbia, 1962

TUESDAY, JULY 19, 1966, AT 3:30 P.M.
IN ROOM 261, CHEMISTRY BUILDING

COMMITTEE IN CHARGE

Chairman: C. V. Finnegan

A. V. Bree	C. A. McDowell
D. C. Frost	R. Nodwell
L. G. Harrison	R. Stewart

Research Supervisors: D. C. Frost
C. A. McDowell

External Examiner: G. L. Weissler
Department of Physics
University of Southern California
University Park
Los Angeles, California

THE PHOTOIONIZATION AND DISSOCIATION OF MOLECULES

ABSTRACT

The photoionization and dissociation of molecules was studied using a combination of a vacuum monochromator and a mass spectrometer. The work was performed to obtain fundamental information about some simple molecules and their ions, and it was hoped that this method would provide a good means for the determination of accurate ionization potentials.

Photoionization efficiency curves of sixteen atoms and molecules, namely: argon, krypton, xenon, oxygen, nitrogen, carbon monoxide, chlorine, hydrogen chloride, ammonia, water, methane, methane-d₄, propylene, acetylene, methyl cyanide and methyl alcohol for the energy range from eight to twenty-one electron volts were obtained. Numerical values of ionization and appearance potentials were determined from the initial onset of the photoionization efficiency curves, and the ionization potentials are discussed and compared with those obtained by other investigators. The threshold ionization potentials of these molecules are in close agreement with the spectroscopic values and are superior to those obtained by the electron impact method.

The shape of the photoionization efficiency curve near the threshold gives an indication as to the type of electron removed in the photoionization process, and the correct electronic configuration of the molecule can sometimes be deduced from the numerical values of the ionization potentials as demonstrated in the case of methyl cyanide.

The dissociation of ammonia, methane, methane-d₄, propylene, acetylene, methyl cyanide and methyl alcohol was studied, and the mechanisms for the dissociation processes were discussed. From the photoionization efficiency curves of the fragment ions, numerical values of bond dissociation energy, ionization potentials of radicals and zero-point difference for the isotopic ions are deduced.

Autoionization processes were observed in the study of krypton, xenon, oxygen, nitrogen, carbon monoxide, hydrogen chloride and acetylene. That the peaks observed in the photoionization efficiency curves of these species are indeed due to autoionization has been confirmed by comparison with corresponding peaks in the optical absorption spectra. The vibrational frequencies of hydrogen chloride and acetylene in the excited states could be deduced from the energy separation between two adjacent autoionization peaks.

GRADUATE STUDIES

Field of Study: Chemistry

Topics in Physical Chemistry	C. A. McDowell R. F. Snider J. A. R. Coope
Topics in Inorganic Chemistry	H. C. Clark N. Bartlett W. R. Cullen
Topics in Organic Chemistry	R. Stewart J. P. Kutney R. E. I. Pincock
Spectroscopy and Molecular Structure	C. Reid L. W. Reeves K. B. Harvey
Seminar in Chemistry	J. N. Butler
Quantum Chemistry	R. Hochstrasser
Statistical Mechanics	R. F. Snider

Related Studies:

Calculus and Differential Equations	S. A. Jennings
Modern Physics	M. Bloom
Elementary Quantum Mechanics	W. Opechowski

PUBLICATION

D. C. Frost, D. Mak and C. A. McDowell, "The
Photoionization of Nitrogen Dioxide",
Canadian Journal of Chemistry, 40,
1064 (1962).

ABSTRACT

The present work is concerned with photoionization efficiencies of gases and vapors determined as a function of photon energy by vacuum spectroscopy and mass analysis. The photoionization work was performed to obtain fundamental information about some simple molecules, and it was hoped that the results would provide a means to explain the apparent discrepancies of threshold ionization potentials previously reported by other workers.

Results on the photoionization of sixteen atoms and molecules, namely: argon, krypton, xenon, oxygen, nitrogen, carbon monoxide, chlorine, hydrogen chloride, ammonia, water, methane, methane-d₄, propylene, acetylene, methyl cyanide and methyl alcohol for the energy range from eight to twenty-one electron volts are presented. Photoionization efficiency curves of these molecules were obtained from which numerical values of ionization potentials, dissociative-ionization appearance potentials and dissociation energies are deduced, and the fine structure and autoionization processes are interpreted.

The results are discussed and compared with those obtained by other investigators. The threshold and inner ionization potentials of these molecules are in close agreement with spectroscopic values and are superior to those obtained by the electron impact method.

A brief account of the historical developments leading to the present work is described, and a few existing methods for the determination of ionization potentials with their

(iii)

advantages and limitations are pointed out. The essential components of the instrument and their special characteristics are briefly discussed, and the major sources of error are also included. The limitations of the apparatus at the present stage are pointed out, and improvements are suggested. The reasons for the choice of molecules for this work is mentioned, and an outline for further work is also suggested.

ACKNOWLEDGEMENTS

It is a pleasure to acknowledge my gratitude to Professor C. A. McDowell and Dr. D. C. Frost for their constant interest and encouragement during the course of this research. I wish to express my gratitude to Dr. C. E. Brion and my colleagues for their many helpful discussions. Thanks are also due to the technical staffs of the Chemistry Department at the University of British Columbia for their skilful assistance.

CONTENTS

	<u>PAGE</u>
ABSTRACT	ii
ACKNOWLEDGMENTS	iv
I. INTRODUCTION	1
A. General	1
B. Ionization Potentials	3
1. Introduction	3
2. Adiabatic and Vertical Ionization potentials	3
3. Determination of Ionization potentials	5
a) Optical Spectroscopy	5
b) Cyclic Method	6
c) Electron Impact Studies	6
d) Photoelectron Spectroscopy	8
e) Photon Impact Method	9
C. Historical Review of Photoionization	11
II. THEORETICAL	15
A. Photoionization	15
B. Autoionization	17
C. Threshold Law of Photoionization	19
D. Theory of Mass Spectrometry	22
E. Hydrogen and Helium Spectra	24
III. EXPERIMENTAL	
A. Introduction	27
B. The Mass Spectrometer	30
1. Ion Source	30
2. Analyser and Electromagnet	31
3. Electron Multiplier	33
4. Vibrating Reed Electrometer	33

<u>CONTENTS</u> (Continued)	<u>PAGE</u>
C. The Monochromator	35
1. Light Source	35
2. Grating System	36
3. Photon Monitor	37
4. Energy Conversion Scale	38
D. The Vacuum System	40
1. Analyser Tube	40
2. Monochromator	40
3. Light Source	40
4. Gas Handling System	41
5. Measurement of Pressure	41
E. Experimental Techniques	43
1. Sampling	43
2. Procedure	43
3. Photoionization Efficiency Curve	44
F. Sources of Error	46

RESULTS AND DISCUSSION

IV. Photoionization of Atoms	
A. Argon	47
B. Krypton	49
C. Xenon	51
V. Photoionization of Diatomic Molecules	
A. Oxygen	53
B. Nitrogen	58
C. Carbon Monoxide	62
D. Chlorine	66
E. Hydrogen Chloride	68

CONTENTS (Continued)PAGE

VI. Photoionization of Polyatomic Molecules	
A. Ammonia	71
B. Water	76
C. Methane and Deutero-methane	78
D. Propylene	84
E. Acetylene	87
F. Methyl Cyanide	91
G. Methanol	95
VII. CONCLUSION	98
BIBLIOGRAPHY	102

(viii)
LIST OF TABLES

	<u>PAGE</u>
I. The Threshold Laws of Photon and Electron Impact	21
II. Autoionization Peaks of Krypton	50
III. Autoionization Peaks of Xenon	52
IV. Ionization Potential of Oxygen	54
V. Autoionization Peaks of Oxygen	56
VI. Threshold I.P. of Nitrogen	59
VII. Autoionization Peaks of Nitrogen	61
VIII. Autoionization Peaks of Carbon Monoxide	63
IX. Autoionization Peaks of Hydrogen Chloride	70
X. Ionization Potential of Ammonia	73
XI. Ionization Potential of Methane, Deutero-Methane.	79
XII. Ionization Potential of Propylene	85
XIII. Autoionization Peaks of Acetylene	88
XIV. Relative Ionization Probabilities of Methyl Cyanide	94
XV. Ionization Potential of Methanol	96

(ix)
LIST OF FIGURES

	<u>AFTER PAGE</u>
1. Potential Energy Curves	3
2. Autoionization	17
3. Single Ionization Region	20
4. Hydrogen Spectrum	24
5. Helium Spectrum	25
6. The Monochromator and Mass Spectrometer	27
7. Mass Spectrometer Ion Source	30
8. Light Source	36
9. Photoionization of Argon	48
10. Photoionization Efficiency Curve of Krypton.....	49
11. Photoionization Efficiency Curve of Xenon.....	51
12. Photoionization Efficiency Curve of Oxygen, I...	53
13. Photoionization Efficiency Curve of Oxygen , II.	53
14. Photoionization Efficiency Curve of Nitrogen....	58
15. Photoionization Efficiency Curve of Carbon Monoxide, I	62
16. Photoionization Efficiency Curve of Carbon Monoxide, II	62
17. Photoionization Efficiency Curve of Chlorine....	66
18. Photoionization Efficiency Curve of Hydrogen Chloride	68
19. Photoionization Efficiency Curve of Ammonia.....	71
20. Photoionization Efficiency Curve of Water.....	76
21. Photoionization Efficiency Curve of Isotopic Methane	78
22. Mass Spectrum of Isotopic Methane	83
23. Photoionization Efficiency Curve of Propylene...	84
24. Photoionization Efficiency Curve of Acetylene...	87

LIST OF FIGURES (Continued)AFTER PAGE

25.	Photoionization Efficiency Curve of C_2H^+	90
26.	Photoionization Efficiency Curve of Methyl Cyanide,.....	91
27.	Ionization Efficiency Curves of Krypton and Methyl Cyanide.....	91
28.	Mass Spectrum of Methyl Cyanide	94
29.	Photoionization Efficiency Curve of Methanol.	95

CHAPTER ONE

INTRODUCTION

A. General

This thesis is mainly concerned with the results of the ionization and dissociation of molecules when subjected to photon impact in the wavelength region $1500\text{\AA} - 500\text{\AA}$ (about 8 to 21 eV.). Ultraviolet radiation in this energy range is capable of removing the valence electron from the atom or molecule, and sometimes electrons which are somewhat more strongly bound. This radiation is also capable of breaking chemical bonds.

A 1-meter Seya-Namioka type scanning vacuum ultraviolet monochromator coupled with a Nier-type mass spectrometer was used to measure ionization potentials of molecules and appearance potentials of their fragment ions.

Mass spectrometric studies of photoionization results have often led to a better understanding of the various reactions which occur when molecular and fragment ions are formed by photon impact. Careful examination of the detailed form of the photoionization efficiency curves has in general enabled ionization and fragmentation processes to be distinguished and identified, and the shapes of the curves to be interpreted in terms of electronic and vibrational energy states.

This work is concerned with three problems: (a) to determine accurately the photon energy necessary for the removal of an electron from a molecule to form an ion, this amount of energy being equal to the ionization potential of the molecule, (b) to determine the photon energy required to form X^+ ion from a molecule XY, and from this energy to obtain the dissociation energy

of the bond X-Y, and (c) to determine the products of molecular photoionization, if any, e.g. whether in methane, the absorption of photon of a given energy produces CH_4^+ or CH_3^+ ions, and if both are possible, what the relative probabilities are of forming them.

B. Ionization Potentials

1. Introduction

During the last forty years, the study of ionization potentials of gaseous atoms and molecules has occupied an increasing number of workers, and a considerable number of fairly accurately determined ionization potentials have appeared in the literature. These have been made possible by methods of optical spectroscopy, photoelectron spectroscopy, theoretical and semi-empirical calculations, charge transfer spectra, and electron and photon impact ionization.

2. Adiabatic and Vertical Ionization Potentials

The adiabatic ionization potential of a molecule is defined as the energy required to remove an electron completely from the ground vibrational level of the lowest electronic state of the molecule to the ground vibrational level of the relevant electronic state of the molecule-ion.

The probability of ionization of a diatomic molecule by electron impact as well as photoionization can be considered to be governed by the Born-Oppenheimer approximation:-

$$P_{v',v''} \propto \left| \int \Psi_{v'} \Psi_{v''} dr \right|^2 \quad \dots\dots\dots 1.1$$

where $\Psi_{v'}$ is the vibrational wavefunction of the level v' of the ion, $\Psi_{v''}$ is the vibrational wavefunction of the ground state ($v''=0$) of the neutral molecule, and r is the internuclear separation.

Diatomic molecules can be treated as anharmonic oscillators, and the vibrational wavefunctions for different vibrational levels of the molecule and its ion have the form shown in Figure 1.

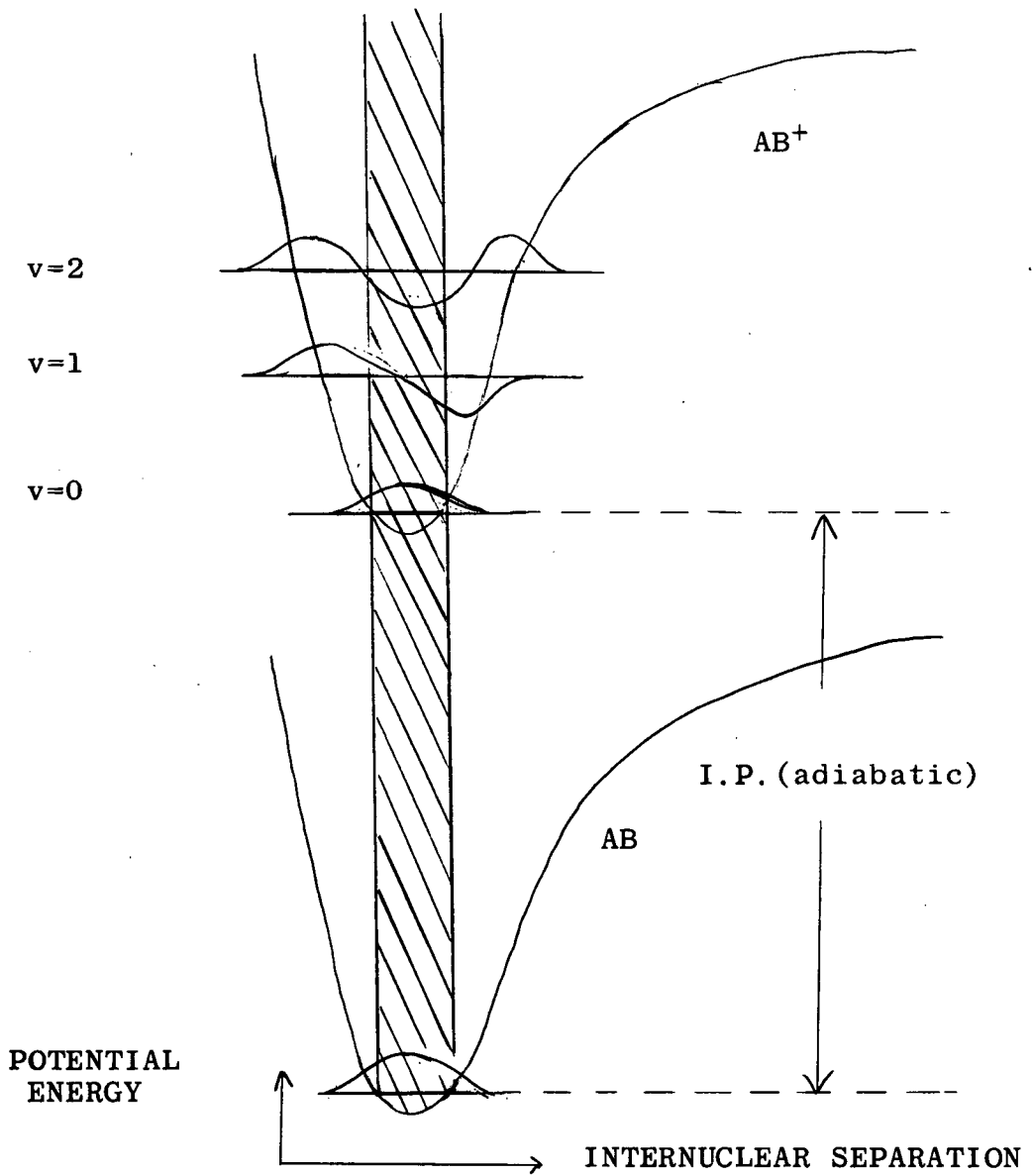


Figure 1 - POTENTIAL ENERGY CURVES

Suppose the minima of the two electronic states are vertically above one another. It is clear that the (0-0) transition has high probability, whereas (0-1), (0-2) etc. transitions have a much lower probability, because the negative part of the integral partly cancels the positive part.

The adiabatic ionization potential is the difference in energy between the ground vibrational state of AB and the ground vibrational state of AB^+ . If the equilibrium internuclear distances for the molecule and its ion are the same, the ionization potentials obtained by optical spectroscopy, electron impact and the photoionization method should all correspond to the adiabatic value, provided that the instruments used are sensitive enough.

But when the equilibrium internuclear distance of the ionic state is greater than that of the molecular ground state, the most probable transition is to a higher vibrational level and the ionization potential found by these methods may be higher than the adiabatic value. The same is true when the equilibrium internuclear distance of the ionic state is less than that of the molecular ground state, and the higher value for the ionization potential is usually called the vertical ionization potential. The (0-0) transition however, still has small finite probability, and the value for the ionization potential obtained by electron and photon impact should depend largely on the sensitivity for detection of ions. The general picture for polyatomic molecules should be similar.

In photoionization studies, ionization potentials obtained from the onset of the photoionization efficiency curves are in general in good agreement with the adiabatic ionization potentials obtained by other methods. When ionization is caused

by the removal of a bonding electron and the minima of the ground and ionic electronic states are not vertically above one another, the photoionization efficiency curve usually shows curvature near the threshold. The vertical ionization potential can be measured from the curve at the point of steepest slope before the curve reaches the first maximum.

The vertical ionization potential of a molecule will always be equal to or higher than the adiabatic value. In fact, experimental evidence has shown that the difference is usually between 0.02 to 0.5 electron volt.

3. Determination of Ionization Potentials

Ionization potentials are among the most important properties of a molecule, and it is desirable to have methods of determining them accurately.

a) The Optical Spectroscopic Method

One of the most accurate methods for the determination of ionization potentials employs optical spectroscopy. This involves a study of absorption spectra, and the fitting of the data into Rydberg series:-

$$v = I - \frac{R}{(n + a)^2} \quad \dots\dots\dots 1.2$$

where: I and a are constants specific to a particular molecule,

v is the wavelength of a particular molecule,

R is the Rydberg constant,

n is an integral value representing the particular Rydberg band.

Once the Rydberg (0-0) transition is identified by analysis of the Rydberg bands of the absorption spectra, or by comparison with the spectra of isotopic molecules, the ionization

potential of a molecule can readily be calculated. The wavelength of spectral bands in spectroscopic work can be measured with a high degree of accuracy, and the uncertainty in the value of the ionization potential derived from it is usually only a few parts of a thousand. However, this method cannot be applied to quite a large number of molecules which give continuous or diffused spectra, and an unambiguous assignment of the Rydberg transitions is not then possible.

b) The Cyclic Method

When the absorption spectrum of a molecule is so complex that the Rydberg series leading to the ground state of the ion cannot be obtained, some workers (84) have used a cyclic method to determine the adiabatic ionization potential indirectly. This method is based on the following equation:-

$$I(XY) + D_0(XY^+) = I(X) + D_0(XY) \dots\dots\dots 1.3$$

where $I(XY)$ is the ionization potential of XY , $I(X)$ is the ionization potential of X , $D_0(XY)$ and $D_0(XY^+)$ are the dissociation energies of the molecule and the ion respectively. If $I(X)$, $D_0(XY)$ and $D_0(XY^+)$ are known accurately, the I.P.(XY) of the molecule can be determined.

c) The Electron Impact Method

The essentials for making electron impact measurements are a beam of electrons of known energy which may be passed through the gas under investigation, and a device for detecting the ions produced and for measuring their intensity. Electron impact studies have been highly developed, and are far more generally applicable because molecules with strongly bound

electrons may be investigated. For many molecules, the electron impact method provides the only way to determine the ionization potential.

The electron impact method suffers from several defects. The first arises through using an electron beam emitted from a hot filament. This electron beam will not be monoenergetic in character but will possess an energy spread of about one electron volt which will be mainly Maxwell-Boltzmann in nature, and is, of course, governed by the temperature of the filament. In addition, a further energy spread will be imparted to the electron beam by the variation of temperature along the filament due to conduction of heat through the supporting leads, and by the voltage drop across the filament. Since electrons are charged particles, the electric field which is necessary to produce an ion beam in the ion source usually also perturbs the electron energy. The difficulty of obtaining an electron beam with sufficiently low energy spread causes much of the information obtained by the electron impact method to be of low precision, and fine details in the ionization efficiency curves to be unresolved.

The diminution of the energy spread in the electron beams used in the electron impact method is at present under investigation in this and other laboratories using electrostatic selectors. Success in this field of study will greatly improve the accuracy of values of the ionization potentials obtained by the electron impact method.

Wannier (131) proposed a theory for the ionization of molecule by electron impact near the threshold. He stated that the two slow electrons, upon emerging from the ion, remain

within the reaction zone at the threshold energy of the impacting electron. Only when each slow electron has appreciable kinetic energy can it escape from this region and only then does the ion current start to grow. For this reason, it is quite possible that ionization cross sections are zero or vanishingly small for electron (impacting) of an energy equal to or just exceeding the threshold ionization energy. If this is so, it places a restriction on the ultimate accuracy obtainable for electron impact measurements of ionization potentials, even with improved methods of obtaining effectively monochromatic electron beams.

d) Photoelectron Spectroscopy

This is a rather new technique reported by Kurbatov, Vilesor and Terenin (66), Schoen (107) and Turner and Al-Joboury (127-129), for the direct measurement of ionization potentials of a molecule less than 21.21 eV. The gas under study is illuminated by a beam of photons of energy 21.21 eV. These photons can cause the emission of photoelectrons, and a cylindrical energy analyzer is used to study the photoelectron energy distribution. A photoelectron energy spectrum consists of peaks which can be shown to lead directly to the vibrational and electronic energy levels of the molecule. The ionization potentials of quite a number of molecules have been reported using this method and in some favorable cases vibrational structure can also be seen.

Frost, McDowell and Vroom (41) have reported recently the use of a spherical energy analyzer of greatly improved resolution to study the photoelectron energy distribution of hydrogen. They have been able to measure accurately the first five vibrational energy levels of H_2^+ ($3 \Sigma_g^+$), and the relative transition probabilities

to them. The vibrational structure of the hydrogen ion in the photoionization efficiency curve is known (13, 20) to be obscured completely by autoionization, and the five clearly resolved "steps" in the photoelectron retarding curve for hydrogen indicate that autoionization may be avoided in spherical photoelectron spectroscopy.

e) The Photon Impact Method

This method consists of a combination of both photoionization and mass spectrometry. A sample of gaseous molecules to be investigated is illuminated by a beam of monochromatic ultraviolet radiation. If the photon energy of the radiation is gradually increased, successive stages of excitation can be reached until the energy of the photon reaches a certain value when ionization takes place. The ionization potential of a molecule can be obtained from the point of initial onset of ionization. With further increase of photon energy, a curve of photoionization efficiency as a function of photon energy can be derived. In favourable cases the upper energy states and the vibrational levels of the molecule and its ions can be studied from photoionization efficiency curves. A mass spectrometer is used to focus the particular ion under investigation, and to measure the intensity of ion currents produced.

The photoionization method is far more generally applicable than optical spectroscopy, as some molecules with complex spectra which do not exhibit well defined Rydberg series can readily be investigated by the former method.

The reasons for the superiority of this method are threefold. Firstly, it is much easier to obtain monoenergetic photons than it is to obtain monoenergetic electrons; secondly, a gas to calibrate the energy scale needs not be introduced into the

mass spectrometer concurrently with the molecule to be studied as is the regular practice in the electron impact method; and thirdly, the steep rise in photoionization cross section at the ionization threshold permits a sharp separation of ion-formation processes.

The photon impact method is inherently more accurate, and numerical values of ionization and appearance potentials based on this method are in excellent agreement with those obtained by optical spectroscopy. Precise data have thus been made available for a large number of molecules, and information obtained from the photoionization efficiency curves can be correlated with molecular properties and molecular structure, and to check the theories of threshold laws and processes of autoionization. The results furnish reliable information for some theoretical and semi-empirical molecular quantum mechanical calculations which are now being made.

C. Historical Review of Photoionization

Since the discovery of the ionization of gases by X-rays, and the photoelectric effect of light on solids and metals, several investigations have been made on the ionization of gases when exposed to ultraviolet radiation.

Hertz (46) in 1887, when performing experiments on the sparking between electrodes, observed that ultraviolet radiation could be used to ionize gases. Lenard (67) in 1901, carried out some similar experiments and found that air was made conducting under the action of a very absorbable kind of ultraviolet light.

Stark (110) investigated the effect of ultraviolet light on the conductivity of gases and obtained results with certain organic compounds in the vapor state: anthracene, diphenylmethane, diphenylamine and α -naphthylamine.

During the period 1920-1930, experiments on photoionization were conducted mostly with vapors of the alkali metals, especially caesium, rubidium and potassium. The experimental techniques were, as a whole, greatly improved after 1920. However, lack of high resolving power and the relatively low sensitivity of the instruments used has left the data of many of these workers in a somewhat uncertain state. A considerable amount of data has been collected and reviewed by several writers (57,97).

Between 1930 and 1950, very little work concerning photoionization appeared in the literature, and the study of molecular ionization seemed to be dominated mainly by electron impact studies using mass spectrometers. Many investigators have used the electron impact method to measure ionization potentials of molecules and appearance potentials of fragment ions, to determine the energy needed to split up a polyatomic molecule into

specified radicals, and to determine ionization potentials of radicals. Hundreds of papers have already been published in this field and ionization potentials of several hundred molecules have been studied. In many cases, this method has provided the only available data.

The difficulty of obtaining an electron beam with sufficiently low energy spread and accurately known energy caused much of the information from the electron impact method to be inaccurate. The form of the ionization probability curve for a single process is such that when several are superimposed, the resolution of separate threshold potentials is difficult.

After 1950, photoionization studies resumed their steady pace, largely due to the development of ingenious designs for grating monochromators and better means for producing and measuring photon radiation in the far ultraviolet.

The development of a low-cost grating monochromator by Seya (108) and Namioka (89) helped to facilitate the studies of photoionization. It is basically a one-meter monochromator, and the gas pressure in the monochromator is maintained at a pressure of about 10^{-5} mm of Hg. by differential pumping. It has a fixed entrance and exit slit system, and the wavelength of the monochromatic light passing through the exit slit may be altered by rotating the grating.

Johnson et al (62) in 1951, found that coating a photoelectron multiplier with a thin layer of fluorescent material rendered it satisfactory for the measurement of far ultraviolet radiation intensity. Sodium salicylate was found to be best suited since it is stable, does not evaporate in vacuo and gives reproducible results up to 850\AA . Furthermore, its response is

excellent and its quantum efficiency is nearly constant (62).

In 1953, Watanabe, Marmo and Inn (133) and Wainfan, Walker, and Weissler (141) reported data on photoionization measurements in the vacuum ultraviolet region. The total absorption cross-section of a molecule was measured in an absorption cell, and the ionization was found to correspond to the long wavelength limit of the ionization continuum. They showed that the accurate determination of ionization potentials is possible by utilizing monochromatic light of 0.001 eV. band width. However, their methods do not give any information about the products which are formed by photoionization, and no mass analyses were introduced to differentiate between the parent and fragment ions. Also ions may arise from any impurities in the sample. Because of the lack of mass analysis, one has to be quite sure that the sample being studied is free of impurities with lower ionization potentials.

Threshold ionization potentials of more than a hundred molecules were reported in 1959 by Watanabe (139). His results are comparable to those obtained by spectroscopic methods.

Terenin and Popov (124) were the first to use mass analysis (in the photoionization of thallium halides). More recently, Lossing and Tanaka (70) used a vacuum ultraviolet light source for the generation of ions in a mass spectrometer. A krypton discharge lamp with a lithium fluoride window, emitting the two resonance lines 1236\AA (10.03 eV.) and 1165\AA (10.64 eV.) provided enough energy to cause photoionization of acetone, butadiene, butene, propylene, anisole, allyl iodide, dimethyl mercury etc., but not enough to form ionic fragments. Their experiments suffered from the defect of a fixed photon energy, so the photoionization yield could not be studied as a function of energy.

Terenin and Vilessov (125) and Morrison, Hurzeler and Inghram (58, 83) used a combination of vacuum monochromator and mass spectrometer in a detailed study of the formation of ions by photon impact. The source of light was a high voltage hydrogen lamp, and a lithium fluoride window was used to isolate the residual gases in the light source from the ionization chamber. The lithium fluoride window cuts off radiation below 1050\AA (11.50 eV.) and molecules with ionization potentials greater than this cannot be studied.

Weissler, Samson, Ogawa and Cook (146) and Comes and Lessmann (10), using a low-pressure repetitive spark source and differential pumping to retain a low pressure in their apparatus were able to obtain photoionization results up to about 30 eV. without using a lithium fluoride window. However, their light source provided a widely-spaced line spectrum, and so there were of course "gaps" in their photoionization efficiency curves. This frequently made it impossible to determine the onset of ionization processes within several tenths of a volt.

Recently, Dibeler, Krauss, Reese and Hartlee (19) have developed a Hinteregger type photon source which provides a Hopfield helium continuum, and have studied normal and deuterated hydrogen, methane and benzene. Cook and Metzger (12) have computed photoionization cross-sections of several hydrogen-containing molecules from ionization spectra using the Hopfield helium continuum as a continuous background-radiation source. The development of continuous photon spectra marked a major advance in this field.

CHAPTER TWOTHEORETICALA. Photoionization and Dissociative Ionization

In this work, we are concerned mainly with ionizing collisions of photons with atoms and molecules. A photon of energy $h\nu$ can be absorbed by an atom or a molecule to take the system from a state of lower energy E'' to a state of higher energy E' , i.e.

$$h\nu = E' - E'' \quad \dots\dots\dots 2.1$$

where h is Planck's constant, ν is the frequency of the radiation. The absorption of radiation by the molecule XY can be represented by:-



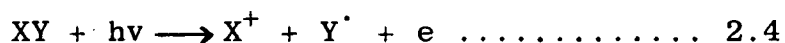
where XY and XY^* are ground and excited states of the molecule respectively. This process is called photoexcitation.

Ionization can be caused by the interaction of a photon of sufficiently high energy to cause the process:



this process is called photoionization, and the photon energy necessary for this process is called the threshold ionization potential of XY . Beyond the energy of the ionization threshold, there will be a region of continuous absorption. The measurement of positive ion current as a function of photon energy provides the usual method of studying this process.

If the absorption of radiation leads to the following reaction:



the process is called dissociative ionization, and the photon energy necessary for this reaction is called the appearance potential of X^+ . The dissociation energy or bond strength of the molecule $D(X-Y)$, can be calculated from the appearance potential by the following relationship:

$$V(X^+) = I(X) + D(X-Y) + K.E. + E.E. \dots\dots 2.5$$

where $V(X^+)$ is the appearance potential of X , $I(X)$ is the ionization potential of radical X , $K.E.$ is the kinetic energy with which X^+ and Y^{\cdot} may be endowed and $E.E.$ is any excitation energy they may have. Most atomic ionization potentials are known from optical spectroscopy, and if $K.E.$ and $E.E.$ are known, the dissociation energy can be obtained by measurement of the appearance potential. Otherwise, the appearance potential gives an upper limit for the energy necessary to break the $X-Y$ bond plus the ionization energy of X .

B. Autoionization

In ionization efficiency curves for molecular ions produced by electron impact, breaks are often observed at energies which do not correspond to any known electronic state of the positive ion species formed. Many peaks in photoionization efficiency curves are also observed at energies above the threshold ionization potential, and the positions of these peaks correspond closely with some of those obtained from absorption spectra. This phenomenon has been established by several workers (10, 27, 54, 91) as due to autoionization of a highly excited state of the atom or molecule concerned.

Autoionization phenomenon can be explained by reciprocal interaction of discrete states with one or more continua as shown in Figure 2. The excitation of an electron in series 2 from the ground state to a discrete state above the ionization continuum of series 1 is followed rapidly by a non-radiative transition to the continuum at the same energy. The excited atom or molecule becomes ionized by losing one of its electrons. Since this process is governed mainly by photoexcitation, and the threshold law for excitation is a delta function, peaks should be observed in the photoionization efficiency curve for autoionization processes.

Massey (78) proposed another mechanism for the autoionization process. It is possible to imagine discrete states of the normal molecule in which two or more electrons are excited. An atom or molecule in such a condition will not usually give up its energy of excitation by radiation. Instead it will break up much more quickly in the following way. Of the two excited electrons, one drops to a more firmly bound state, thereby releasing energy which is absorbed by the other to take it free of the atom or

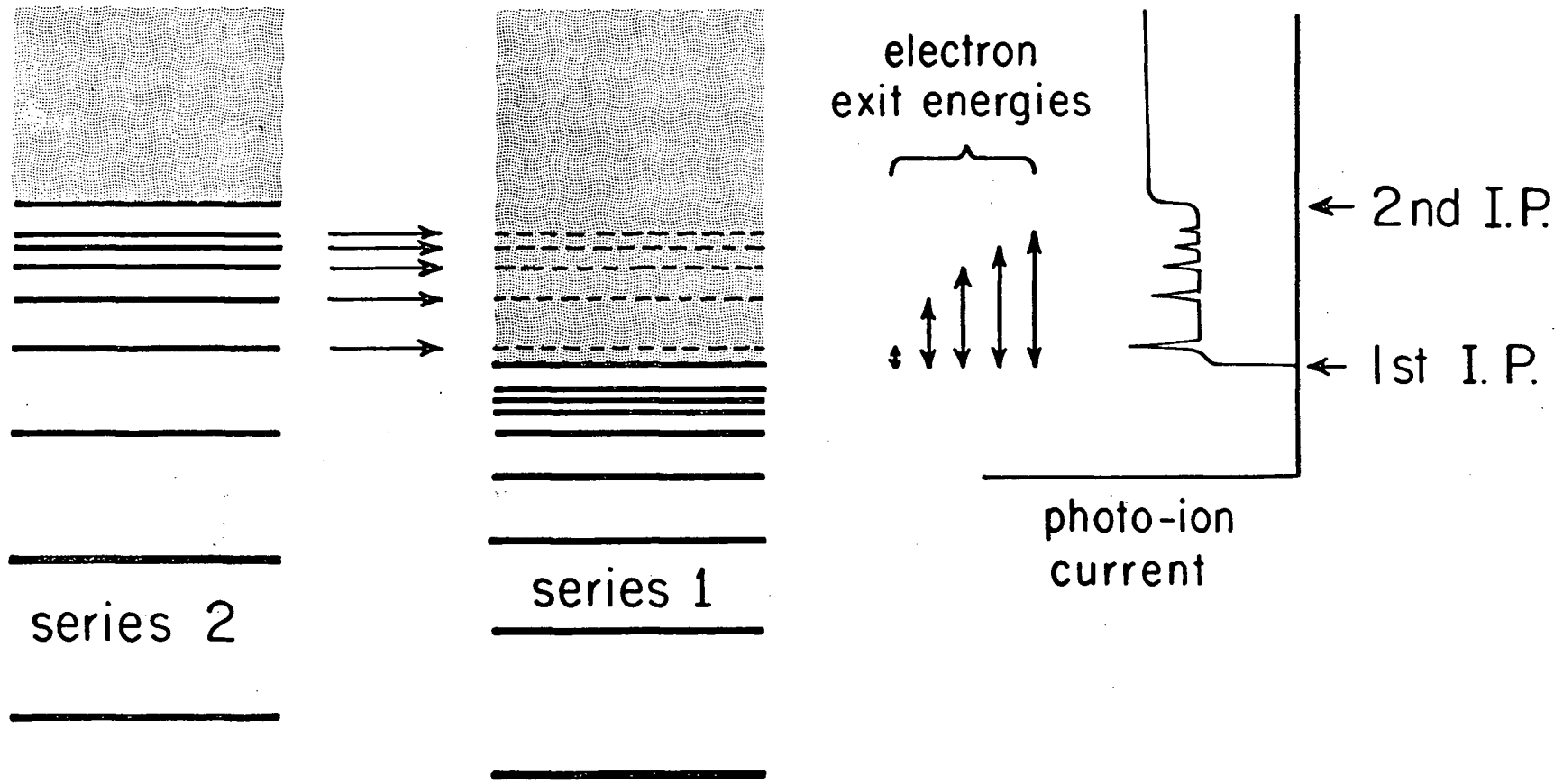


Figure 3

molecule altogether. The excited atom or molecule therefore becomes ionized.

In the work reported here, autoionization processes are found to occur strongly in atoms and diatomic molecules such as krypton, xenon, oxygen, nitrogen, carbon monoxide and hydrogen chloride. For methane and numerous hydrocarbon molecules, no autoionization structure seems to be present. The possible excitations in such molecules appear to result only in continuous absorption, and do not give discrete peaks in the photoionization efficiency curves.

C. The Threshold Laws

In order to determine reliable ionization limits from observed photoionization efficiency curves, it is necessary to interpret the shape of the curves, especially near the threshold. The threshold law describes the variation of the ionization efficiency with energy above the threshold.

The ion current produced by electron impact increases linearly as the energy of the impacting electron is increased above the threshold. Wigner (147) has shown that for a singly charged atom or molecule the ionization efficiency varies with the 1.12th power of the excess energy. However, Fox (51) showed that the ionization efficiency curve for helium singly charged is linear over the first eight volts above the threshold.

It has been established by photoionization studies (83,91,136,146) that the threshold law for direct single ionization, when induced by photon impact, is approximately a step function of excess photon energy, and that for double ionization is approximately a linear function. The autoionization process, induced by photon impact, is governed mainly by the photoexcitation of an electron in the normal molecule. The appearance of sharp peaks for the autoionization process in the photoionization efficiency curve indicates that the threshold law for photoexcitation is a delta function.

Wannier (131) proposed a theory of the threshold law for multiple ionization. The two slow electrons, upon emerging from the ion after the single ionization by electron impact, remain within a spherical reaction zone of radius b

around the ion. Only when each electron has a kinetic energy T greater than e^2/b can it escape from this region. In Figure 3, the kinetic energies T_1 and T_2 of the two emerging electrons are plotted, and the region in which ionization occurs is limited by two straight lines parallel to the axes. Now a line of constant energy excess ΔE in this diagram is straight and of slope -1 ; the segment of it leading to ionization is marked in the figure. Clearly, the length of this segment is proportional to the energy excess and so the ionization efficiency increases linearly with the excess energy.

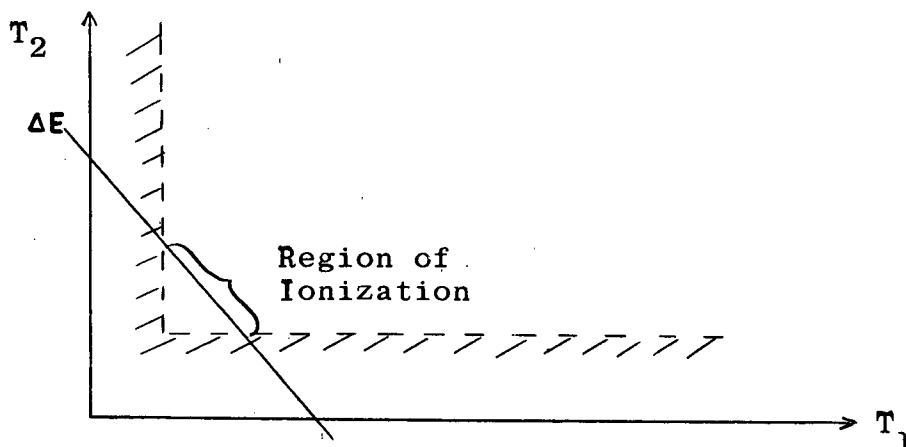


Fig. 3. Region in which ionization occurs in the case of single ionization. T_1 and T_2 are the kinetic energies of the two emerging electrons, and E is the energy excess.

In single ionization by photoionization, only one slow electron emerges from the ion. When the electron has a kinetic energy T greater than e^2/b , photoionization takes place. The photoionization efficiency remains constant after the threshold energy plus the kinetic energy T , and the excess energy of the incident photon is carried away by the slow electron. The photoionization efficiency for single ionization is therefore a step function.

Detailed theoretical calculations by Geltman (43) of ionization by photon and electron impact have established that the ionization efficiency above the threshold energy would be determined by the conditions of the distribution of excess energy of the incident particles among the separating particles. Table I summarises the threshold laws for ionization and excitation by photon and electron impact.

Table I
The Threshold Laws

Number of separating particles	Types of reactions	Ionization Efficiency	Function
1	$A + h\nu \rightarrow A^*$ $A + e \rightarrow A^-$		delta
2	$A + h\nu \rightarrow A^+ + e$ $A + e \rightarrow A^* + e$		step
3	$A + h\nu \rightarrow A^{++} + 2e$ $A + e \rightarrow A^+ + 2e$		linear

Thus, we would expect from the photoionization efficiency curves a delta function for a photoexcitation process, and a step-function for a single photoionization process. These are, however, idealized situations, and the actual curves obtained do not always show perfect steps or delta functions. Some fine structure and steps corresponding to the higher ionization potentials of several molecules cannot be obtained because of the interference and competition of multiple autoionization processes.

D. Theory of the Mass Spectrometer

The term 'mass spectrometer' is now usually restricted to an instrument in which separated ion beams are measured electrically. It will be useful to write down the simple equations governing the motion of a charged ion in a mass spectrometer.

If the charged particle of mass $M(g)$, charge $e(e.s.u.)$ and velocity v (cm per sec) is sent into a magnetic field of force $H(e.s.u.)$, the equation of motion may be described as follows.

Since the force is always at right angles to the direction of motion of the particle, there is no linear, but a constant angular acceleration. From elementary mechanics, it is seen that the particle will experience a centrifugal force, and for equilibrium this must balance the force due to the magnetic field, i.e.

$$\frac{Mv^2}{R} = Hev \dots\dots\dots 2.6$$

where R is the radius of curvature of the ion beam.

If it is assumed now that the charged particle acquires its velocity by falling through an electrostatic potential difference $V(e.s.u.)$, the potential energy must be the same as the kinetic energy of the particle after acceleration, i.e.

$$\frac{Mv^2}{2} = eV \dots\dots\dots 2.7$$

If equations 2.6 and 2.7 are combined, eliminating v , then

$$\frac{M}{e} = \frac{R^2 H^2}{2V} \dots\dots\dots 2.8$$

The equation 2.8 may be termed the mass spectrometer equation. In the mass spectrometer used in the present work, the radius of curvature of the charged particle is fixed, and when analysis of the ions formed from a given molecule is desired, either the ion accelerating voltage is maintained constant, and the magnetic field strength varied continuously (magnetic scanning), or the accelerating voltage is varied keeping the magnetic field strength constant (voltage scanning).

E. The Hydrogen and Helium Spectra

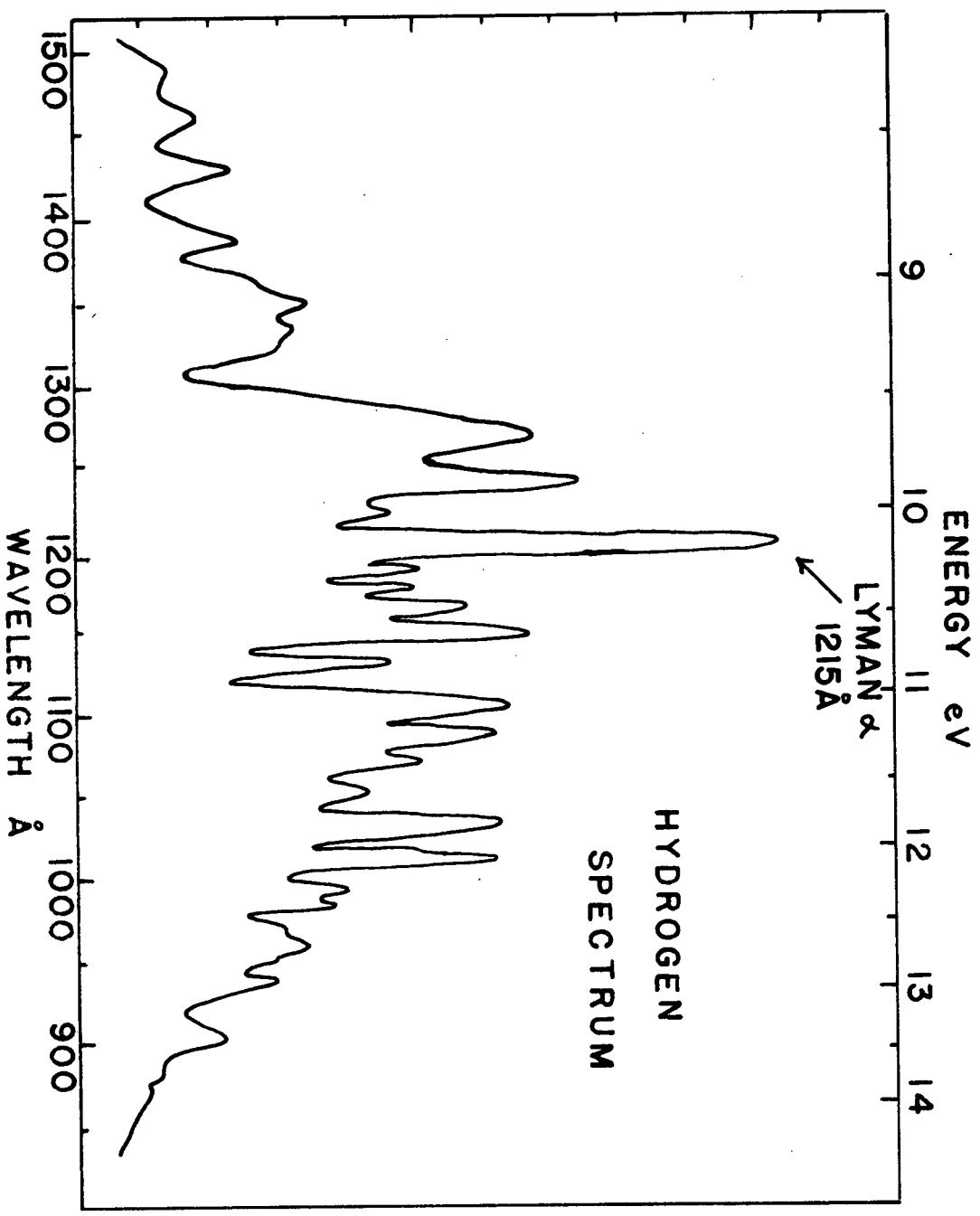
In order to obtain a monochromatic photon beam of varying energy it is necessary to excite gaseous molecules such as hydrogen or helium in the light source. The light emitted from the source is scanned by a 30,000-lines per inch grating to give a spectrum of photon intensity as a function of photon energies. The spectrum obtained is characteristic of the gas employed in the light source: that of hydrogen is useful from 900\AA - 1500\AA (8 - 14 eV.), and that of helium is useful from 500\AA - 1200\AA (10 - 21 eV.). By employing a combination of both spectra, it is possible to obtain photoionization results in the energy range of 500\AA - 1500\AA (8 - 21 eV.).

a) The Hydrogen Spectrum

The hydrogen lamp gives an intense "many-line" spectrum in the 900\AA - 1500\AA region, and the spectral characteristic of the hydrogen spectrum is illustrated in Figure 4. The rapid change in intensity with wavelength of the "line" causes a problem in the interpretation of the photoionization efficiency curve. The contour of the hydrogen spectrum appears in the photoionization efficiency curve for almost every molecule studied. There is an additional complication due to the fact, as Nicholson (92) has indicated, that a strong isolated line in a region of the spectrum where the true photoionization efficiency curve is increasing linearly with energy will produce a false 'hump' in the curve at an energy just below the line and a false 'dip' above it.

Judging from the shape of the hydrogen spectrum, it is reasonable to assume that the spectrum consists of peaks

PHOTOELECTRIC CURRENT



HYDROGEN
SPECTRUM

Figure 4

superimposed on a hydrogen continuum. The photoionization efficiency (P.E.) at the top of a peak represents the true P.E. at that photon energy, and the P.E. at the bottom of the valley between two photon peaks represents the contributions among three factors: the two neighbouring peaks and the hydrogen continuum. The P.E. contributions from the neighbouring peaks are functions of the peak heights and the distance between the valley and the "peak maximum". Taking these factors into consideration, data points on the hydrogen continuum and their corresponding ion intensities are calculated, and the true P.E. curve drawn. In this way false structure on the P.E. curve can be eliminated.

b) The Helium Spectrum

The helium lamp gives an intense continuum in the 500\AA - 1200\AA region, and the spectral characteristic of the helium continuum is illustrated in Figure 5. The slow variation of intensity with photon energy and the continuous nature of this emission spectrum are of particular advantage in this work, and the problem caused by the "many-line" hydrogen spectrum previously discussed is not significant here. The helium spectrum was used for most of the molecules studied in this work.

It can be seen in Figure 5 that the continuum has two principal intensity maxima, at about 810\AA and 670\AA . The resonance line of atomic helium at 584\AA is very small because it is strongly self-absorbed. The several lines observed around 900\AA are impurity lines from nitrogen atoms and oxygen molecules as indicated by Weissler, Samson, Ogawa and Cook

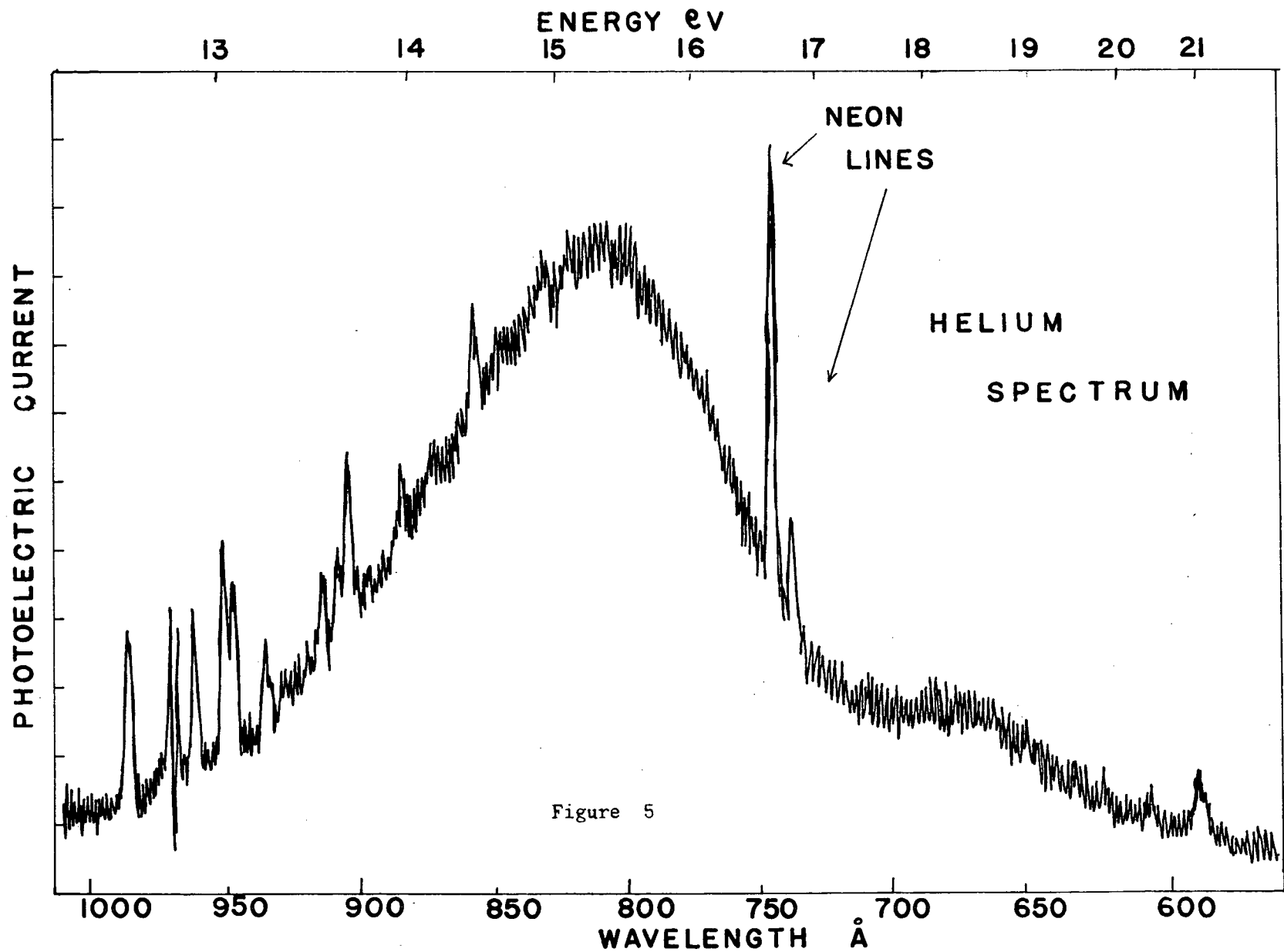


Figure 5

(146). The two lines at 736\AA and 744\AA are resonance lines of atomic neon impurity which appear with considerable intensity. Because of its favourable position in the spectrum and its considerable intensity, the ionization caused by the 744\AA resonance line of the atomic neon is used for the location of the ion beam.

The helium emission continuum is produced by transition from the excited state to the ground state of the helium molecule. The two main continuum maxima at 810\AA and 670\AA are the result of transitions $A^1\Sigma_u - X^1\Sigma_g$ and $D^1\Sigma_u - X^1\Sigma_g$ respectively (123).

The helium continuum is a function of the helium pressure in the light source. At low helium pressure, the resonance line of the atomic helium at 584\AA appears with considerable intensity, while both maxima at 810\AA and 670\AA are at low intensities. As the pressure of helium is increased, the intensities of the two continuum maxima increase while the 584\AA line diminishes because of strong self-absorption.

CHAPTER THREEEXPERIMENTALA. Introduction

The work described in this thesis was done in a photoionization mass spectrometer which was a combination of two major components: the 60 degree Nier type single focusing mass spectrometer and the Seya-Namiooka type 1-meter scanning vacuum monochromator. The two parts could be isolated by a two and a half inch diameter Crane wedge-type valve, so that either side could be opened to air for servicing. This valve was fitted with an appropriate O-ring.

A simple form of the apparatus was illustrated schematically in Figure 6. A sample of gaseous or liquid compound to be studied was stored in a sample tube, a fraction of it was expanded into three large evacuated glass bulbs. The gas then moved through a very fine leak into the ion source of the mass spectrometer, where the pressure was measured with an ionization gauge. This pressure was kept constant at about 5×10^{-5} mm. of Hg. for several hours.

The monochromator utilized an aluminized, 30,000 lines per inch grating, and a repetitive, high voltage spark through gas in a pyrex glass capillary served as a light source. The gases used in the light source were either pure hydrogen or pure helium maintained at about 50 microns pressure. Entrance and exit slit widths of 0.020 to 0.040 inch limited the resolution to 4\AA or about 0.05 eV. at a photon energy of 10 eV.

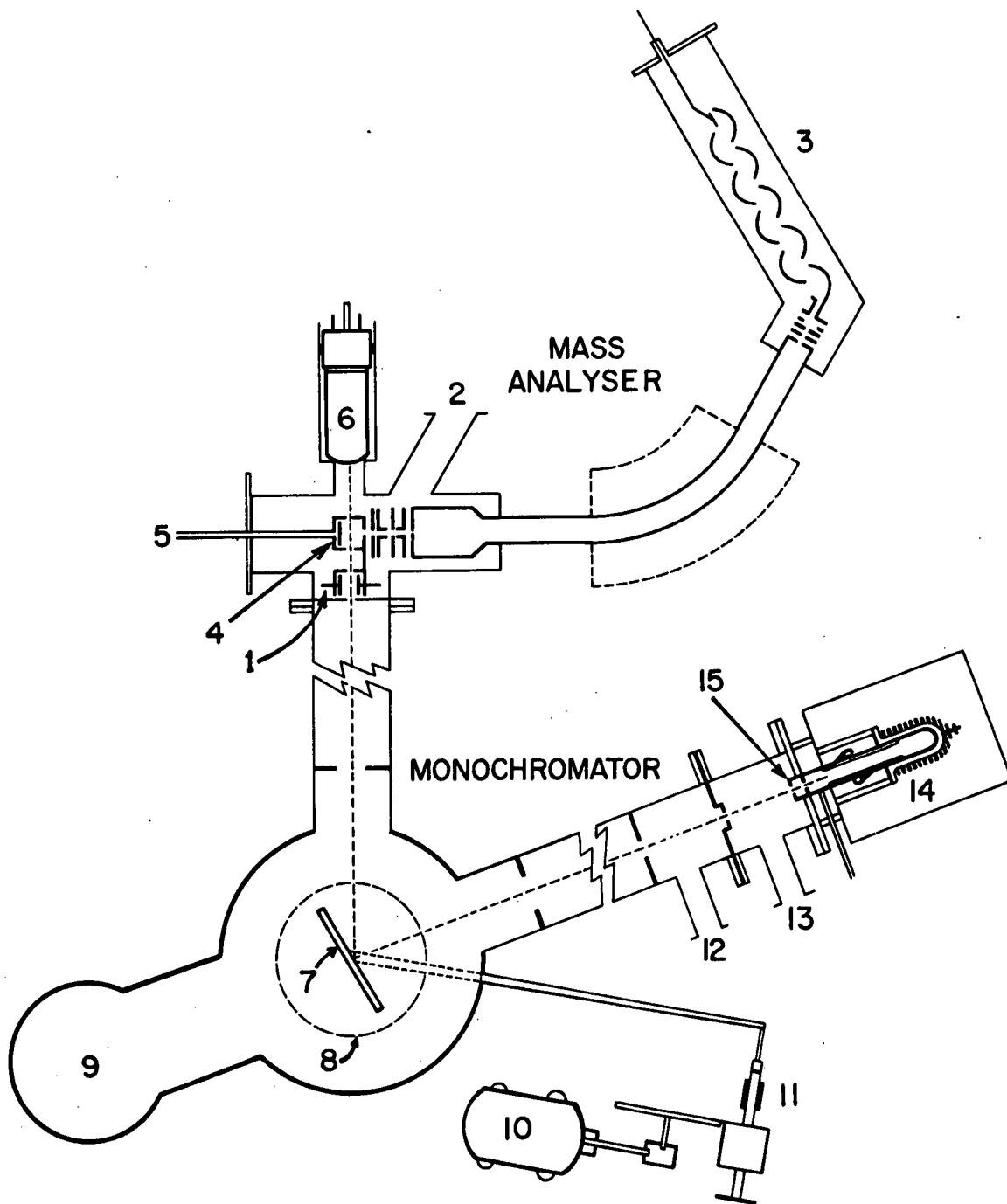


Figure 6: The Monochromator and Mass Spectrometer

Vacuum ultraviolet radiation was generated from the light source L, and passed through a narrow entrance slit to a grating G, sitting on a table T. By turning the arm A, monochromatic radiation of different wavelengths could be selected. The refracted monochromatic light traversed the exit slit of the monochromator, passed through the ion chamber and was incident on a photodetector which had been sensitized to vacuum ultraviolet radiation by coating it on the outside with a thin layer of sodium salicylate.

Positive ions were formed in the ion source by the absorption of vacuum ultraviolet light if it had sufficient energy. The positive ions formed in the ion source were forced through a small slit by a repeller (with a positive potential of a few volts), and were then accelerated by a potential difference of about 2000 volts. They passed through a system of slits of controlled voltage which caused them to be collimated into a narrow beam, and thence down to the magnetic analyser.

In the magnetic field region, the ions were deflected and followed a circular path. The radius of the path depended upon the mass, the velocity of the ion and upon the magnetic strength. By suitable adjustment of the magnetic field strength, a homogeneous beam of ions of the same mass per charge ratio could be focussed at the exit slit.

The small current due to the ion beam was then amplified by a 17-stage electron multiplier. Near the mass spectrometer exit slits, two parallel plates were installed, one of them at ground potential and the other at 100 volts positive or negative. The potential of the second plate was

adjusted so that the ion beam through the exit slit was focussed on the first stage of the electron multiplier. The output electron current from the electron multiplier was fed into a vibrating-reed amplifier and then into a recorder.

Currents from the photodetector and from the vibrating reed were recorded separately as the grating was rotated, and a plot of ions per photon (arbitrary units) against photon energy constituted the photoionization efficiency curve.

B. The Mass Spectrometer

The mass spectrometer was a Nier (93) type instrument, using a 60° sector shaped magnetic field for mass analysis; the permitted radius of ion path was 15 cm. The ion source used yielded an ion beam nearly homogeneous in energy. A calibrated potentiometer supplied the ion accelerating voltage which was continuously variable over the range of 580 to 2800 volts. The magnetic field was provided by a steel electromagnet, and enabled focussing over the range of mass numbers 10 to 300 with an ion accelerating voltage of 2500 volts.

1. The Ion Source

The ion source was placed behind the exit slit of the monochromator as shown in Figure 6. A diagram of the end and side section of the ion source was illustrated in Figure 7. The electrodes 1, 2, 3, 4, 5 and 6 were made of stainless steel, chosen for its non-magnetic properties and corrosion resistance. The ion source and its associated members were also made of stainless steel. All the spacers, insulators and the sample inlet tube were made of pyrex glass.

At the section through A (Figure 7), two deflection plates, at a potential of 500 volts were installed to deflect secondary photoelectrons which were produced when photons hit the metallic part of the monochromator exit slit.

A tungsten filament mounted behind a slit provided a beam of electrons which passed over the ion exit slit at right angle to the direction of the photon beam. This filament provided a means of obtaining electron impact results for comparison. Photoionization cross sections were one or two

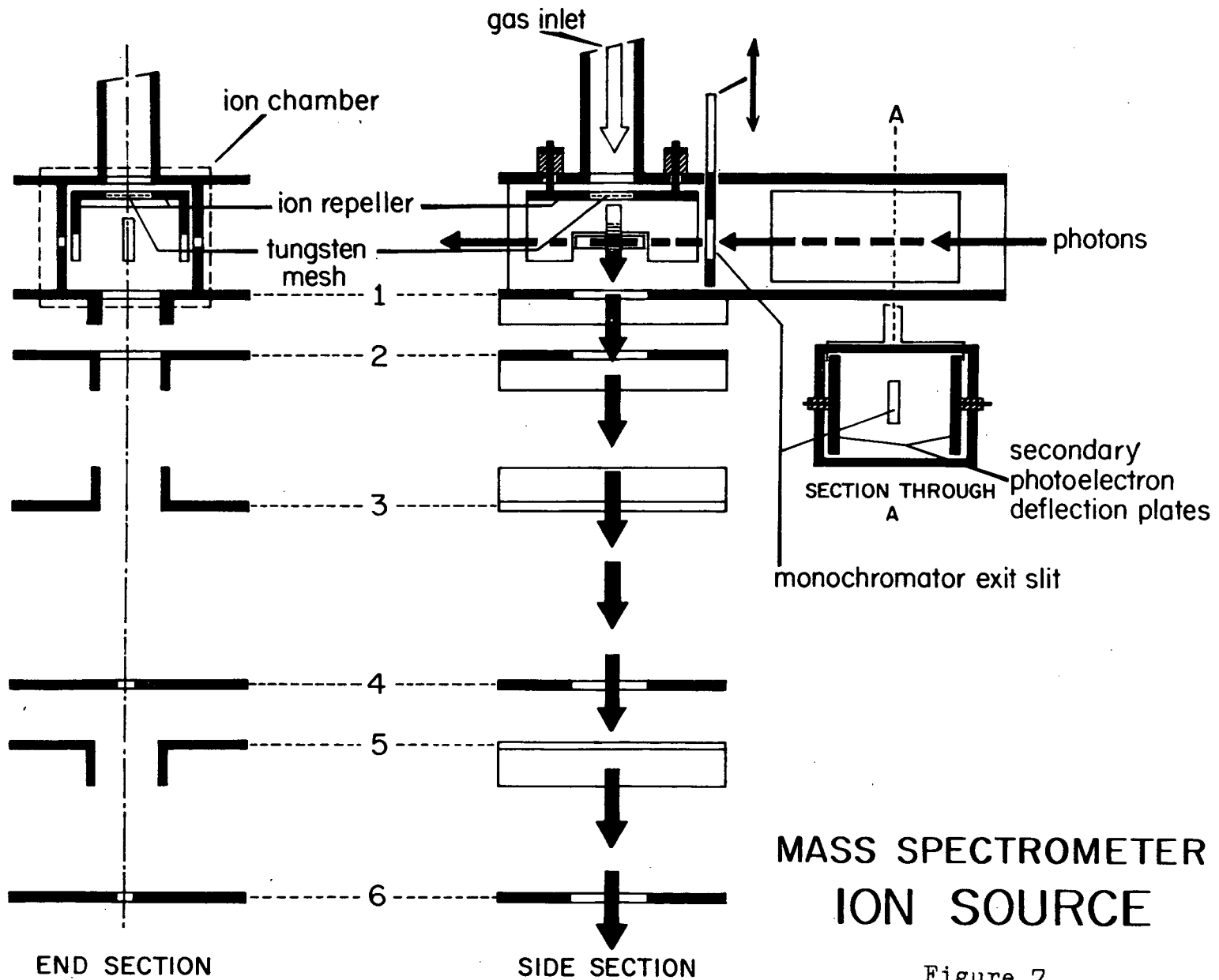


Figure 7

orders of magnitude less than those for impact by 70-volt electrons, (ionization cross section for electron impact is about 10^{-16} cm²), but the ion currents obtained were smaller by two or three orders of magnitude, because the flux density in terms of ionizing particles was much less for any presently available light source than in the case of electron beams (25).

An ion accelerating potential of 2000 volts was applied to electrode 1, and a small fraction of it to the electrodes 2, 3 and 5. The potentials on electrode 2 and each half of 3 and 5 could be adjusted to align the ion beam in the ion source. Electrodes 4 and 6 were at ground potential.

Gaseous molecules entered the ion chamber and diffused into the photon beam. Positive ions produced by photon impact were drawn out of the ion chamber by a small electric field between the ion repeller and the electrode 1. The ion repeller was made of tungsten mesh and was maintained at a positive potential of a few volts, so that neutral molecules could diffuse through it, but positive ions formed in the ion chamber were forced down through the electrode 1. After passing through the ion chamber, the ion beam was accelerated by electrode 1 and focussed by electrodes 2, 3 and 5, and finally passed the exit slit 6 into the mass analyser.

2. The Analyser and the Electromagnet

The analyser tube was made from a 5 cm. diameter copper tube bent through 90° on a radius of curvature of 17.2 cm. It was flattened over the centre section to fit between the 2.2 cm. pole gap of the analyser magnet. The complete unit was rigidly locked to the framework of the

instrument so that its position could be fixed with respect to the magnet.

The electromagnet comprised five 10,000-turn coils wound on a low carbon steel core of 6" x 3" section. The machined pole pieces were made of the same material and had a gap of 2.2 cm. The maximum field strength in the pole gap was approximately 5,000 gauss, and could be varied for the detection of ions over the range of mass numbers of 10 to 300 with an ion accelerating voltage of 2,500 volts.

In the analyser, a beam of ions passing at right angle through a homogeneous magnetic field was deflected by an amount which was determined by the momentum of the ions. Since, in general, the beam emerging from the ion source was inhomogeneous in momentum, the several types of ions having different momenta would be deflected by different amounts. In practice, the ion accelerating potential was maintained constant, and ions of equal charge in the original beam were homogeneous in energy the momentum depended only on the mass of the ion. For a fixed system of slits, one could collect a homogeneous beam of ions of the same mass at the exit slit. By continuously changing the magnetic field strength, one could determine the mass spectrum of the ions formed from a given compound.

On emerging from the magnetic analyser, the resolved ion beam passed through the 2 mm. wide slit, and fell on to the first plate of the electron multiplier. Between the slit and the electron multiplier a suppressor electrode (maintained at negative $22\frac{1}{2}$ volts) suppressed any secondary electrons from ion bombardment of the slit. Furthermore, two parallel plates were recently installed to focus the ion beam. The potential

difference between the two plates was of the order of 100 volts, and could be varied continuously in order to obtain the maximum ion current.

3. The Electron Multiplier

The 14 stage electron multiplier was a sensitive detector of ions. The positive ions from the magnetic analyzer impinged upon the first plate of the detector giving rise to secondary electrons. These electrons were in turn caused to strike a succession of plates, each giving a secondary electron yield greater than unity. The plates were made of 2% Be-Cu, and were connected to 14 successively higher positive potentials, and the secondary electrons were directed from plate to plate by the potential difference across them. The principal merits of the electron multiplier were its extreme sensitivity, fast response and low-noise, wide-bandwidth amplification.

The final electron current from the last plate was collected by a fine tungsten mesh, and then directed to a Cary Model 31 vibrating reed electrometer.

4. The Vibrating Reed Electrometer

The main usefulness of a vibrating reed electrometer is in the measurement of small d.c. currents. The electrometer consisted of two parts: the head unit and the main amplifier. The input d.c. potential which arose from the passage of the electron current through a large resistor of the order of 10^{12} ohms, was converted to a.c. potential by applying it through a series resistor to a capacitor whose capacitance was periodically varying with time. This a.c. signal then underwent several

stages of amplification and the rectified output was displayed on a meter situated in the rack unit.

The input resistor and capacitor were mounted in small individual plug-in units to facilitate changes of range and response time. The input capacity could also be varied internally in the range of 0 to 10 pf. Internal sensitivity controls enabled the amplifier gain to be adjusted in the range 1 to 30,000. This was useful for scaling the output to reduce ionization curves to almost equal sensitivity.

With an input resistance of 10^{12} ohms and capacitance of 5 pf., currents as low as 10^{-16} amperes could be measured. The time constant in this range was about five seconds. The amplifier output was fed into a chart recorder which enabled automatic recording of current from the ion source.

C. The Monochromator

Essentials for making photon impact experiments are a beam of monochromatic light of known energy passing through the gas under study and a device for detecting and measuring the photon intensity. A 1-meter monochromator based on the Seya-Namioka (89,108) mounting was constructed. The body of the monochromator was constructed as a compact brass unit, with fixed entrance and exit slits. The instrument was especially good for the vacuum region because the source and exit slits did not need to be moved as the wavelength was changed. The only mechanical motion involved was a simple rotation of the concave grating, which greatly simplified the vacuum seal problems.

1. The Light Source

The light source used in this work was basically a repetitive, high voltage spark discharge through gas in a pyrex capillary capable of emitting a vacuum ultraviolet continuum from 8 to 21 eV. when it was scanned by the grating. The light source consisted of two major components:

a) The McPherson Model 720 high voltage A.C. power supply which was capable of supplying 0 - 10,000 volts at a maximum current of 60 milliamperes, from a controlled high frequency tungsten spark source. Stable operation was achieved by adjustment of the jet of air blowing across the spark gap. The air jet removed the ionized gases and metal vapors resulting from each electrical breakdown. Further stability was gained by the use of a mercury vapor ionization lamp which illuminated the spark gap.

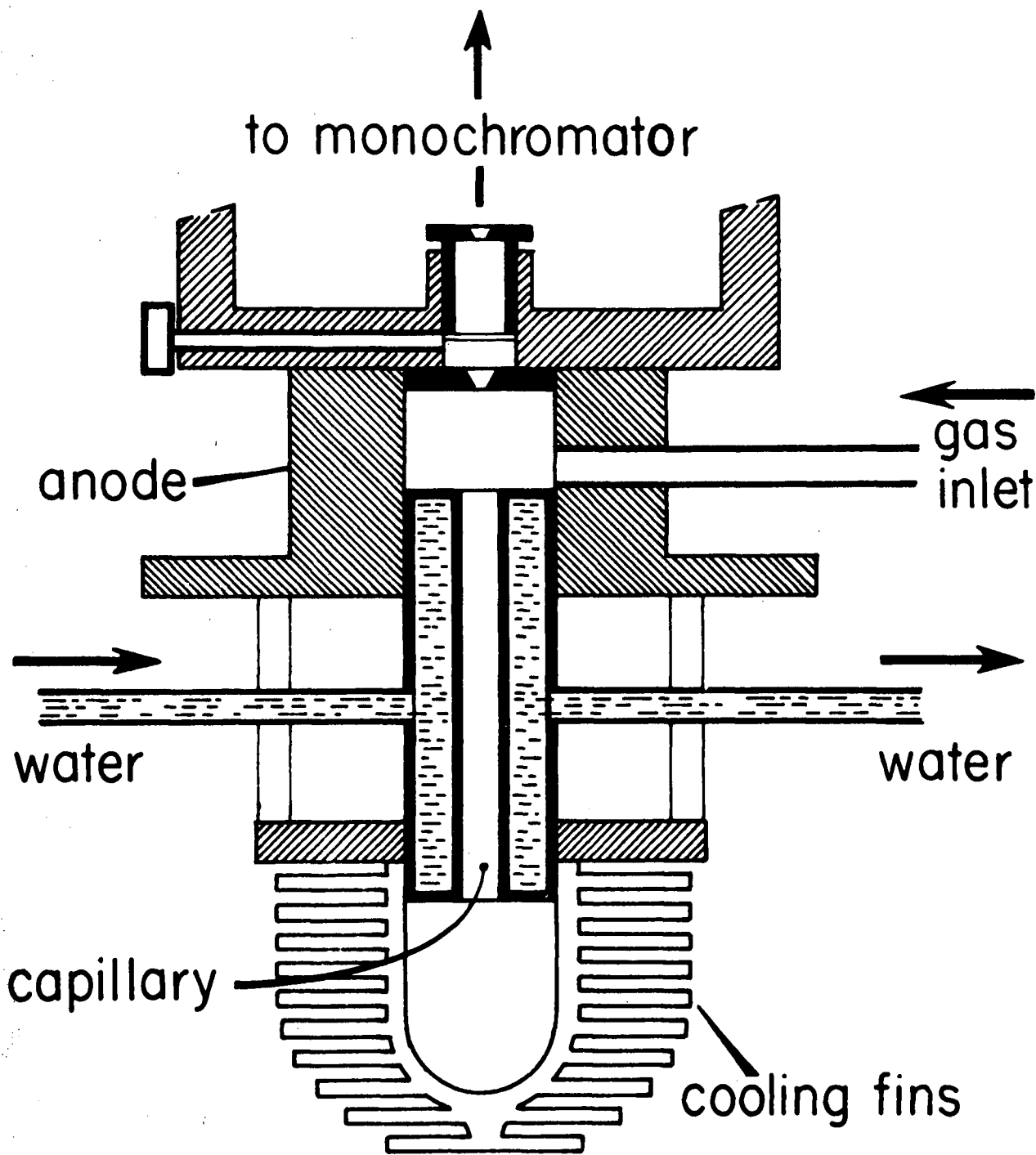
b) The McPherson Model 630 vacuum ultraviolet light source and a diagram of the light source is illustrated in Figure 8. It was a capillary discharge light source, consisted of water cooled capillary, a water cooled Anode and an air cooled cathode. The cathode was air cooled by a built in blower. In operation, this light source could produce a line spectrum or continuum, and it was connected to the monochromator with or without a lithium-fluoride window. In the present work a windowless light source was used. Therefore it was necessary to keep gas pressure in the mass spectrometer as small as possible, and so differential pumping was employed between the source and monochromator inlet slit. A cam operated sliding plunger sealed against the entrance slit jaw, and the monochromator was further evacuated by a 6" oil diffusion pump at the grating housing.

A gas regulating system consisting of a two-stage tank regulator, throttling valve and absolute pressure indicator calibrated 0 to 100 mm. Hg. was connected between the gas tank and the light source. Before the gas from the gas tank entered the light source, it first passed through a U-tube containing Linde synthetic zeolites (molecular Sieves) cooled to liquid nitrogen temperature in order to eliminate any impurities from the gas.

The gases used in the light source were mainly hydrogen or helium. A continuous spectrum was produced by helium from 500\AA to 1200\AA (10 to 21 eV.), and hydrogen was useful for the wavelength region of 900\AA to 1500\AA (8 to 13 eV.). The gas pressure was usually maintained constant at 50 mm. Hg. as indicated in the absolute pressure indicator.

2. The Grating System

In the present work, a 30,000 lines per inch, 54 cm. focal



LIGHT SOURCE

Figure 8

length concave grating with an active area of 25 x 30 mm. was used. The grating rotated about a vertical axis through the centre of the grating which enabled wavelengths between 500\AA and 1500\AA (about 8 to 21 eV.) to be selected with a resolution of about 4\AA .

The grating G, and the external driving system were shown schematically in Figure 6. The grating was clamped in a holder in position on a table T inside the grating housing. The grating was rotated by moving the 12-inch arm A which was connected to a spindle passing through a vacuum seal to the grating table base. The arm A bore against a precision micrometer screw Z which could either be turned manually or by the variable speed motor U. D was a rubber-ringed gear wheel which helped to transmit a smooth drive to the micrometer.

3. The Photon Monitor

A RCA-1P28 glass-enclosed photomultiplier tube was used to measure the photon intensity. It was capable of multiplying the feeble photoelectric current produced at the cathode by a mean value of 1.0×10^6 when operated at 100 volts per stage. The output current of the 1P28 was a linear function of the photon intensity under normal conditions.

The photomultiplier was sensitized to vacuum ultraviolet radiation by coating it on the outside with a thin layer of sodium salicylate dissolved in methyl alcohol. The quantum efficiency of fluorescence of this material has been measured and found to be constant in the wavelength region above 1000\AA , and is a linear function of the photon energy in the wavelength region below 1000\AA (134).

The output current of the photomultiplier was amplified further by a Keithley d.c. electrometer, capable of measuring down

to 10^{-12} amperes. The final output signal from the Keithley electrometer was recorded in a Speedomax recorder.

4. The Energy Conversion Scale

The wavelength of a particular beam of monochromatic light depends on the angular position of the diffraction grating, and is given by the Bragg Equation:-

$$n \lambda = 2d \sin \phi \quad \dots\dots\dots 3.1$$

where n is the order of the line, d is the grating spacing, and ϕ is the angle of the diffraction for wavelength λ . The order n , can be roughly determined by spectrum analysis. (Only $n = 1$ was used in this work). The grating spacing d is an accurately determined constant. A relation therefore exists between the wavelength and the angle of diffraction for any wavelength in the spectrum. The grating table used in the present work was connected to a 12-inch arm A which bore against a precision micrometer screw. The $584\overset{\circ}{\text{A}}$ helium resonance line, the $744\overset{\circ}{\text{A}}$ neon impurity line of the helium spectrum and the $1215\overset{\circ}{\text{A}}$ α line of the hydrogen spectrum were focussed separately, and the micrometer readings were recorded for each line. Using these three readings, a calibration curve was drawn, which is a straight line relating wavelength to micrometer reading, from which the wavelength of any other spectral line could be determined directly from the micrometer reading.

The relation $E = \frac{hc}{\lambda}$ gives us a means of comparing our results which are in terms of photon wavelength with the electron impact data which are in electron volts. E is the energy of the radiation in electron volts, h is Planck's constant, c is the velocity of light, and λ is the wavelength of the radiation.

A conversion table for wavelengths to electron volts based on this equation was published in 1961 by Samson (106) and the conversion factor used was $1 \text{ cm}^{-1} = 12397.8 \pm 0.5 \times 10^{-8} \text{ eV}$. This table was used throughout this work for all energy conversions.

D. The Vacuum System

A good vacuum is essential in photoionization work, because atmospheric species such as oxygen and nitrogen absorb ultraviolet radiation strongly in the wavelength region below 2000\AA . Also atom-atom and ion-atom reactions will arise if the ion source pressure of the mass spectrometer is not under a good vacuum. The vacuum system used follows the conventional lines for mass spectrometers, and can be subdivided into four different sections.

1. The Analyser Tube

The analyser tube was pumped from the source end by a 2-inch all-metal MCF-60 fractionating oil diffusion pump fitted with a cold trap, and backed by a Welch duo-seal vacuum pump. The ultimate vacuum of these pumps was about 5×10^{-7} mm. Hg., and net pumping speed was between 20 to 30 litres per second.

A NRC-518 ionization gauge mounted near the ion source, was used to measure the pressure in this region.

2. The Monochromator

The monochromator was pumped near the grating mounting by a 6-inch all-metal MCF-700 fractionating oil diffusion pump fitted with cold-baffles, and backed by a large Welch duo-seal rotary pump.

A NRC-501 thermocouple, mounted on the top of the grating housing, was used to measure the pressure of this region before the oil diffusion pump was switched on.

3. The Light Source

Two Welch duo-seal vacuum pumps, one in front and the other behind the monochromator entrance slits, were employed to

minimise the gas pressure in the light source region. It is important to evacuate this region, because the photon intensity will be diminished if the radiation is allowed to cause ionization there.

4. The Gas Handling System

A Welch duo-seal type rotary pump was used to evacuate the gas particles in the three storage glass bulbs. It was separated from the bulbs by means of a tap before samples were introduced into the storage bulbs and also during a run. The pressure in this region was usually maintained in the order of 10^{-4} mm of Hg.

5. The measurement of Pressure - Gauges

The Thermocouple Gauge

This type of gauge consists of a wire through which a fixed current of about 6 mA is passed. The temperature of the wire depends upon the rate of heat loss from the wire and, therefore, upon the gas pressure, and is measured by means of a thermocouple attached to the wire. The output of the thermocouple is observed on a meter, which is calibrated directly in terms of pressure.

Ionization Gauge

The NRC-518 ionization gauge is simply a discharge tube relying on ionization for its principle of operation. It consists of a tungsten filament, a grid at constant potential, and a plate. The filament emits electrons which ionize gas molecules in the gauge, and the plate (negative with respect to the grid) is used to collect the ions. The number of ions hitting the plate depends on the gas pressure, and the plate current is amplified and observed on a meter calibrated directly in terms of pressure.

The ionization gauge is equipped with a safety relay which will automatically turn off the gauge when the pressure reaches some set value, say $1\frac{1}{2}$ times the full scale indication of the particular range selected.

E. Experimental Techniques

1. Sampling

The water used was distilled and the gaseous compounds used in this research were pure samples supplied by Matheson of Canada Co. Ltd. and were not further purified.

Before the study of a molecule by photon impact was carried out, a mass spectrum of the sample was first taken. This was done by focussing the intense $744\overset{\circ}{\text{A}}$ (about 16.64 eV.) neon impurity line of the helium spectrum and keeping the ion accelerating voltage at about 2000 volts, the magnetic field strength was scanned slowly by a motor, and the ion current was measured and displayed on the recorder. In each case, peaks corresponding to the parent and fragment ions were observed on the mass spectrum, but impurities if any, were not observed. The reasons for taking the mass spectrum were threefold, firstly, to detect the approximate positions of the parent and its fragment ions in the mass spectrum; secondly, to measure their relative ionization probabilities at a certain photon energy; and thirdly, to detect impurities in the sample.

2. Experimental Procedure

In order to obtain photoionization data for various molecular ions, the following procedure was followed for each gas.

The system was pumped down to approximately 10^{-6} mm Hg. and the electronic equipment was allowed to warm up for a period of half an hour. The sample to be studied was introduced into the gas handling system and subsequently leaked into the ion chamber of the mass spectrometer. The gas pressure in the ion chamber was maintained at 3×10^{-5} mm Hg., and remained constant for a period of at least three hours.

When all these preparations had been completed, the intense 744\AA (about 16.64 eV.) neon impurity line of the helium spectrum was focussed. The magnetic field strength was adjusted to bring the ion to be studied to focus at the collector with an ion accelerating voltage at about 2000 volts. Sometimes it was also necessary to adjust the ion accelerating voltage, the potentials at the repeller electrode, electrodes 2, 3 and 5 (Figure 7), and the two electrodes between the ion exit slit and the electron multiplier, to give the maximum ion current.

The spectrum of hydrogen or helium was scanned at 3\AA per minute by rotating the grating with a multiple-speed motor, and light of various wavelengths contained in the source was allowed to enter the ion chamber. The scanning was started at a photon energy well below the threshold ionization potential of the molecule, and the ion and photon current intensities for each wavelength were measured separately on two recording charts. Finally, a photoionization efficiency curve was obtained. For each molecule, the experiment was repeated six or more times until close agreement between the successive runs was obtained.

When the ion and photon current intensities became very low, both the rotary and diffusion pumps were stopped, and air was introduced into the system. The grating was taken out, dismantled, and sprayed with pure toluene. The photoelectron detector was cleaned with methanol, and coated with a fresh layer of sodium salicylate. After these operations, both the ion and photon current intensity were found to be greatly improved.

3. The Photoionization Efficiency Curve

The significance of the detailed shape of the photoionization efficiency curves, is not only for the accurate measurement.

of ionization and appearance potentials, but also for the identification of the various processes leading to the ion and the detection of higher energy states. These curves were drawn, from the experimental data, relating the number of ions of a given kind per number of incident photons, produced by photon impact, against the photon energy of the ionizing radiation.

The photoionization efficiency for a given molecule at a certain photon energy is defined by the equation:-

$$\begin{aligned} \text{Efficiency} &= \frac{\text{number of primary ion-pairs formed}}{\text{number of incident photons absorbed}} \\ &= \frac{\text{amplitude of the ion current}}{\text{amplitude of the photon current}} \quad \dots 3.2 \end{aligned}$$

These photoionization efficiencies have been found to be relatively unaffected by external perturbations such as gas pressure, applied field, and the geometry of the ionization chamber (139).

The instrument used in this work has a resolution of 4\AA , and as a result, the actual 'threshold' value of the ionizing photon energy will be greater than the value obtained from the photoionization efficiency curves by a half-width of the resolution, namely 2\AA . A correction has been made for all measurements reported in this work.

F. Sources of Error

One of the major sources of error was due to the interpretation of the photoionization efficiency curves. The threshold ionization potentials of all the molecules could be determined to a high degree of accuracy. However, the noise to signal ratio of the ion and photon intensity measurements after the threshold in some cases was rather high, and it was difficult to localize the point where maximum change of slope indicated the inner ionization potentials. Only estimated positions were obtained from the experimental curves in spite of the fact that the band width of the photon beam used was only 0.05 eV. at 10 eV. photon energy.

The second source of error was caused by the variation of the gas pressure during a run. In the early phase of the work, a three-litre storage bulb was used for sample, and the gas was allowed to leak slowly into the mass spectrometer. It was found that after about three hours of operation, the gas pressure dropped to nearly half its original value, and as a result the ion current decreased significantly while the photon current remained constant. Two five-litre gas bulbs were since then added to the supply system making a total capacity of thirteen litres. The gas pressure drop for the same period of time was very small, and the drop in ion current per photon at a particular wavelength during a run was negligible.

The threshold ionization potentials of all the molecules studied represent the average of six or more runs. The photoionization efficiency curves of several runs exhibited good reproducibility, and the difference of this ionization potential between each run was usually less than 0.05 eV.

CHAPTER FOUR

PHOTOIONIZATION OF ATOMS

The photoionization efficiencies of 'noble' gaseous atoms are of special interest in that the ionization potential of these atoms is known accurately from spectroscopic data. A comparison of data obtained by the two methods provides a means of determining the accuracy and reliability of the photoionization results. Photoionization results on the 'noble' atoms also provide a check for the validity of theoretical models of excitation and autoionization processes.

Argon, krypton and xenon each has an outer mp^6 shell, where $m = 3$ for argon, 4 for krypton and 5 for xenon, and the ionization of these molecules refers to the removal of one of the six p electrons. The ground state of the ion formed is split into two levels, the $^2P_{3/2}$ and $^2P_{1/2}$. The latter has the higher energy.

Beutler (3) studied the absorption spectra of these gases, and obtained ionization thresholds of the $^2P_{3/2}$ and $^2P_{1/2}$ states of the ions from the analysis of the Rydberg series. He observed that the series members converging to the higher energy sublevel of the ground state of the ion ($^2P_{1/2}$) become very diffuse near the ionization limit, and proposed that this was due to autoionization, i.e. the 'noble' atom was first excited to one of its excited states, and subsequently ionized by a radiationless transition to the ionization continuum.

A. Argon

The absorption coefficients for argon have been measured by Weissler and Lee (142) and Huffman, Tanaka and Larrabee (54). The photoionization efficiency of argon has been

measured by Wainfan, Walker and Weissler (143), Weissler, Samson, Ogawa and Cook (146) and Comes and Lessman (9). All their data were obtained using a line spectrum as their light source. Frost and McDowell (35), Foner and Nall (29), Marmet and Kerwin (77) studied argon using the electron impact method.

Figure 9 shows the photoionization efficiency for argon as a function of the photon energy. The threshold ionization of argon to give a $^2P_{3/2}$ state of the ion is obtained from the point of initial onset of the argon curve at 15.73 ± 0.05 eV., which is in good agreement with the spectroscopic value at 15.76 eV. (1), with the photoionization results at 15.7 eV. by Weissler et al. (146) and with the electron impact data at 15.76 eV. by Dibeler et al. (17), at 15.77 eV. by Morrison (81) and at 15.74 eV. by Foner and Nall (29).

From this threshold, the ionization efficiency is observed to rise steeply as would be expected in the case of a monatomic gas. The spectroscopic separation between the $^2P_{3/2}$ and $^2P_{1/2}$ state of Ar^+ is 0.18 eV., and with our present monochromator resolution we do not expect to resolve any structure between these two states. That autoionization peaks appear in this region has been demonstrated by the total absorption experiment of Huffman, Tanaka and Larrabee (54), and Cook and Ching (14).

The photoionization efficiency of Ar^+ remains fairly constant at higher energies up to about 16.5 eV. However, Comes and Lessman (9) found several peaks in their Ar^+ curve up to 18 eV., and they correlated these with breaks found by various workers using electron impact methods. We would expect to be able to resolve most of the peaks appearing

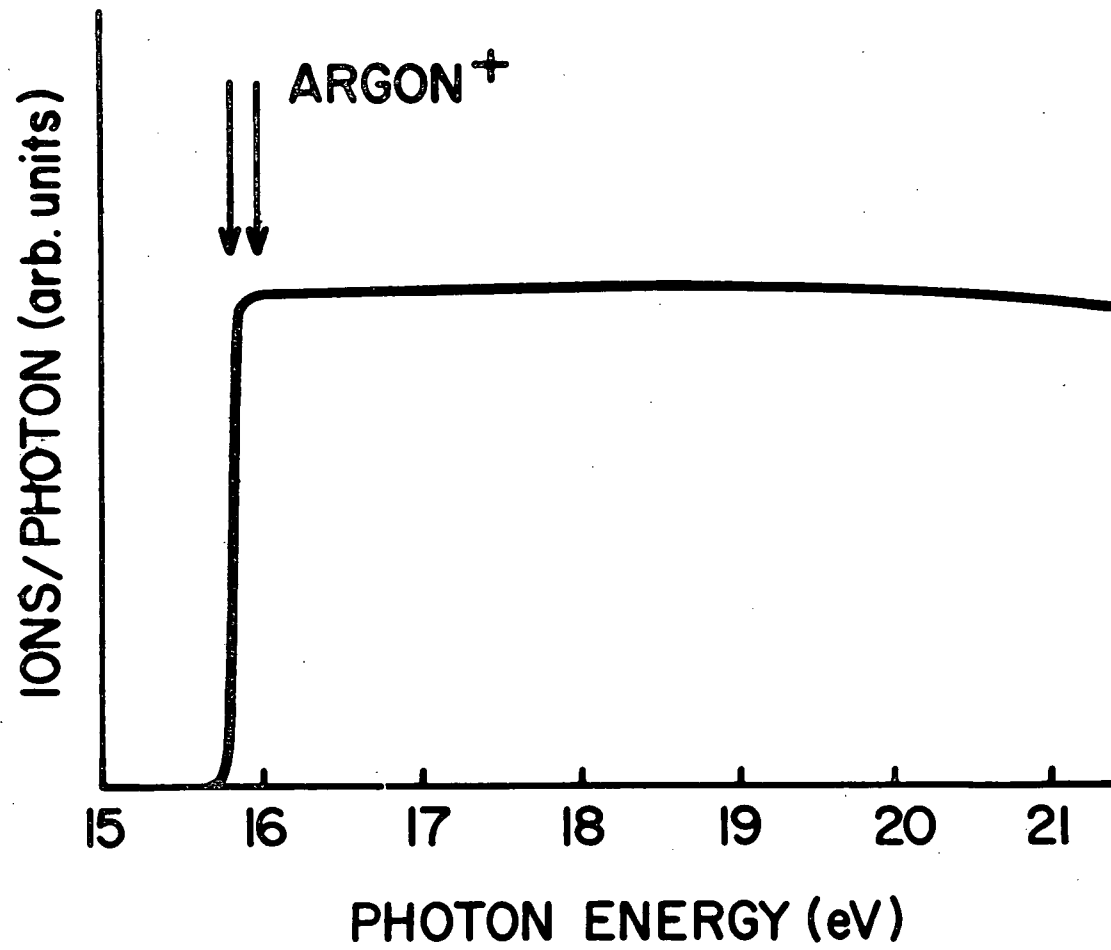


Figure 9

in the Comes and Lessman curve, but we find no evidence for them. Huffman, Tanaka and Larrabee (54) using a much smaller energy bandwidth (0.02 eV. at 600 \AA) found no evidence for these transitions either, and it seems unlikely that photoionization efficiency curves should be very different from total absorption curves for this simple case. Of course, there are different selection rules for electron impact excitation, and their observed transitions may be optically forbidden. This would explain their absence in the results reported here but not in the Comes and Lessman observations. The main difference between the two sets of data lies in the light source - the Comes and Lessman data was obtained using a line spectrum, and ours using a helium continuum.

B. Krypton

Krypton has been studied by Beutler (3), Huffman, Tanaka and Larrabee (53) using the spectroscopic method. Frost and McDowell (35) using the electron impact method studied Kr^+ ion and found that the ground state of Kr^+ consists of two components, $^2\text{P}_{3/2}$ and $^2\text{P}_{1/2}$ states, whose separation is 0.68 eV.

The photoionization efficiency curve of krypton is shown in the lower half of Figure 10, and the top curve is the absorption coeff. curve of krypton by Huffman, Tanaka and Larrabee (53) for comparison. The threshold ionization potential of krypton obtained at the point of initial onset of the former curve is found to be 13.99 ± 0.05 eV. which is in good agreement with the spectroscopic ionization potential of

krypton at 14.009 eV. (1) and the electron impact data of Dibeler (17) at 13.96 eV.

After the threshold energy, the curve of Kr^+ is observed to rise steeply as would be expected in the case of a monatomic gas. A strong photoionization peak is observed at 14.09 eV. which partially obscures the ionization continuum of the $^2\text{P}_{3/2}$ state of Kr^+ . Several less intense ionization peaks are also observed at higher energies. These peaks have been found previously by Beutler (3) and Huffman (53) as autoionized in their absorption spectra.

The position of the peaks in Figure 10 are compared with those found by Huffman (53) in the absorption spectra of Kr in Table II.

Table II
Peak Energies for Krypton Ion (eV.)

This work	13.99 (IP.)	14.08	14.26	14.37	14.47
Huffman (53)		14.09	14.26	14.36	14.47

The good agreement between absorption spectroscopy and the photoionization data strongly suggested that the peaks determined here arise from autoionization.

At 14.75 eV. another small ionization continuum is observed from the curve for Kr^+ (Figure 10), this continuum corresponds to the ionization of krypton to the $^2\text{P}_{1/2}$ state. The $^2\text{P}_{3/2}$ and $^2\text{P}_{1/2}$ ground state separation in Kr^+ is found to be 0.78 eV. which is higher than the value of 0.666 eV.

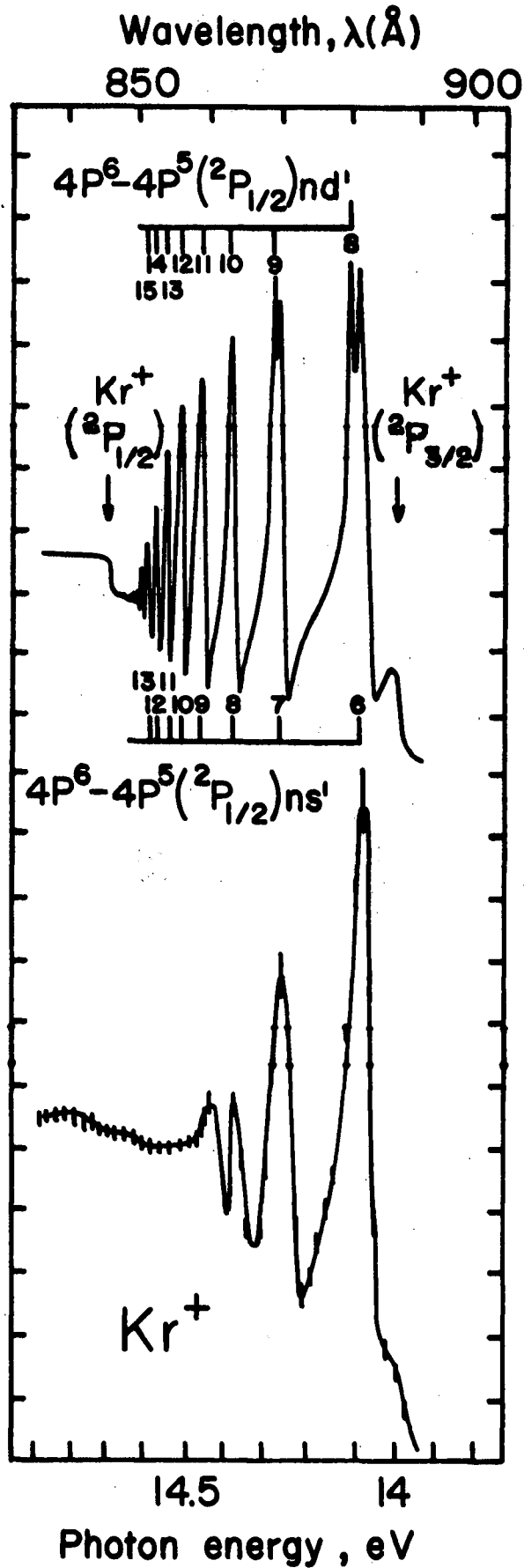


Figure 10

obtained by the spectroscopic method (1). The large difference in energy is probably due to the fact that the ionization continuum for the $2P_{1/2}$ state of Kr^+ is very small, and the accurate determination of the ionization potential responsible for this process is difficult with the resolution at present attainable with the apparatus.

C. Xenon

Xenon has been studied by Beutler (3), Huffman, Tanaka and Larrabee (53) (Absorption Spectroscopy), by Nicholson (91), Matsunaga, Jackson and Watanabe (79) (Photoionization) and by Dibeler, Mohler and Reese (17), and Foner and Nall (29) (Electron Impact).

The photoionization efficiency curve of xenon is shown in Figure 11. The threshold ionization potential of xenon measured at the point of steepest slope is found to be 12.13 ± 0.05 eV. which is in excellent agreement with the spectroscopic value 12.129 eV. (1).

After the threshold energy, several peaks appear on the efficiency curve for xenon. These peaks have been found previously by Beutler (3) as autoionized in his absorption spectrum, and that they are indeed due to this type of process has been recently confirmed by Nicholson (91) in a total photoionization apparatus.

The present photoionization work was done with mass analysis and with much lower sample pressure (10^{-5} mm. of Hg.) than those used by Nicholson (20 - 100 μ). Atom-atom and ion-atom reactions are therefore virtually eliminated.

In Table III below the position of peaks in Figure 11 are compared with those found by Beutler (3), Huffman (53) and

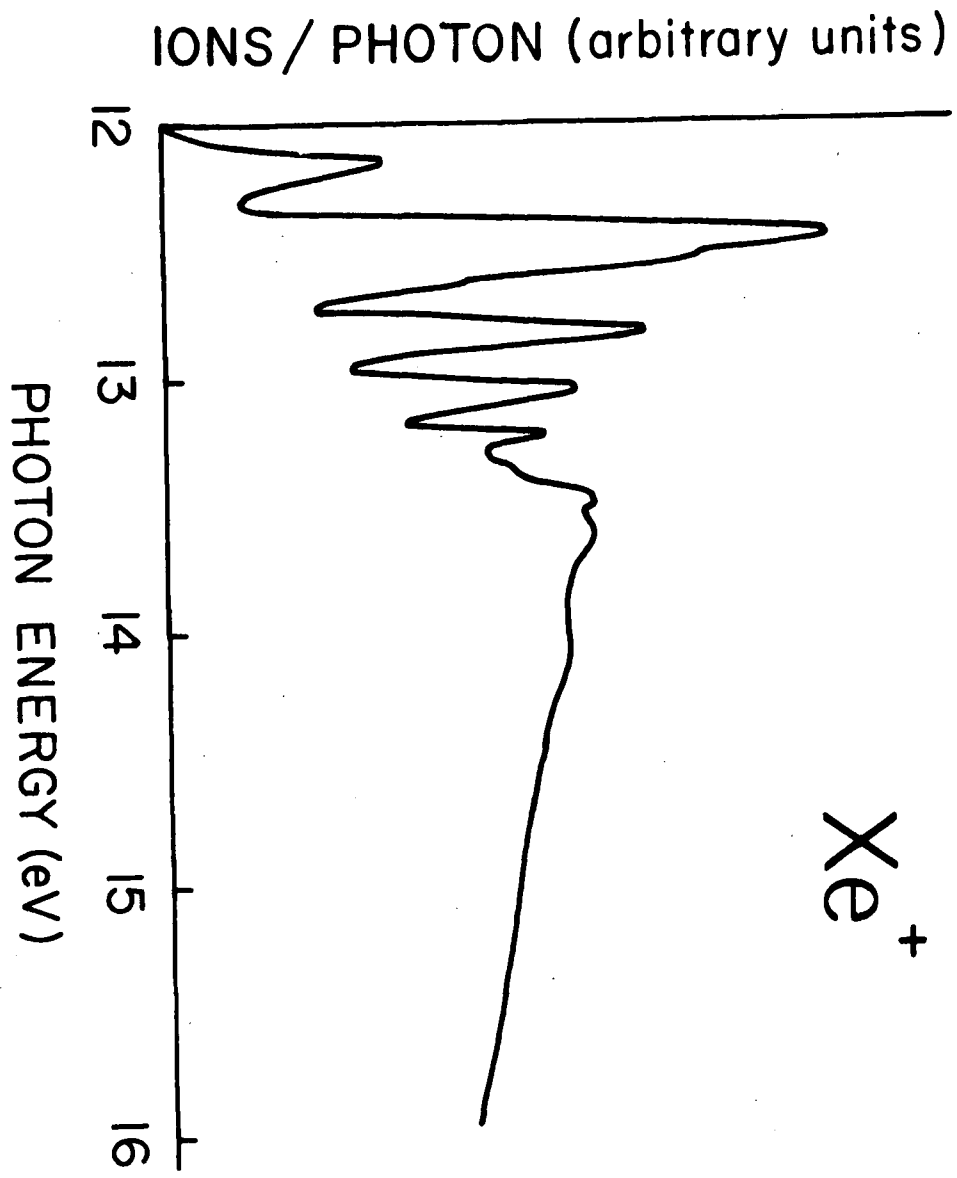


Figure 11

Watanabe (79) in the absorption spectrum of xenon, and also by Nicholson (91) using the total photoionization apparatus.

Table III
Peak Energies for Xe⁺ (eV).

This work	Beutler(3)	Huffman(53)	Watanabe (79)	Nicholson(91)
12.12 (IP.)			12.15 (IP.)	12.129 (IP.)
12.43	12.45	12.46	12.46	12.48
12.81	12.82	12.83	12.83	12.86
13.03	13.02	13.02	13.00	13.05
13.18	13.14	13.15		13.16
13.23	13.21	13.21		13.25
13.45			13.48	
13.63				

The closeness of the agreement between the absorption spectroscopy and the photoionization data prove beyond doubt that the peaks determined here arise from the process of autoionization.

The $^2P_{3/2} - ^2P_{1/2}$ ground state separation in Xe⁺ is found to be 1.32 eV., which is in good agreement with the separation of 1.31 eV. obtained by the spectroscopic method (1).

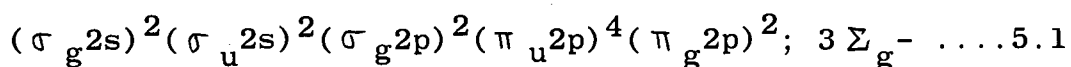
CHAPTER FIVE

PHOTOIONIZATION OF DIATOMIC MOLECULESA. Oxygen

Oxygen is a major component of the atmosphere, and the study of its photoionization is of fundamental importance in molecular spectroscopy and ionospheric physics.

Oxygen has been the subject of many fairly detailed studies. Price and Collins (89) studied the molecule by the optical spectroscopic method, and Mulliken and Stevens (84) using the cyclic method have obtained the first ionization potential of oxygen as 12.2 eV. Photoionization studies of oxygen have been done by Inn (60), Watanabe (138), Nicholson (91) and Samson and Cairns (105). Tate and Smith (122), Hagstrum (44), Frost and McDowell (38), Clarke (5) and Brion (4) have studied oxygen by the electron impact method.

The ground state of the oxygen molecule has the electronic structure:



The molecular orbitals are listed in the order of decreasing binding energy, omitting the inner ones. The first ionization potential refers to the removal of an electron from the outer antibonding ($\pi_g 2p$) orbital leaving the O_2^+ ion in its $X^2 \Pi_g$ ground state.

The photoionization efficiency curves for oxygen are shown in Figures 12 and 13. The ionization potential of oxygen measured from the point of initial onset of the curve is 12.06 ± 0.05 eV. which is in excellent agreement with other photoionization values at 12.065 eV. by Nicholson (91), 12.063 eV. by

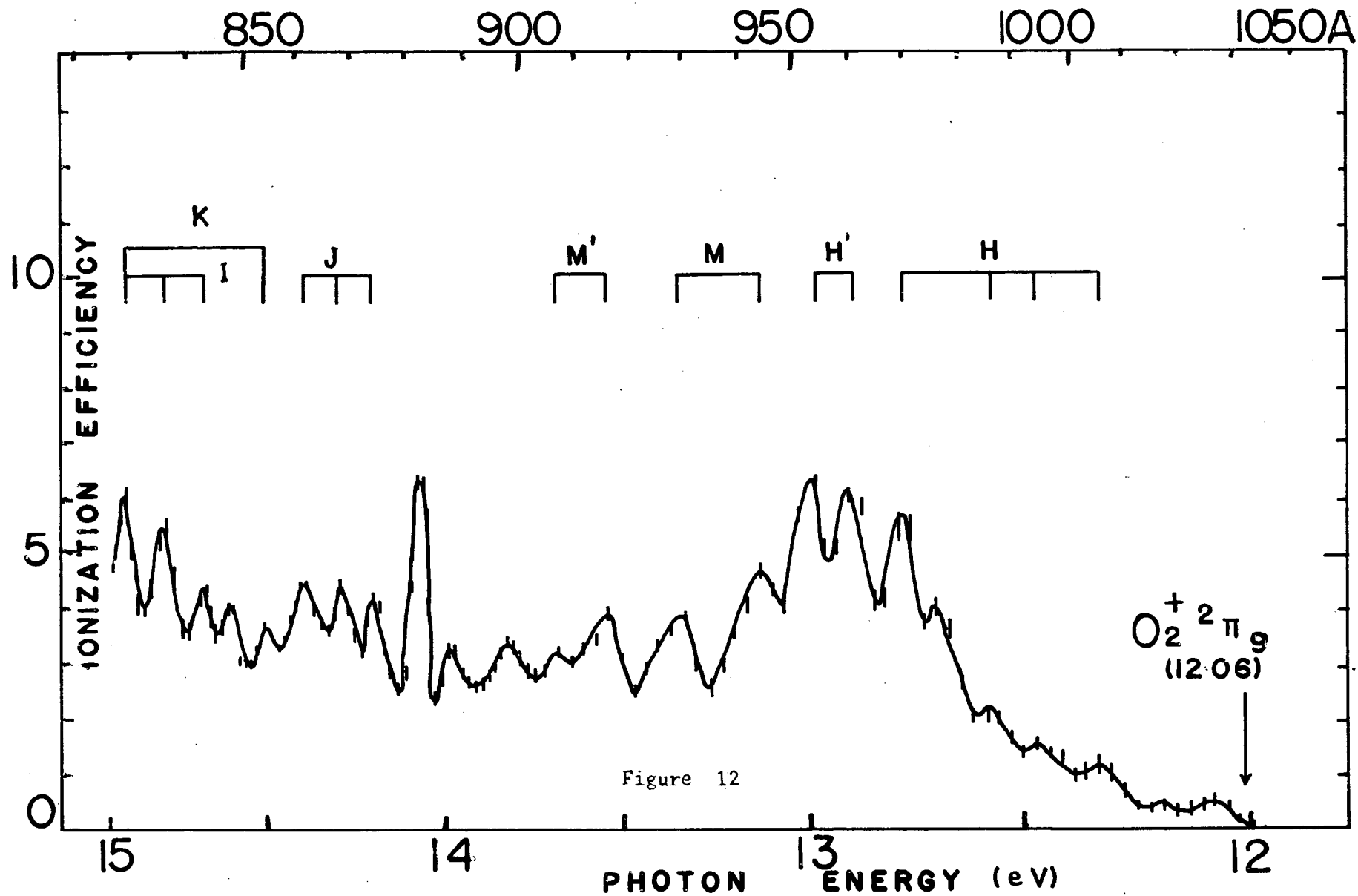
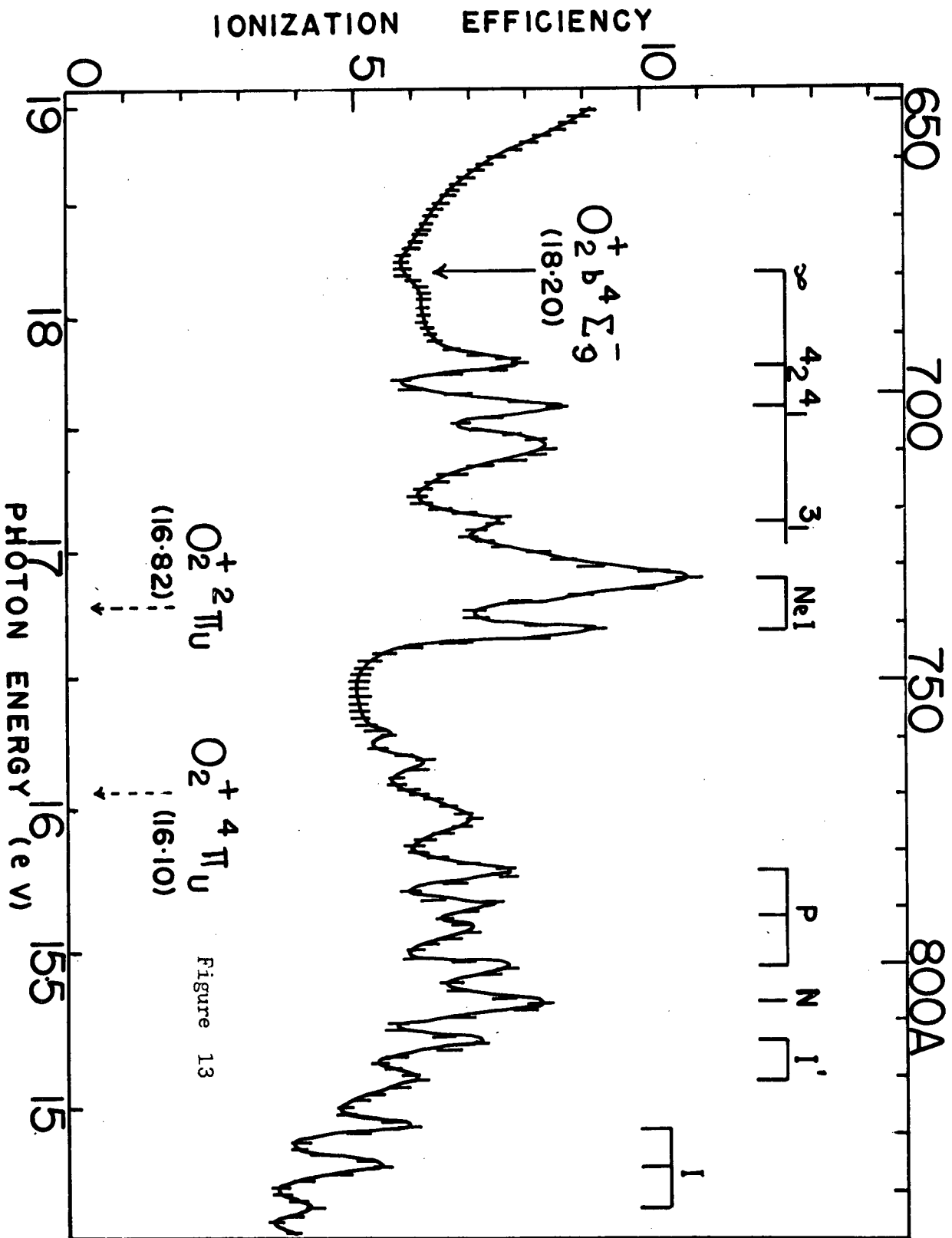


Figure 12



Samson (105) and 12.07 eV. by Watanabe (138). The close agreement between the photoionization results using different techniques proves beyond doubt that the photoionization methods of obtaining ionization potentials are reliable. Values obtained by electron impact methods are slightly higher. The various electron impact, spectroscopic and photoionization ionization potentials of oxygen found by different workers are summarised in Table IV.

Table IV
Threshold Ionization Potential of Oxygen

I.P. (eV.)	WORKERS	METHODS	YEAR
12.06 \pm 0.05	Present result	Photoionization	1966
12.04 \pm 0.01	Inn (60)	Photoionization	1953
12.07 \pm 0.01	Watanabe (138)	Photoionization	1957
12.065	Nicholson (91)	Photoionization	1963
12.063	Samson (105)	Photoionization	1965
12.2	Mulliken (84)	Cyclic Method	1933
12.2 \pm 0.1	Price (99)	Spectroscopy	1934
12.5 \pm 0.1	Tate (122)	Electron Impact	1941
12.1 \pm 0.2	Hagstrum (44)	Electron Impact	1951
12.21 \pm 0.04	Frost (38)	Electron Impact	1958
12.04 \pm 0.02	Clarke (5)	Electron Impact	1964
12.20 \pm 0.05	Brion (4)	Electron Impact	1964

After the threshold ionization potential of oxygen, the photoionization efficiency curve exhibits many peaks. The whole region after the threshold energy is known to be overlaid with many autoionization states (130), and a comparison of the absorption spectrum and the photoionization efficiency curve shows that the peaks in the photoionization spectrum correspond well with

peaks in the absorption spectra. Table V shows a comparison of peaks in photoionization efficiency curves obtained in this work with those obtained in the work of Nicholson (91) and Watanabe (138), and in the absorption spectra of Huffman (55), Cook (11) and Price and Collins (99). The agreement between photoionization and absorption peaks establish with certainty that certain of the oxygen peaks arise from autoionizing levels.

The lettering scheme of figure 12 and 13 is such that bands in the groups H, I, J, K , H', I', , M, N, O , M', N', , belong to Rydberg series' approaching the limit characteristic of each particular group (99).

The well established states of oxygen ions are $X^2\pi_g$, $a^4\pi_u$, $A^2\pi_u$ and $b^4\Sigma_g^-$. The energy state of O_2^+ $^2\pi_g$ is obtained by the removal of a ($\pi_g 2p$) electron, the $a^4\pi_u$ and $A^2\pi_u$ states are obtained by the removal of ($\pi_u 2p$) electrons, and $b^4\Sigma_g^-$ state is obtained by the removal of an ($\sigma_g 2p$) electron. The present photoionization data for oxygen gives evidence for the excitation of only two types, namely the transitions to $X^2\pi_g$ and $b^4\Sigma_g^-$ states. In the region of the π_u electronic transitions, autoionizing transitions especially the neon impurity lines are so intense that the electronic levels of the ions are obscured by the resolutions of the monochromator.

The ionization potential of oxygen leading to the $b^4\Sigma_g^-$ state is obtained from the break of the curve at 18.20 eV. This value is in close agreement with those at 18.16 eV. by Price and Collins (99) and 18.17 eV. by Huffman, Larrabee and Tanaka (55). The electron impact work of Frost and McDowell (38) gives a value of 18.42 eV.

Table V

Comparison of Peaks in Photoionization Efficiency

Curves and Absorption Spectrum of Oxygen

Designation (56)	This Work	Huffman (55)	Cook (11)	Nicholson (91)	Price (99)	Watanabe (138)
-	12.16	12.16	-	-	-	-
H ₁	12.30	12.30	-	12.33	12.33	12.33
H ₂	12.45	12.47	-	12.47	12.48	12.48
H ₃	12.53	12.53	12.56	12.61	12.61	12.61
-	12.68	12.69	12.68	-	-	-
H ₄	12.76	12.75	12.75	12.75	12.75	12.76
H ₃ '	12.87	12.88	12.88	12.84	12.84	12.84
H ₄ '	12.97	12.97	12.97	12.97	12.97	12.98
M ₂	13.10	13.08	13.08	13.09	13.08	13.09
M ₄	13.31	13.31	13.31	13.31	13.31	13.31
M ₃ '	13.51	13.52	13.52	13.52	13.52	13.53
M ₄ '	13.63	13.62	13.63	13.62	13.62	13.62
-	13.77	13.76	13.77	13.75	-	13.77
-	13.94	13.95	13.95	13.96	-	-
-	13.99	13.98	13.99	13.99	-	13.98
J	14.14	14.11	14.13	-	-	-
J	14.25	14.25	14.25	-	-	-
J	14.34	14.33	14.34	-	-	-
K	14.49	14.48	14.48	-	-	-
-	14.57	14.56	14.57	-	-	-
I	14.67	14.66	14.66	-	-	-
I	14.79	14.79	14.79	-	-	-
I, K	14.92	14.91	14.91	-	-	-
I'	15.07	15.07	15.06	-	-	-
I'	15.16	15.17	15.17	-	-	-
N	15.32	15.33	15.33	-	-	-
P	15.45	15.45	15.45	-	-	-
-	15.56	15.55	15.55	-	-	-
P	15.60	15.60	15.60	-	-	-
P	15.77	15.77	15.77	-	-	-
-	15.80	15.80	15.80	-	-	-

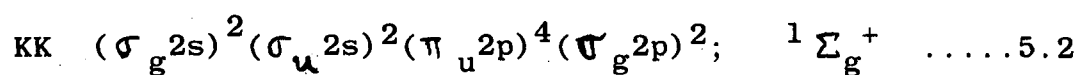
The interatomic distance, according to Frost and McDowell (38), for the various states of oxygen and its molecular ions are: O_2 1.204Å ($X^3 \Sigma_g^-$); O_2^+ : 1.1227Å ($X^2 \Pi_g$), 1.3813Å ($a^4 \Pi_u$), 1.4038Å ($A^2 \Pi_u$) and 1.2795Å ($b^4 \Sigma_g^-$). The most probable transitions in photoionization according to the Franck-Condon Principle (and with the interatomic distances between the molecule and the ion in mind), will be those near the vertical line rising from the ground state of the oxygen molecule to one of the low lying vibrational levels of $X^2 \Pi_g$ and $B^4 \Sigma_g^-$ states of the oxygen ion. The transitions to a $a^4 \Pi_u$ and $A^2 \Pi_u$ states of the oxygen ion are less probable since they lie at a greater interatomic distance.

B. Nitrogen

Nitrogen has been studied by many workers. The absorption coefficients of nitrogen have been measured by Huffman, Tanaka and Larrabee (55), Cook and Metzger (11), Ogawa and Tanaka (95), Watanabe and Marmo (136), Itamoto and McAllister (61) and Clarke (5). Only a few papers on the photoionization of nitrogen, particularly those measuring photoionization efficiencies, have been published. Earlier work was done by Wainfan, Walker and Weissler (141), Cook and Metzger (11), Samson and Cairns (103) and Comes and Lessman (8).

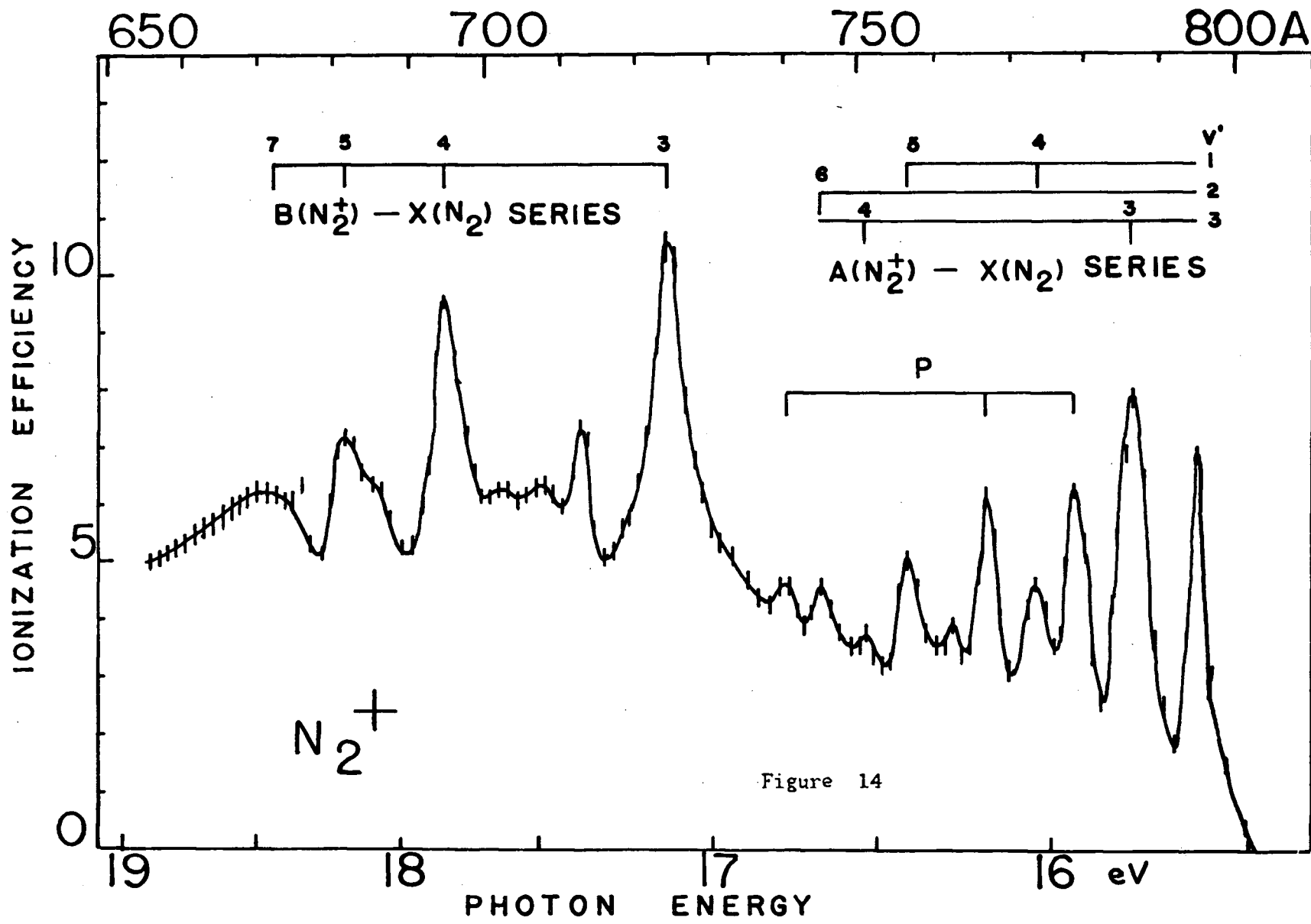
Earlier workers, however, measured absorption coefficients using a well-resolved line source. In some cases, the source emission line used by these authors did not coincide with an actual nitrogen absorption maximum or minimum so that the coefficients listed for comparison are those at the two nearest maxima or minima. The present data is based on a continuum source, and such difficulties are not expected.

The electron configuration of nitrogen predicted from elementary molecular orbital theory is:-



The molecular orbitals are listed in the order of decreasing binding energy, omitting the inner orbitals.

The photoionization efficiency of nitrogen as a function of the photon energy is shown in Figure 14. The threshold ionization potential of nitrogen measured from the point of initial onset of the curve is at 15.55 ± 0.05 eV. This value refers to the removal of an electron from the outer ($\sigma_g 2p$) orbital, to leave the N_2^+ ion in its $X \quad {}^2 \Sigma_g$ ground state. The



value of 15.55 eV. is in good agreement with the spectroscopic value of 15.576 eV. (48), and the photoionization ionization potential of nitrogen at 15.580 eV. by Watanabe and Marmo (136), and by Ogawa and Tanaka (95). Numerous workers have obtained electron impact value for the first ionization potential of nitrogen. Frost and McDowell (38), Fox and Hickman (30) and Cloutier and Schiff (6) have used a R.P.D. method and obtained values of 15.63 eV., 15.60 eV. and 15.58 eV. respectively for the threshold ionization potential of nitrogen. The various electron impact, spectroscopic and photoionization ionization potentials of nitrogen are summarised in Table VI.

Table VI

Threshold Ionization Potential of Nitrogen

<u>I.P. (e.V.)</u>	<u>WORKERS</u>	<u>METHODS</u>	<u>YEAR</u>
15.55 \pm 0.05	Present result	Photoionization	1966
15.6 \pm 0.1	Weissler (146)	Photoionization	1956
15.580	Watanabe (136)	Photoionization	1956
15.580	Ogawa (95)	Photoionization	1962
15.58	Huffman (55)	Photoionization	1963
15.576	Herzberg (48)	Spectroscopy	1950
15.65	Tate (121)	Electron Impact	1936
15.60	Fox (52)	Electron Impact	1954
15.63 \pm 0.02	Frost (35)	Electron Impact	1955
15.58 \pm 0.02	Cloutier (6)	Electron Impact	1959

The photoionization efficiency curve of nitrogen (Figure 14) exhibits a slight curvature near the threshold energy, and this confirms the fact that there is a small difference in

equilibrium interatomic distance between the ground states of the nitrogen molecule and its ion. The equilibrium interatomic distances of the ground states of the molecule and its ions are 1.094\AA and 1.116\AA respectively (48).

There has been some question in the electron impact data concerning the shape of the ionization efficiency curve of nitrogen in the region of a few volts above the threshold energy. Clarke's data (5) using an electrostatic selector shows a non-linearity in this region of his N_2^+ curve, which was not observed by other investigators using conventional electron impact methods (30). Fox (32) using a R.P.D. method confirmed the nonlinearity in the same region of the N_2^+ curve, and attributed this to an additional ionization process such as autoionization.

The photoionization efficiency curve for nitrogen exhibits a series of sharp peaks above the threshold. Table VII shows a comparison of these peaks with the absorption spectra of Huffman Tanaka and Larrabee (55) and Cook and Metzger (11). The close agreement in peak energies found by the two techniques proves beyond doubt that they arise from the process of autoionization and that the region above the threshold energy is overlaid with autoionized states.

More peaks appear in the absorption spectrum of nitrogen than in the photoionization spectrum in the same region. This may be due to two reasons: firstly, the resolution of the photoionization monochromator is very much less than that in the absorption spectroscopy, so that a separation of less than 4\AA between two peaks cannot be resolved in the photoionization spectrum but are easily resolved in the absorption spectrum; and secondly, the autoionization process is governed by certain selection rules

Table VII
Comparison of Peaks in the Photoionization Curve
and Absorption Spectrum of Nitrogen

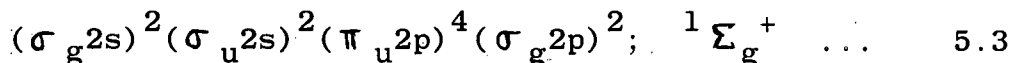
Designation	This work	Huffman (56)	Cook (11)
	15.55 (IP.)		
R _x 8.1	15.65	15.65	15.65
R _a 3.3	15.79	15.81	15.80
P 0.0	15.97	15.98	15.98
R _a 4.1	16.06	16.06	16.06
P 1.0	16.18	16.19	16.19
R _a 5.1	16.38	16.39	16.39
R _a 4.3	16.53	16.52	16.52
R _a 6.2	16.75	16.76	16.76
P 3.0	16.65	16.65	16.65
R _b 3.0	17.14	17.14	17.13
-	17.41	-	-
R _b 4.0	17.84	17.84	17.84
R _b 5.0	18.18	18.18	18.18
R _b 7.0	18.46	18.46	18.46

which determined the reciprocal interaction between the excited states of molecule and the ionization continuum. Not all excitation of electrons to the excited states of the molecule results in ionization, and this explains why peaks observed in the absorption spectrum are absent in the photoionization spectrum.

C. Carbon Monoxide

The absorption spectrum of carbon monoxide in the vacuum ultraviolet has been studied by many workers. The most recent work on photoionization is by Huffman, Tanaka and Larrabee (56), Watanabe, Zelikoff and Inn (132), Sun and Weissler (145), Tanaka, Jursa and LeBlanc (120) and Watanabe, Nakayama and Mottl (140). Fox and Hickam (30) and Hagstrum (44) have studied carbon monoxide by the electron impact method.

The carbon monoxide molecule has 14 electrons, and the ground state has the following electron configuration:



where the molecular orbitals are arranged in the order of decreasing binding energy, omitting the inner orbitals.

The photoionization efficiency curve for carbon monoxide is shown in Figures 15 and 16. The threshold ionization potential measured from the point of initial onset of the curve is 13.98 ± 0.05 eV. which refers to the removal of an $(\sigma_g 2p)$ electron to give an ion in the $X \ 2 \Sigma^+$ ground state. The value of 13.98 eV. is in close agreement with the spectroscopic value of 14.01 eV. by Watanabe (140) and the electron impact value of 13.98 eV. by Fox and Hickam (30) and 14.1 eV. by Hagstrum (44).

The efficiency curve of carbon monoxide rises sharply after the threshold onset as predicted from the Franck-Condon principle since the equilibrium interatomic distance of the normal molecule is almost the same as the CO^+ ion in the $X \ 2 \Sigma^+$ state.

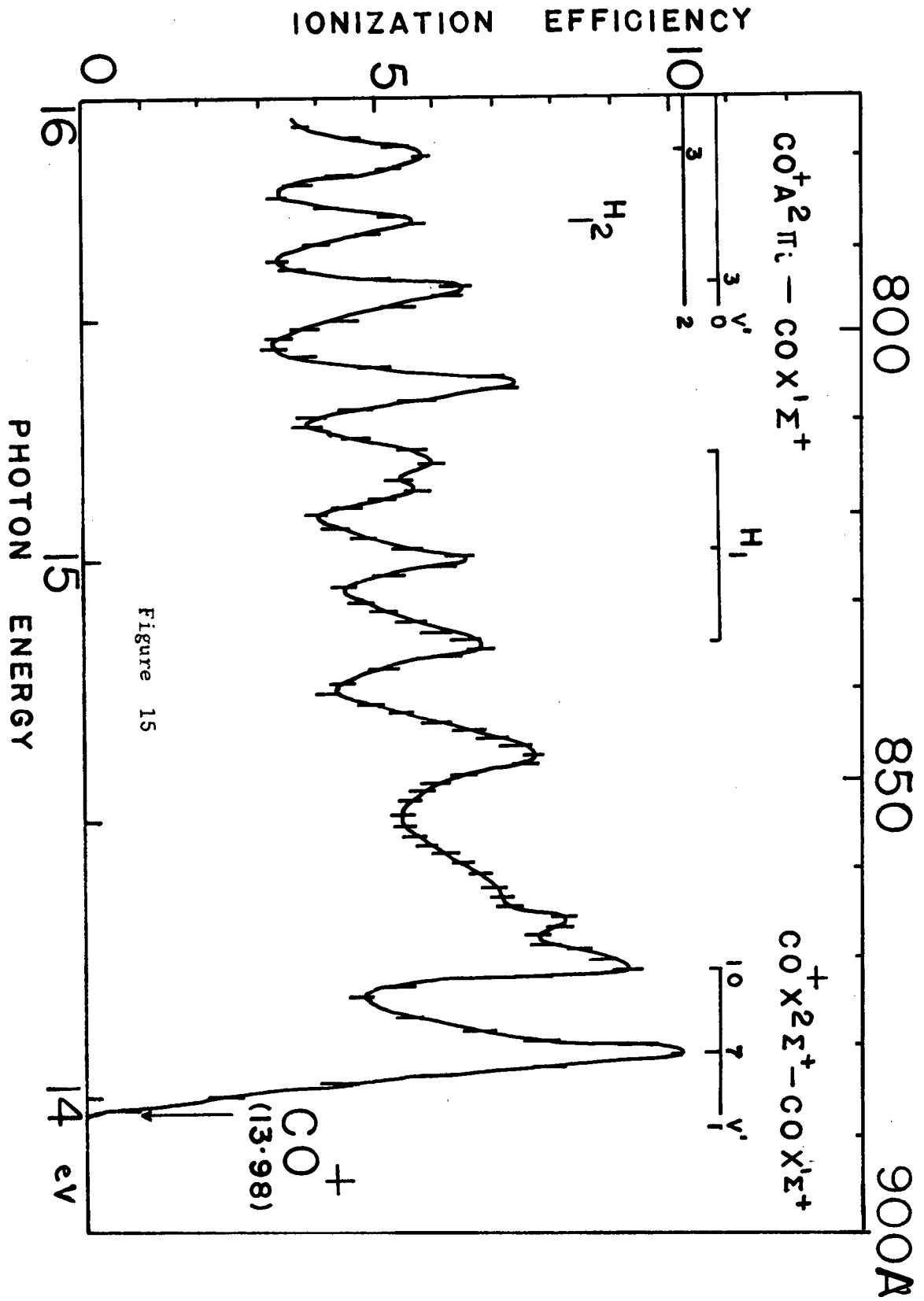
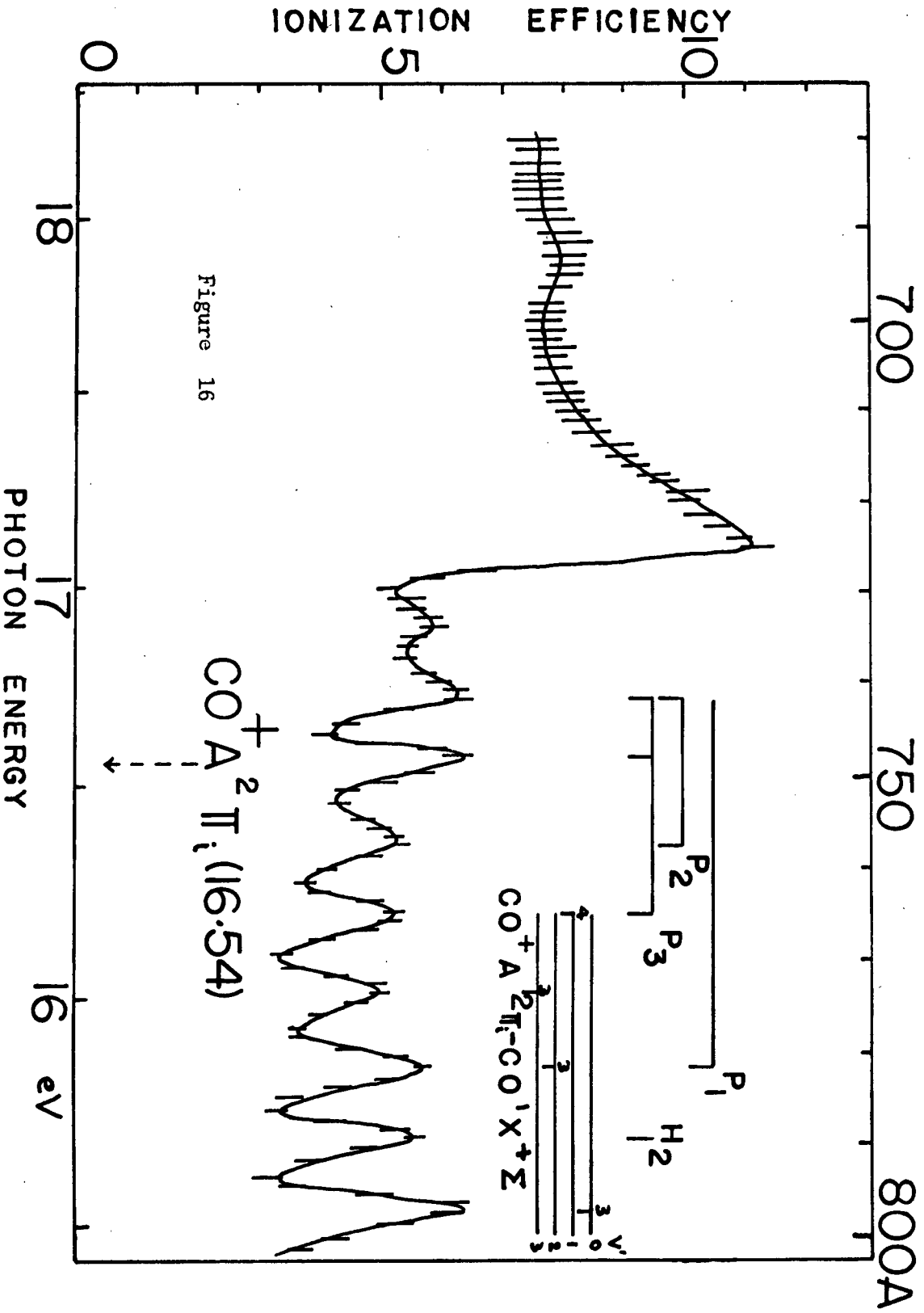


Figure 15



Fox (32) observed a deviation from linearity in his electron impact data points in the vicinity of the $X^2\Sigma^+$ threshold, and Wallace (130) has measured the carbon monoxide autoionization bands in his absorption spectra. The photoionization efficiency curve of carbon monoxide also exhibits many peaks above the threshold ionization potential. Table VIII shows a comparison of the position of peaks in the photoionization spectrum and the absorption spectra of Huffman (56) and Cook (14).

Table VIII
Comparison of Peaks in Photoionization Curves
and Absorption Spectrum of Carbon Monoxide

Designation	This work	Huffman (56)	Cook (14)
	13.98 (IP.)		
R _x 7.1	14.01	14.01	14.01
R _x 10.1	14.17	14.17	14.17
-	14.26	14.25	14.26
-	14.31	14.31	14.31
-	14.57	14.56	14.56
H ₁	14.77	14.78	14.78
H ₁	14.98	14.98	14.98
-	15.08	15.09	15.08
H ₁	15.16	15.16	15.16
R _a 3.0	15.29	15.29	15.29
H ₂	15.54	15.55	15.54
R _a 3.2, P ₁	15.66	15.66	15.66
R _a 3.3,	15.84	15.84	15.84
R _a 4.1, P ₃	15.99	15.99	15.99

Table VIII (continued)

Designation	This work	Huffman (56)	Cook (14)
P ₂	16.33	16.33	16.33
P ₃	16.54	16.54	16.54
P ₂ , P ₃	16.71	16.71	16.72
-	16.87	16.88	16.88
B	17.04	17.07	17.04
P ₄	17.96	17.96	17.96

A comparison of the photoionization efficiency curve and the absorption spectra shows that the peaks in the photoionization spectrum agree well with the corresponding peaks in the absorption spectra. Close agreement between the two shows that the peaks (fig. 15 and 16) in our photoionization efficiency curve are from autoionizing levels.

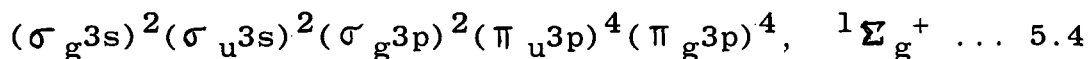
The second ionization potential of carbon monoxide refers to the removal of electron to form CO⁺ in the excited A ²Π_i state, and the spectroscopic value for this limit is 16.536 eV. (119) as shown in Figure 16 by broken arrow. This ionization potential was not observed for the following reason. The equilibrium interatomic distances as given by Herzberg (48) are: 1.1281Å, X ¹Σ_g⁺ of CO; 1.1150Å, X ²Σ⁺, and 1.2436Å, A ²Π_i of CO⁺. The large difference in equilibrium interatomic distance for the CO(X ¹Σ_g⁺) and CO⁺(A ²Π_i) states results in the probability for this transition being distributed fairly equally over several vibrational levels, and the 0-0 transition between the X ¹Σ_g⁺ of the molecule and the A ²Π_i state

of the ion is small. This means that there are probably several steps in the continuum threshold for this state, and apparently the competition of the autoionization process in the same region is so intense that the steps are obscured at the resolution of the experiment.

D. Chlorine

The only spectroscopic ionization potential of the chlorine molecule has been reported by Gaydon (42). Watanabe (138), using the photoionization method has obtained the threshold ionization potential, and Morrison and Nicholson (90) and Thorburn (126) have measured the electron impact ionization potentials. Frost and McDowell (39) using the R.P.D. electron impact method have been able to measure first and inner ionization potentials of the molecule.

According to Mulliken (86), the electronic structure of chlorine may be represented by the formula:



The inner electrons are omitted and the orbitals are listed in order of decreasing binding energy.

The photoionization efficiency curve for the chlorine molecule is shown in Figure 17. The threshold ionization potential (obtained from the point of initial onset of the curve) at 11.47 ± 0.05 eV. refers to the removal of an electron from the anti-bonding ($\pi_g 3p$) orbital. This value is higher than the spectroscopic value at 11.32 eV. found by Gaydon (42), but it is in excellent agreement with the value at 11.48 eV. found by Watanabe (138). The electron impact method gives the threshold ionization potential of the chlorine molecule at 11.8 eV. (Morrison and Nicholson (90)), 11.8 eV. (Thorburn (126)) and 11.63 eV. (Frost and McDowell (39)). It is noted that the electron impact figures are considerably higher than the value found in this work, and this is probably due to the difference in the ionization cross-section at the threshold, and in the degree of sensitivity in the ion current measurement.

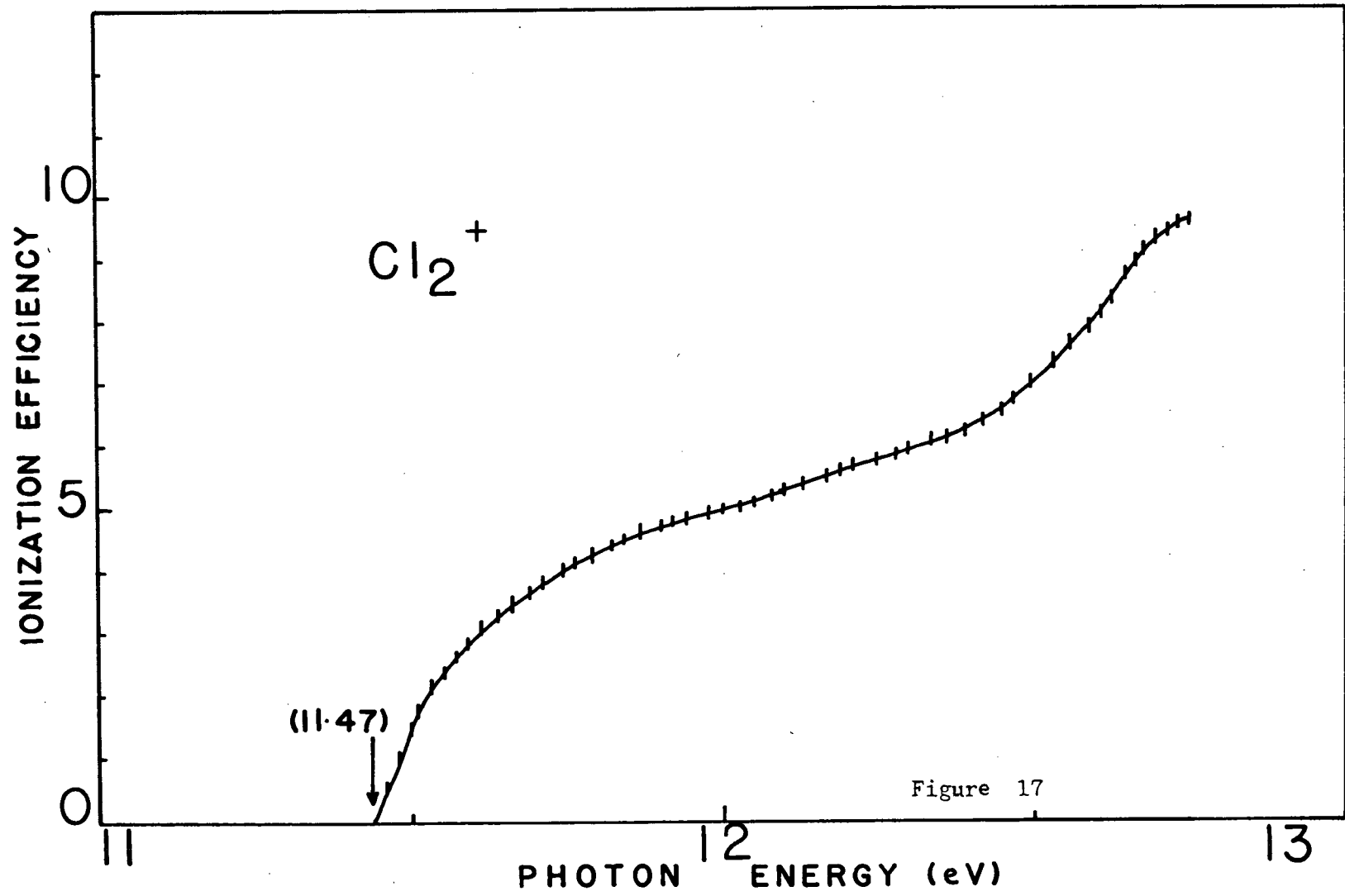


Figure 17

The ionization efficiency shows a slight curvature near the threshold, and this indicates a change of equilibrium internuclear distance between the molecule (normal) and Cl_2^+ ion ($^2\pi_g$), and confirms that the primary ionization involves the removal of an antibonding electron.

The outer ($\pi_g 3p$) and ($\pi_u 3p$) orbitals are mainly atomic in character, and the ions formed by the removal of electrons from these orbitals will be in $^2\pi_g$ and $^2\pi_u$ states, and each of these $^2\pi$ states would be a doublet. Frost and McDowell (39) indicated that there appear to be several ionic energy levels within about 0.6 eV. of the ionization threshold, but we have not been able to resolve these ionic energy levels. Since the curve for Cl_2^+ above the threshold energy appears abnormal in shape, this suggests the overlapping of several ionization processes.

E. Hydrogen Chloride

Hydrogen chloride has been studied extensively by infrared and Raman spectroscopy, but data in the far ultraviolet region are scarce. The photoionization efficiency curve of hydrogen chloride is shown in Figure 18. From the curve the threshold of ionization is 12.56 ± 0.05 eV., which refers to the removal of a non-bonding electron localized in the halogen atom as discussed by Mulliken (88) and Price (100) leading to a $X \ 2\pi_{3/2}$ ground state for the molecular ion. This value is in good agreement with the value of 12.56 eV. found by Fox (31) using the R.P.D. method, and 12.53 eV. by Morrison (81) using the electron impact method. However, it is lower than the value at 12.74 eV. by Watanabe (138) using the photoelectric measurement, and at 12.90 eV. by Price (100) using spectroscopic means.

The curve for hydrogen chloride rises sharply after the threshold energy, agreeing with the fact that the single photoionization process is indeed a step function. There is a further sharp increase of photoionization efficiency around 14 eV. and the steepest ascent of the curve is selected as the onset of the ionization to the $A \ 2\Sigma^+$ excited state of the hydrogen chloride ion at 14.04 eV. and it is 1.48 eV. above the ionic ground state. This value agrees with the values at 1.6 eV. by Fox (31) and 1.5 eV. by Morrison (81), and is consistent with the values of 1.14 eV. and 2.83 eV. for the similar states in HF^+ and HI^+ respectively by Frost and McDowell (37), if one assumes that the energy separation of the $X \ 2\pi_{3/2} - A \ 2\Sigma^+$ states should increase progressively. However, it is not in agreement with the spectroscopic value

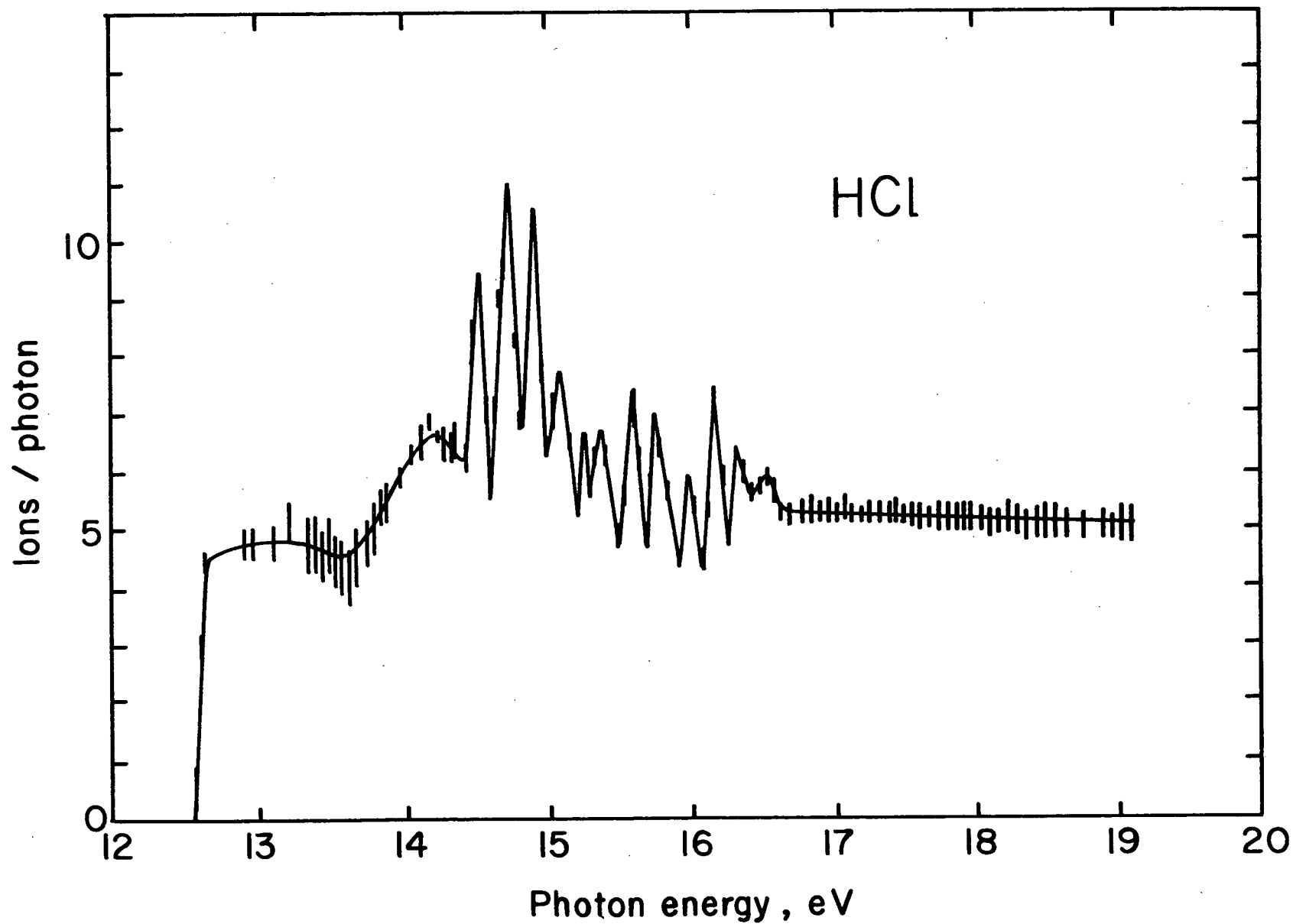


Figure 18

of 3.48 eV. obtained by Norling (94).

The $A^2\Sigma^+$ state for the hydrogen halide results from the removal of an electron from a $2p\sigma$ type bonding orbital, and thus one might expect the binding energy of the electron to vary as the dissociation energy of the H - X bond. Since the dissociation energy decreases progressively for these molecules (5.83 eV. for HF, 4.43 eV. for HCl, 3.75 eV. for HBr and 3.06 eV. for HI), one might expect the value of the $X^2\Pi_{3/2} - A^2\Sigma^+$ energy separation to vary in a progressive manner. If this is so, the 1.48 eV. value for the energy separation of these two states is consistent whereas the 3.48 eV. value by Norling is not.

The photoionization efficiency curve exhibits many peaks of nearly equal energy separation after the second ionization potential leading to the $A^2\Sigma^+$ state of the HCl^+ ion. These peaks can be explained as the autoionized peaks which are caused by the excitation of an electron to an excited state of the molecule which has an energy greater than the second ionization potential, and followed rapidly by a radiationless transition to the ionization continuum with the formation of an ion. The photon energy at the top of each peak is given in Table IX. The energy separation between two adjacent peaks (Δv) differs by the order of 100 cm^{-1} which corresponds to only 0.008 eV. The average energy separation between the peaks is 1450 cm^{-1} which gives the vibrational frequency for the excited state of the hydrogen chloride molecule. Since the internuclear distance for HCl (normal) is nearly equal to that for $HCl^+(2\Sigma)$, the vibrational frequency for HCl (excited) should be the same order of magnitude as that for $HCl^+(2\Sigma)$.

Table IX
Autoionized Peaks of Hydrogen Chloride

Transitions	E (eV.)	ν (cm^{-1})	$\Delta \nu$ (cm^{-1})	
0-0	14.55	117371		
0-1	14.74	118906	1535	
0-2	14.92	120337	1431	
0-3	15.10	121803	1466	
0-4	15.26	123076	1273	
0-5	15.40	124224	1148	
0-6	15.60	125825	1601	Average:
0-7	15.78	127307	1472	1450 cm^{-1}
0-8	16.00	129067	1760	
0-9	16.18	130503	1436	
0-10	16.34	131792	1189	
0-11	16.54	133422	1630	

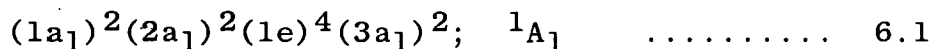
The vibrational frequency for the $A^2\Sigma^+$ state of HCl^+ ion is given by Herzberg (47) as 1526.5 cm^{-1} . Therefore it is reasonable to interpret the autoionized peaks as being due to the vibrational structure of the excited state of the hydrogen chloride molecule.

CHAPTER SIX

Photoionization of Polyatomic Molecules.

A. Ammonia

The ammonia molecule is known (47) to have pyramidal symmetry C_{3v} , and its molecular orbital formula is:-



The molecular orbitals are listed in the order of increasing energy. The electronic structure of the ground state of the ammonia molecule can be compared with that of the nitrogen atom, which has a configuration of $1s^2, 2s^2, 2p^3$. When a nitrogen atom and three hydrogen atoms combine to form an ammonia molecule, the two $1s$ electrons of the nitrogen atom occupy the $(1a_1)$ orbital, the innermost orbital of the ammonia molecule. The two $(2a_1)$ orbital electrons are bonding electrons to a certain extent, and the electrons occupying this orbital are the $2s$ electrons of the nitrogen atom. One of the $2p$ electrons of the nitrogen atom, and the three electrons of the hydrogen atom form the four $(1e)$ orbitals in ammonia. These are strongly bonding orbitals. The two remaining $2p$ electrons of the nitrogen atom form the non-bonding orbital of $(3a_1)$, which is an orbital consisting a pair of unshared electrons and is localized largely on the nitrogen atom of ammonia.

The photoionization efficiency curve for the ammonia molecule is shown in Figure 19. The photon energy at the point of initial onset of ionization at 10.12 ± 0.05 eV. obviously refers to the energy required to remove an electron from the non-bonding $(3a_1)$ orbital to form an NH_3^+ ion in its 2A_1 ground state, assuming the C_{3v} symmetry is retained in the ion.

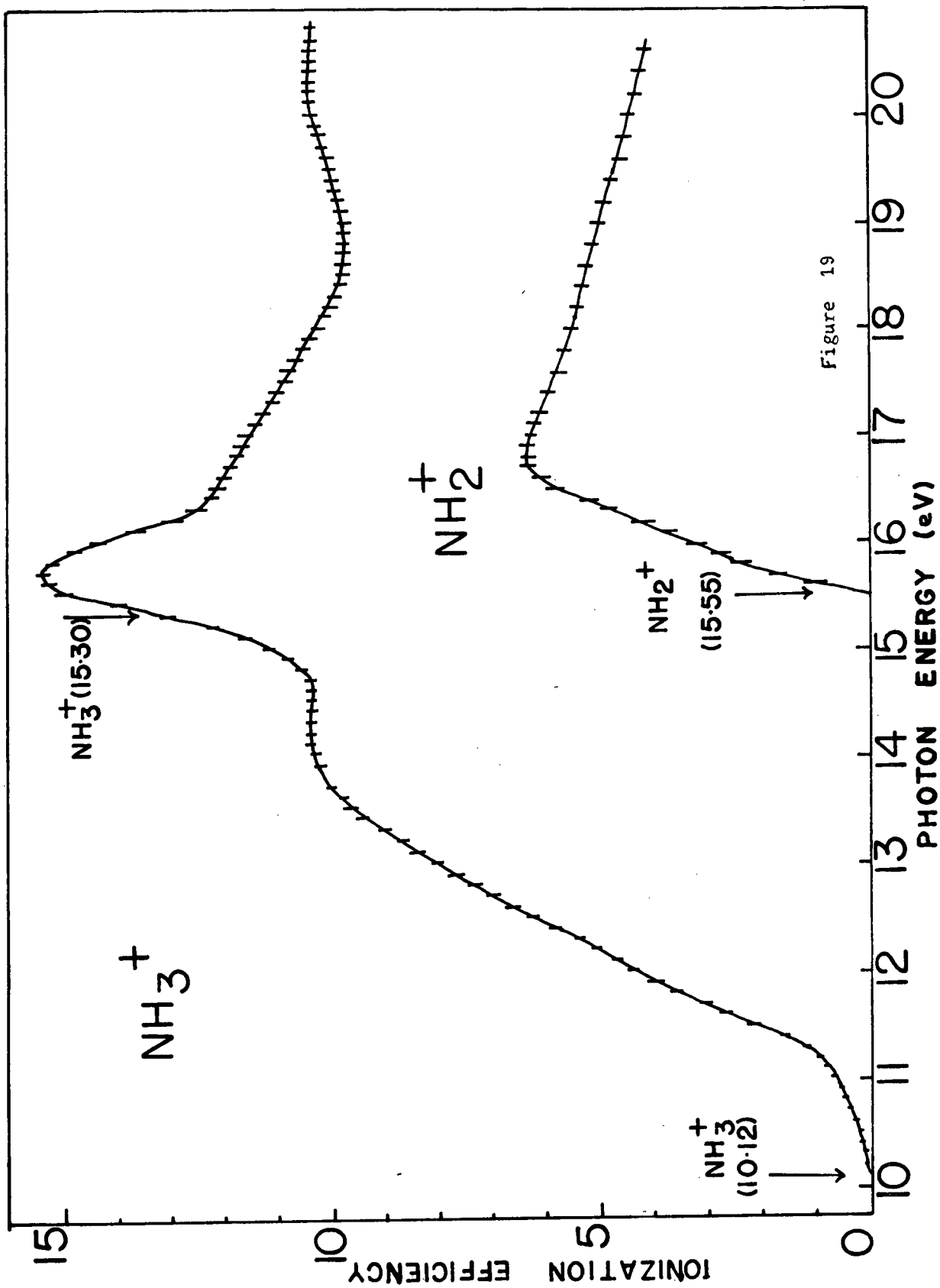


Figure 19

The threshold ionization potential of ammonia at 10.12 eV. is in good agreement with the results obtained by other workers using different methods. Inn (60) in 1953 and Watanabe (137) in 1959, measured the absorption and photoionization coefficients of ammonia using far ultraviolet radiation, and determined the threshold ionization potential of ammonia as 10.13 eV. and 10.15 eV. respectively. Walker and Weissler (144) in 1959 measured the photoionization efficiency and cross section of ammonia and found the first ionization potential to be 10.07 eV. All these workers used photoionization instruments of different design, and used different methods for the interpretation of the photoionization data.

The values for the first ionization potential of ammonia obtained by the electron impact method are in all cases slightly higher than those obtained by photoionization. Mann, Hustrulid and Tate (76) in 1940 using the electron impact method, found the first ionization potential of ammonia to be 10.5 eV. Later, Frost and McDowell (37) in 1958, and Morrison and Nicholson (82) in 1952, using a modified and much more sensitive mass spectrometer, found the first ionization potential of ammonia to be 10.40 eV. and 10.42 eV. respectively. The fact that the electron impact method tends to measure the vertical process and not necessarily the minimum energy required for ionization, accounts for the ionization potentials obtained by these methods being generally larger (by 0.02 to 0.5 eV.) than the adiabatic values.

A theoretical calculation on the orbital energies of ammonia was undertaken by Duncan (22) in 1957, and he found the first ionization potential of ammonia to be 9.94 eV., which is

considerably lower than all the reported experimental values.

Table X summarises the reported values of the threshold ionization potentials of ammonia:-

Table X
Threshold Ionization Potential of Ammonia

<u>I.P. (eV.)</u>	<u>Workers</u>	<u>Methods</u>	<u>Year</u>
10.12 \pm 0.05	Present work	Photoionization	1965
10.13 \pm 0.02	Inn (60)	Photoionization	1953
10.07 \pm 0.05	Weissler (144)	Photoionization	1955
10.15 \pm 0.02	Watanabe (139)	Photoionization	1959
10.15 \pm 0.02	Cook (12)	Photoionization	1964
10.5 \pm 0.1	Tate (76)	Electron Impact	1940
10.42 \pm 0.05	Morrison (82)	Electron Impact	1952
10.40 \pm 0.02	Frost (37)	Electron Impact	1958
9.94	Duncan (22)	Theoretical	1957

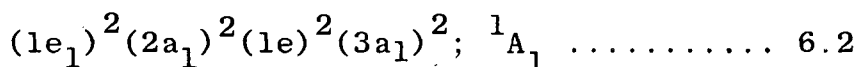
The photoionization efficiency curve of ammonia (Figure 19) shows curvature near the threshold, and this confirms the finding of Watanabe (139) that the 0-0 transition of ammonia from the ground state of the molecule to the ground state of the ion is rather non-vertical. The ionization efficiency rises steadily with increasing photon energy up to about 14 eV. after the threshold ionization potential. Between 14 and 15 eV., the ionization efficiency remains fairly constant. At the latter energy, an inner or second ionization potential is indicated, since the curve begins to rise again. The photon energy at the point of steepest ascent is 15.30 eV. corresponds to the second vertical ionization potential. This second ionization potential is identified as being due to the formation of the first excited

state of the NH_3^+ ion, i.e. the ${}^2\text{E}$ state, formed by the removal of an electron from the (1e) degenerate orbital of the ammonia molecule. This (1e) orbital of ammonia is the main bonding orbital which spans the three N-H bonds, and the removal of an electron from here may cause the dissociation of the molecule with the formation of the NH_2^+ ion. A maximum ionization efficiency was observed at 15.70 eV. on the curve.

Walker and Weissler (144) have found evidence of a second ionization potential of ammonia : a little over 15 eV. Duncan (22) calculated the second ionization potential of ammonia to be at 16.20 eV., and Frost and McDowell (37) used the electron impact method finding the second ionization potential to be 15.31 eV.

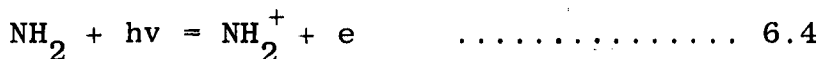
The Dissociation of Ammonia

The photoionization efficiency curve for the NH_2^+ ion is shown in Figure 19. The appearance potential of NH_2^+ is 15.55 ± 0.05 eV. This value is slightly lower than that obtained by Wilkinson and Johnson (148) at 15.8 eV. in 1950. The NH_2^+ ion can be formed from the ${}^2\text{A}_1$ state of the NH_3^+ ion. If the NH_2^+ ion is assumed to have the symmetry C_{2v} , the electronic configuration of the ion is probably:-



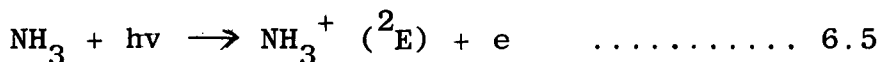
The combination of $\text{NH}_2^+ ({}^1\text{A}_1) + \text{H} (2s)$ correlates with $\text{NH}_3^+ ({}^2\text{A}_1)$, and thus the formation of NH_2^+ from the ${}^2\text{A}_1$ state of NH_3^+ is allowed by group theory.

Recent studies of the photochemical decomposition of ammonia (21) give a mechanism for the NH_2^+ ion formation which requires a primary dissociation and ionization process:



In the initiation step, the ammonia molecule is dissociated into a radical NH_2 and a hydrogen atom. In the second step, the NH_2 radical is ionized to give an NH_2^+ ion. The NH_2^+ ion will be predominant, since the ionization potential of NH_2 is much less than that of the hydrogen atom.

An alternative and equally probable mechanism is:-



All these mechanisms will be operative in the formation of NH_2^+ ions at the expense of the ammonia parent ions. They help to explain the decline of the photoionization efficiency for the ammonia parent ions at about 15.70 eV., if the peak is not caused by autoionization.

The energy required to remove the first hydrogen atom, i.e. $D(\text{NH}_2\text{-H})$, is known (117) to be 104 Kcal. (4.52 eV.). The appearance potential of the NH_2^+ ion, or $V(\text{NH}_2^+)$, has been obtained from Figure 19 as 15.55 eV. Hence, using the following equation:-

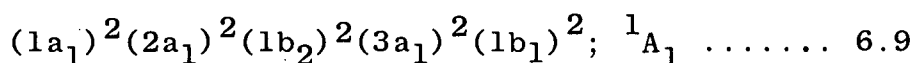
$$V(\text{NH}_2^+) = D(\text{NH}_2\text{-H}) + I(\text{NH}_2) + \text{K.E.} + \text{E.E.} \dots\dots\dots 6.7$$

(where K.E. and E.E. are the kinetic and excitation energies of the NH_2^+ ion), and since the NH_2^+ ion is known to have little excess kinetic and excitation energy (72), the ionization potential of NH_2 is equal to or less than 11.03 eV.

B. Water

Water vapor has been extensively studied by absorption spectroscopy below the threshold ionization potential. However above this energy data is scarce. Photoionization of water vapor is important in upper atmospheric studies, because the extreme ultraviolet light from the sun can ionize the molecule.

According to Mulliken (87), the electronic ground state of water has 1A_1 symmetry and is derived from the electronic configuration:-



Recent self-consistent molecular orbital calculations by Ellison and Shull (24) have shown that this is the correct order of the orbitals and that the $(1b_1)$ is a pure $2p_x$ orbital of oxygen, the main bonding orbitals being $(3a_1)$ and $(1b_2)$.

The photoionization efficiency curve of water is shown in Figure 20. The initial onset of the curve at 12.56 ± 0.05 eV. gives the energy for the removal of an electron from the $(1b_1)$ non-bonding orbital. This value is in excellent agreement with the spectroscopic work by Price, Teegen and Walsh (102) who were able to arrange the bands into four Rydberg series with a common limit at 12.56 eV., and is also in good agreement with the value of 12.59 eV. found by Watanabe, Nakayama and Mottl (140), and Cook and Metzger (12) using the photoionization method, and 12.60 eV. by Frost and McDowell (37), and Foner and Hudson (28) using the electron impact technique.

The photoionization efficiency curve of water rises gradually after the threshold energy and reaches a maximum about 16 eV. Within this range, no excited states or autoionization

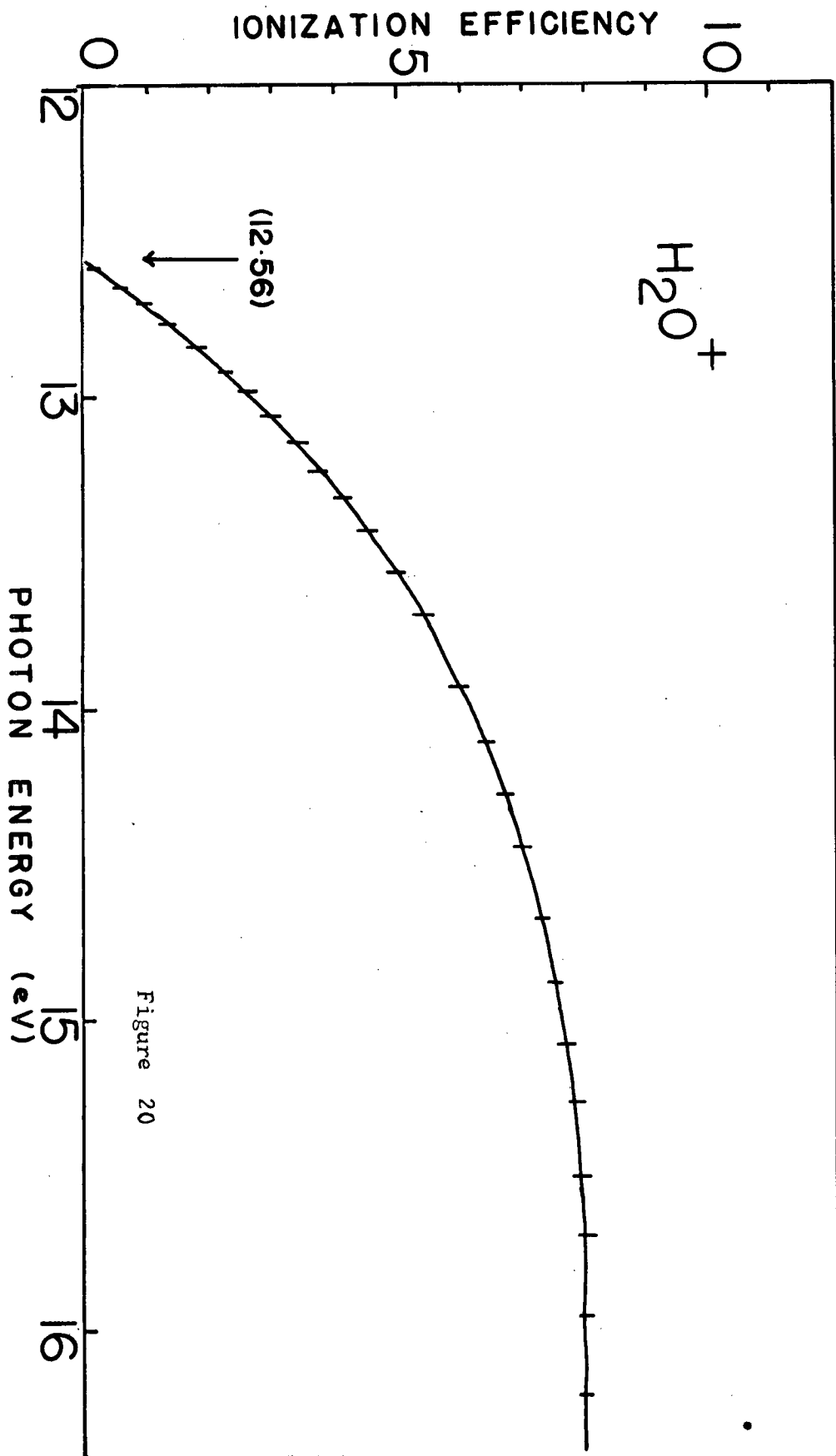


Figure 20

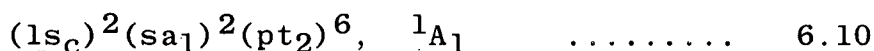
peaks were observed, and this confirms the findings of Cook and Metzger (12). Sugden and Price (116) reported in 1948 the finding of excited states of water ions at 16.2 and 18.0 eV., but Field and Franklin (33) considered these excited states were doubtful probably on the ground that Price's work was done without mass analysis, and the excited states observed might be due to impurities. However, Frost and McDowell (37) reported excited states of the water ion at 14.35 and 16.34 eV. by the electron impact method. The failure to observe the excited states on the photoionization efficiency curves is probably due to the difference in ionization cross sections in the photoionization and electron impact methods.

The excited states of the water ions were probably formed by the removal of electrons from the main bonding orbitals ($1b_2$) and ($3a_1$), and the ions formed will be in 2B_1 , 2A_1 and 2B_2 states. The removal of an electron from the main bonding orbitals may cause the breaking of the O-H bond and dissociation of the water molecule with the formation of H^+ or OH^+ . A survey of the literature found that the appearance potential of OH^+ is at about 18 eV. and that for H^+ is at about 19.6 eV.

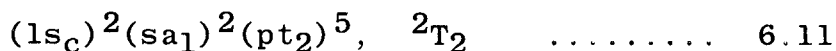
C. Methane and Deutero-methane

Methane, deutero-methane and their fragment ions have been subjected to considerable study by many workers using photoionization and electron impact methods. Several discussions have been reported about possible inconsistencies in the electron impact results, and the accuracy of the derived dissociation energy of the $\text{CH}_3\text{-H}$ bond have been questioned. The appearance of ions in the photoionization efficiency curves of methane and deutero-methane and their fragment ions has been fairly sharp and this permits quite accurate determination of the appearance potentials of the ions and the dissociation energies of the parent molecules.

There are ten electrons in methane, and these can be put into five doubly occupied orbitals. The electronic structure of methane can be represented by:



Mulliken (85) has shown that the triply degenerate (pt_2) orbital has the lowest binding energy, and the ionization potential of methane obtained from the photoionization efficiency curve (Figure 21) at 12.87 eV. can be referred to the removal of an electron from the (pt_2) orbital to leave a CH_4^+ ion with the electronic structure:



This threshold ionization potential of methane at 12.87 eV. agrees with the value at 12.8 eV. found by Weissler (143), at 12.98 eV. by Watanabe (140) and at 12.71 eV. by Dibeler, Krauss, Reese and Hartlee (19) using the photoionization method. The

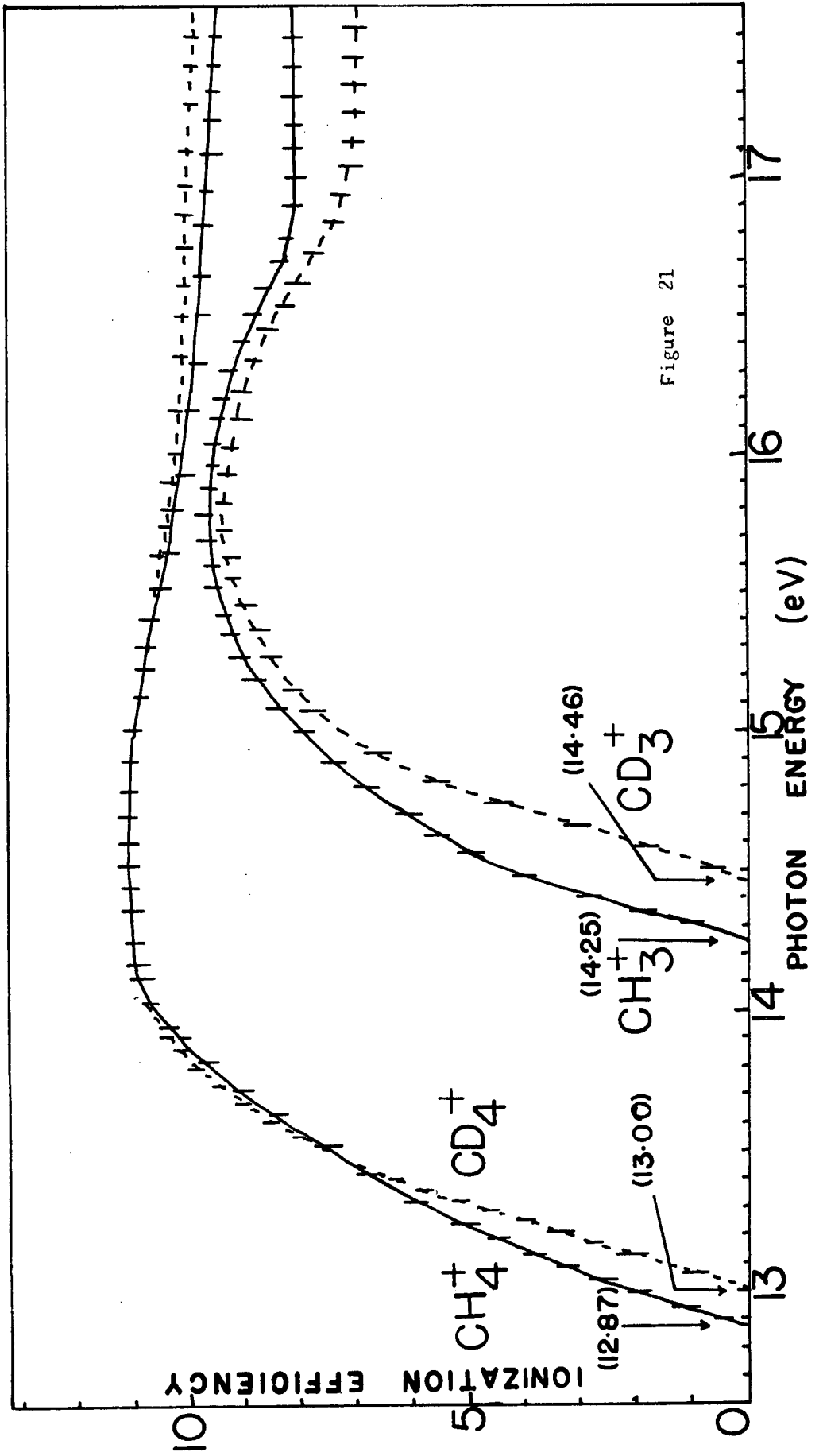


Figure 21

reported values by electron impact methods give a somewhat higher value. Table XI summarizes the ionization and appearance potentials of methane, deuterio-methane and the fragment ions.

Table XI
Ionization Potentials of Methane, Deuterio-methane
and Fragment Ions.

I.P. (eV.)	Workers	Method	Year
<u>CH₄⁺</u>			
12.87 ± 0.05	This work	Photoionization	1966
12.8 ± 0.2	Weissler (143)	Photoionization	1955
12.98 ± 0.05	Watanabe (140)	Photoionization	1962
12.71 ± 0.02	Dibeler (19)	Photoionization	1965
13.2 ± 0.4	Smith (110)	Electron Impact	1937
13.0 ± 0.2	Koffel (64)	Electron Impact	1948
13.04 ± 0.03	Honig (52)	Electron Impact	1948
13.04 ± 0.02	Mitchell (80)	Electron Impact	1949
13.12 ± 0.03	McDowell (71)	Electron Impact	1951
<u>CH₃⁺</u>			
14.25 ± 0.05	This work	Photoionization	1966
14.25 ± 0.05	Dibeler (19)	Photoionization	1965
14.5 ± 0.4	Smith (109)	Electron Impact	1937
14.4 ± 0.3	Koffel (64)	Electron Impact	1948
14.5 ± 0.05	Mitchell (80)	Electron Impact	1949
14.39 ± 0.02	McDowell (71)	Electron Impact	1951
<u>CD₄⁺</u>			
13.00 ± 0.05	This work	Photoionization	1966
12.87 ± 0.02	Dibeler (19)	Photoionization	1965
<u>CD₃⁺</u>			
14.46 ± 0.05	This work	Photoionization	1966
14.38 ± 0.03	Dibeler (19)	Photoionization	1965

The ionization potential of CD₄ at 13.00 ± 0.05 eV.

is a little higher than that obtained by Dibeler et al. (19) at 12.87 eV. However, a study of their curve near the onset showed long tailing extending more than 0.5 eV. The extrapolated values, as they admitted, have no fundamental significance. The values obtained by electron impact are as usual higher: Lossing, Turner and Bryce (69) obtained a value of 13.21 eV., and Honig (52), a value of 13.30 eV. A difference of ionization potentials between CH_4 and CD_4 is also observed, and the difference:

$$I(\text{CD}_4) - I(\text{CH}_4) = 0.13 \text{ eV.} \quad \dots\dots\dots 6.12$$

is also in good agreement with those obtained by Dibeler et al. (19) of 0.16 eV. and by Lossing et al. (69) of 0.18 eV.

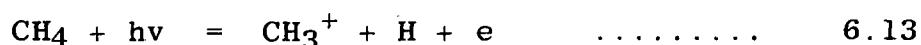
McDowell (72) pointed out that the (pt_2) orbital of the methane molecule will be divided into two orbitals: (πe) of symmetry E and (zb_2) of symmetry B_2 ; and the resultant shift of the potential minimum can lead to a change in the relative populations of the different vibrational levels in the ions of CH_4 and CD_4 as the amount of such vibrational excitation will depend upon the overlap integral between the ground vibrational state and the upper states, which is appreciably greater for CH_4 than for CD_4 . This may provide a possible explanation for the large difference observed in the ionization potentials of CH_4 and CD_4 .

The photoionization efficiency curves of CH_4^+ and CD_4^+ rise after the threshold energy until about 14 eV. where they start levelling off. No autoionization peaks have been observed in the curves for the molecular or fragment ions, and this is consistent with the observed fact that for hydrocarbons, the possible excitations result only in continuous absorption,

and do not give discrete peaks in the photoionization efficiency curves.

The appearance potential of CH_3^+ is obtained from the initial onset of the curve at 14.25 eV. and is in good agreement with that obtained by Dibeler et al. (19) at 14.25 eV., but about 0.2 eV. lower than that obtained by the electron impact method.

The formation of the CH_3^+ ion can be represented by the process:



McDowell (74) indicated that at a photon energy of about 14 eV., the CH_4^+ ion will be formed in a vibrationally excited state, and consequently dissociation to yield the methyl ion and hydrogen atom could take place. The levelling off of the CH_4^+ curve at this energy indicates that the formation of the CH_3^+ ion can indeed arise from the dissociation of CH_4^+ parent ions.

The appearance potential of CD_3^+ measured from the initial onset of the curve at 14.46 eV. is a little higher than that obtained by Dibeler et al. (19) at 14.38 eV. The difference is quite small considering the long tailing at the onset on their curves. The difference between the appearance potentials of CH_3 and CD_3 of 0.21 eV. indicates that there is considerable displacement of the minima of the ground state of the parent ion relative to that of the molecular ground state.

The dissociation energy of $\text{CH}_3\text{-H}$ can be obtained from the following equation:

$$A(\text{CH}_3)^+ = D(\text{CH}_3\text{-H}) + I(\text{CH}_3) + \text{K.E.} + \text{E.E.} \quad \dots\dots\dots 6.14$$

where the appearance potential of CH_3^+ , $A(\text{CH}_3)^+$, has been found to be 14.25 eV., and the spectroscopic ionization potential of

the methyl radical, $I(\text{CH}_3)$, is 9.843 eV. (50). McDowell (72) pointed out that the formation of CH_3^+ ions at this energy does not involve kinetic or excitation energies, and this is in agreement with the finding of Berry (2) from discrimination experiments that the kinetic and excitation energies of CH_3^+ ion are 0.032 eV. in excess of the thermal energy.

Therefore, the dissociation energy of $\text{CH}_3\text{-H}$ can be obtained from equation 6.14 as 4.41 eV. which agrees with the value of 4.41 eV. found by Dibeler et al. (19), 4.42 eV. by Stevenson (113) and 4.42 eV. by Eyring (26).

Similarly, with the appearance potential of CD_3 as 14.46 eV. and the ionization potential of methyl- d_3 as 9.832 eV. (49), the dissociation energy of $\text{CD}_3\text{-D}$ can be obtained as 4.63 eV.

The difference in the appearance potentials between CH_3 and CD_3 can be used to determine the zero-point energy difference for the CH_3^+ and CD_3^+ ions (19).

$$D(\text{CH}_3^+\text{-H}) = E + Z_{\text{CH}_3^+} - Z_{\text{CH}_4^+} \dots\dots\dots 6.15$$

$$D(\text{CD}_3^+\text{-D}) = E + Z_{\text{CD}_3^+} - Z_{\text{CD}_4^+} \dots\dots\dots 6.16$$

where Z_x denotes the zero-point energy of the ion species x.

Also:

$$D(\text{CH}_3^+\text{-H}) = A(\text{CH}_3^+) - I(\text{CH}_4) \dots\dots\dots 6.17$$

$$D(\text{CH}_3^+\text{-D}) = A(\text{CD}_3^+) - I(\text{CD}_4) \dots\dots\dots 6.18$$

Equating 6.15 and 6.17; 6.16 and 6.18, we have

$$E + Z_{\text{CH}_3^+} - Z_{\text{CH}_4^+} = A(\text{CH}_3^+) - I(\text{CH}_4) \dots\dots\dots 6.19$$

$$E + Z_{\text{CD}_3^+} - Z_{\text{CD}_4^+} = A(\text{CD}_3^+) - I(\text{CD}_4) \dots\dots 6.20$$

Subtracting 6.20 from 6.19, we have,

$$\begin{aligned} \text{The zero-point energy difference, } Z_{\text{CH}_3^+} - Z_{\text{CD}_3^+} \\ = (Z_{\text{CH}_4^+} - Z_{\text{CD}_4^+}) - I(\text{CH}_3) + I(\text{CD}_3) + A(\text{CH}_3) - A(\text{CD}_3) \\ = 0.23 \text{ eV.} \end{aligned}$$

where, $(Z_{\text{CH}_4^+} - Z_{\text{CD}_4^+}) = 0.31 \text{ eV. (47).}$

The value at 0.23 eV. is in good agreement with the value at 0.18 eV. found by Dibeler et al (19). For comparison, we note that the zero-point difference for the isotopic ammonias, NH_3 and ND_3 is 0.22 eV. (47).

The mass spectra of methane and deuterio-methane at a photon energy of 16.66 eV. is shown in Figure 22. The relative ionization probabilities of these molecules are:

CD_4	CH_4	CH_3	CD_3
100	96	80	69

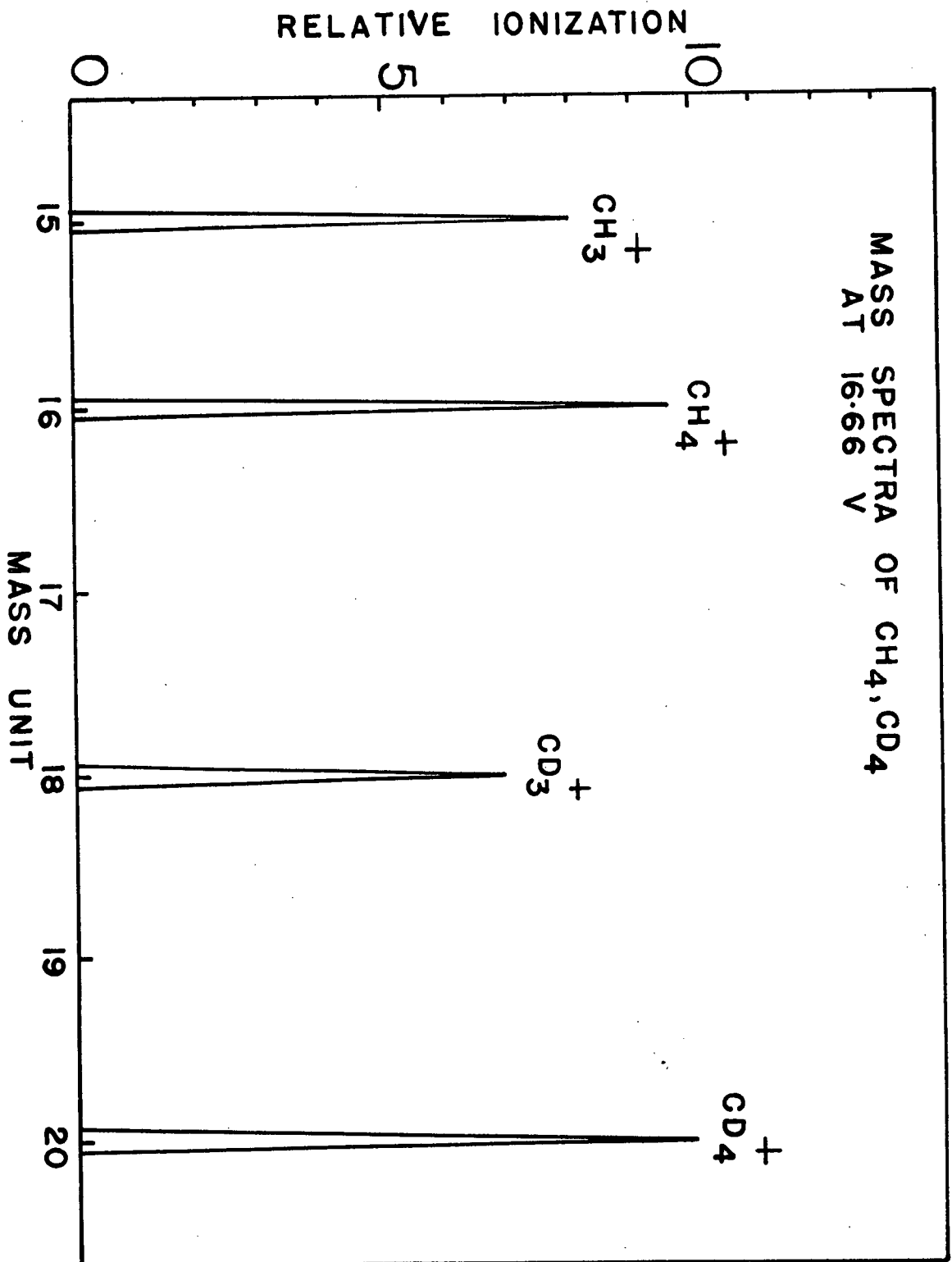


Figure 22

D. Propylene

Because of the great importance to organic chemistry of C=C bonds and the resonance effects which arise from the conjugation of them, the study of propylene has been undertaken by many workers. Price and Tuttle (101) have studied the molecule's absorption spectrum in the far ultraviolet region; Watanabe (139) measured the ionization potential of propylene using the photoelectric method, and Steiner, Giese and Inghram (114) combined mass spectrometer with monochromator and measured the photoionization efficiency between 1050-1300⁰Å. Using the electron impact method, Fox and Hickam (30), Stevenson and Hipple (111), Mitchell and Coleman (80) and Honig (52) have obtained a fairly accurate ionization potential of the molecule.

The photoionization efficiency curves of parent and fragment ions of propylene are shown in Figure 23. It is seen that the curve, unlike those obtained by electron impact, exhibits a sharp onset near the threshold energy. The initial onset of the curve yields the threshold ionization potential of 9.70 ± 0.05 eV. which is in good agreement with the spectroscopic value at 9.70 eV. by Price and Tuttle (101), and the photoionization values at 9.73 eV. by Watanabe (139) and Steiner, Giese and Inghram (114). The ionization potential of the molecule obtained by the electron impact data is a little higher. Table XII summarises the ionization potentials of propylene obtained in this work and by other workers.

At a photon energy below 11 eV. the photoionization efficiency for propylene shows a maximum. Why this should be so is not clear, unless autoionization is responsible for it. The ion intensity begins to rise after 11 eV. indicating an

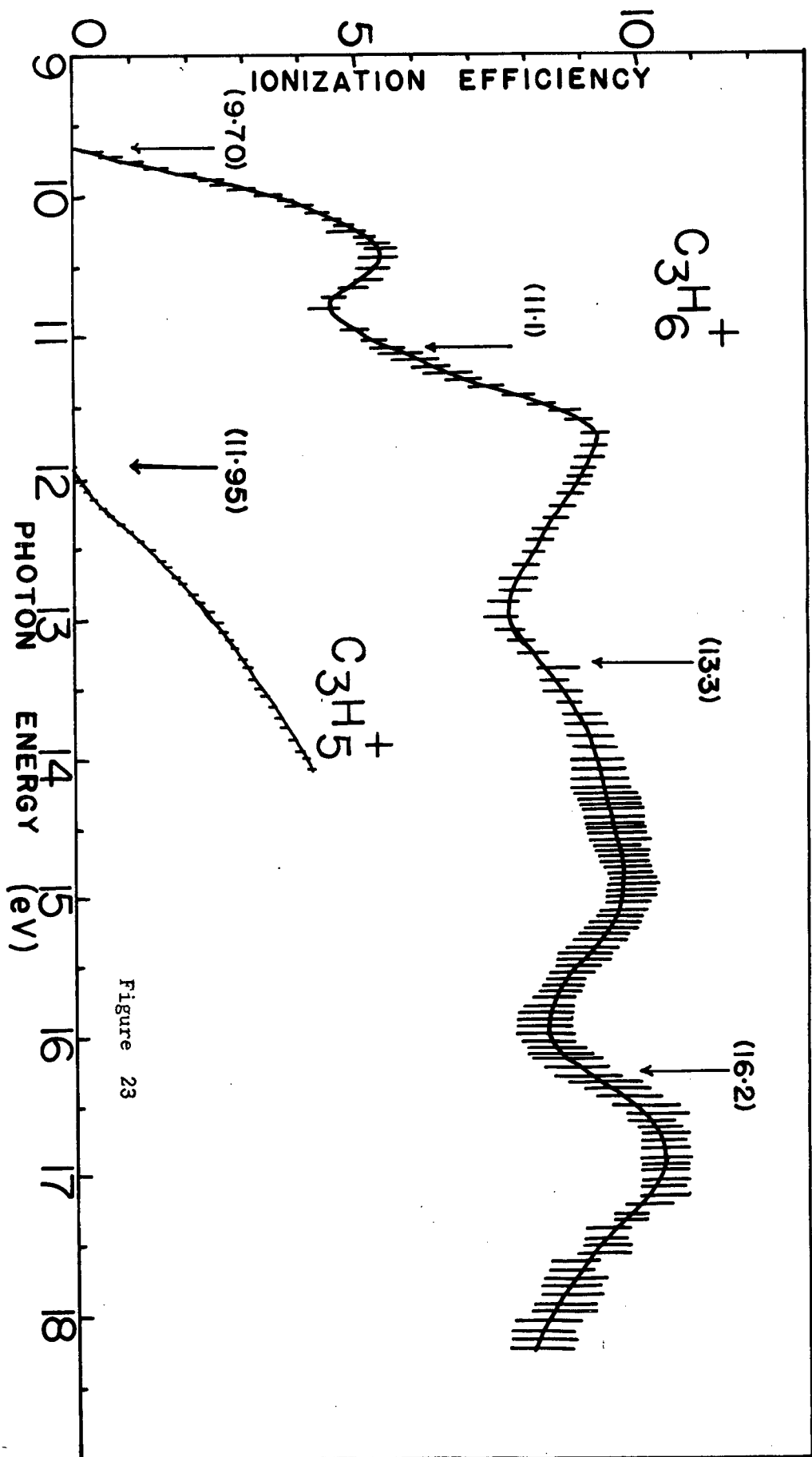


Figure 23

inner ionization potential. The photon energy at the point of the steepest ascent in this region, about 11.1 eV., should correspond to the second vertical ionization potential which refers to the removal of a σ electron. This value at 11.1 eV. is higher than those at 10.54 eV. by Price and Tuttle (101) and 10.54 eV. by Fox and Hickam (30).

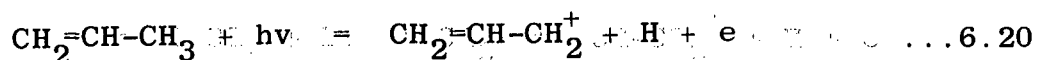
Table XII
Ionization Potentials of Propylene

I.P. (e.V.)	Workers	Method	Year
<u>C₃H₆ (Threshold I.P.)</u>			
9.70	Present result	Photoionization	1966
9.70	Price (101)	Spectroscopic	1940
9.73	Watanabe (139)	Photoionization	1956
9.73	Inghram (114)	Photoionization	1957
9.84	Honig (52)	Electron Impact	1948
10.05	Mitchell (80)	Electron Impact	1949
9.77	Stevenson (111)	Electron Impact	1942
9.78	Fox (30)	Electron Impact	1954
<u>C₃H₆ (second I.P.)</u>			
11.1	Present result	Photoionization	1966
10.54	Price (101)	Spectroscopy	1940
10.54	Fox (30)	Electron Impact	1954
<u>C₃H₅⁺ (appearance potential)</u>			
11.95	Present result	Photoionization	1966
11.96	Stevenson (111)	Electron Impact	1942

The photoionization efficiency curve of propylene shows a decrease at about 11.8 eV., and this may be due to the dissociation of the parent ion with the formation of a C₃H₅⁺ fragment. The appearance potential of the C₃H₅⁺ ion is

obtained from the initial onset of the photoionization efficiency curve (Figure 23) at 11.95 eV., which is in good agreement with the value at 11.96 eV. by Stevenson and Hipple (111). Table XII summarises the ionization potentials of propylene and the appearance potential of $C_3H_5^+$ ion obtained by different workers.

Barring molecular rearrangement, the $C_3H_5^+$ ion formed by the photo-dissociation of propylene should arise from the following mechanism:-



because the (C-H) bonds of the methyl group are generally weaker (more reactive) than the bonds attached to unsaturated carbon atoms.

The bond dissociation energy of propylene, D(allyl-H), can be obtained from the appearance potential of the allyl ion by the following equation:-

$$V(C_3H_5^+) = D(C_3H_5-H) + I(C_3H_5) + K.E. + E.E. \dots 6.21$$

where $V(C_3H_5^+)$ is the appearance potential of the allyl ion (11.95 eV.) and K.E. and E.E.- kinetic and excitation energies of the dissociation products. The ionization potential of the allyl radical, $I(C_3H_5)$, is 8.16 ± 0.03 eV. obtained by Lossing, Ingold and Henderson (68). Since the allyl ion formed is known to have little or no excess kinetic and excitation energies, the bond dissociation energy D(allyl-H) is equal or less than 3.79 eV. in good agreement with the value at 79 ± 6 kcal./mole or 3.43 ± 0.4 eV. obtained by McDowell, Lossing, Henderson and Farmer (75) in a study of the ionization potentials of methyl substituted allyl radicals.

E. Acetylene

A great deal of data has been accumulated on the acetylene molecule. It is known that it is linear and symmetrical, and five frequencies have been identified in the excited and unexcited states. Acetylene has been studied by Dibeler and Reese (18) using the photoionization method, and by Price (98) using a Lyman continuum (who obtained an extensive system of bands from 1520-1050 \AA which yielded a spectroscopic value for the ionization potential and a plausible value for the triple C-C bond). Acetylene has also been studied by Turner (129) using photoelectron spectroscopy, and by Lossing, Tickner and Bryce (69) using the electron impact method.

Acetylene is a linear molecule which has fourteen electrons. The ground state configuration of the molecule can be represented by:

$$[\sigma_g(\text{HC})]^2 [\sigma_g(\text{CH})]^2 [\sigma_g(\text{CC})]^2 [\pi_u(\text{CC})]^4 \dots \quad 6.21$$

The molecular orbitals are listed in the order of decreasing binding energy, omitting the inner electrons.

The photoionization efficiency curve for the acetylene molecule is shown in Figure 24. The curve shows a slight curvature at the initial onset, and this means that the equilibrium internuclear distances are substantially changed in the ions as compared to the neutral molecule, and the electron involved in the ionization process is a bonding or anti-bonding electron. The initial onset of the acetylene curve at 11.40 eV. is selected as the threshold ionization potential which is associated with the energy for the removal of an electron from the (π_u) bonding orbital. The threshold ionization potential is in good agreement

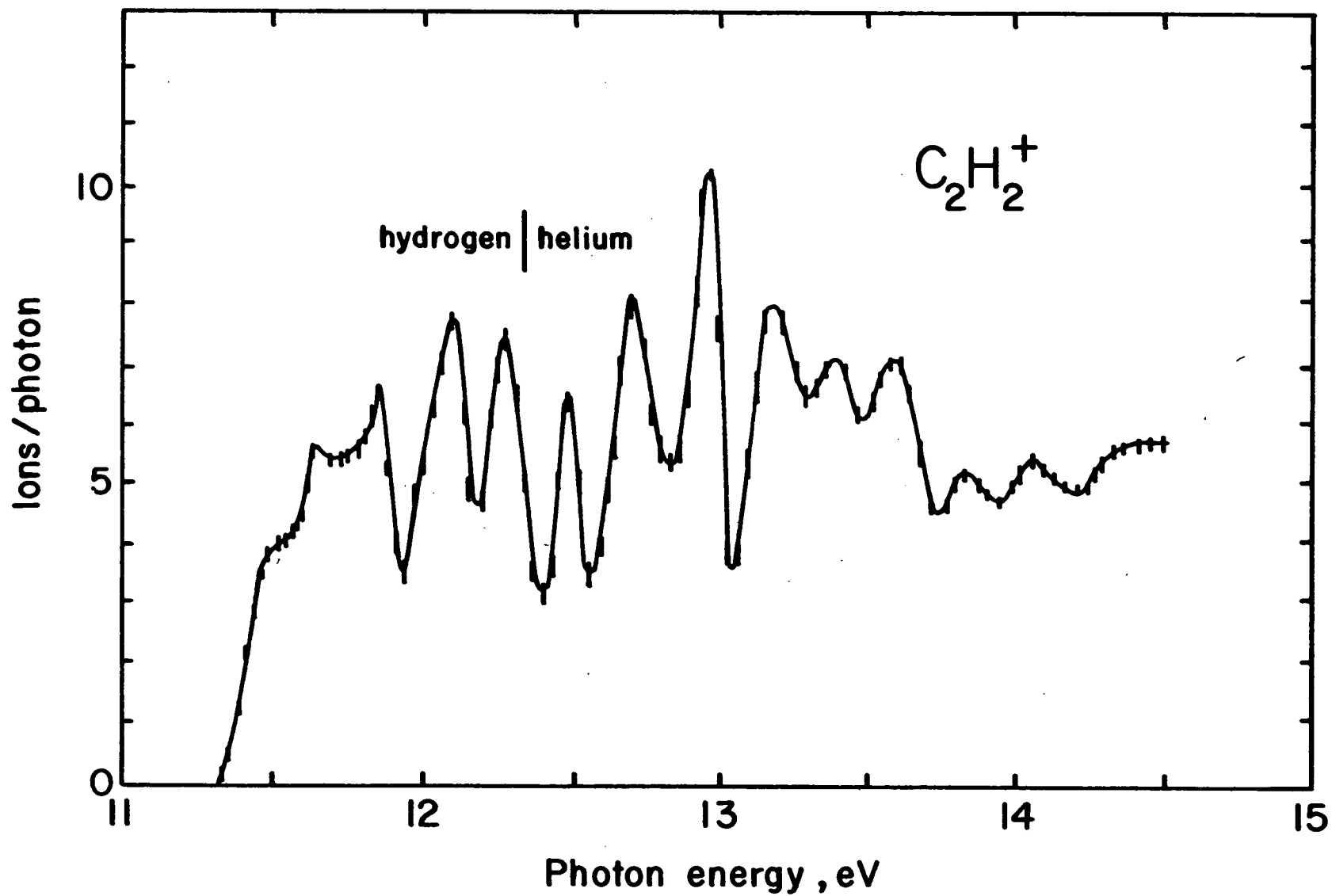


Figure 24

with the value at 11.41 eV. from the spectroscopic determination by Price (98), and the photoionization measurements made by Dibeler and Reese (18). Turner (129) obtained a value of 11.36 eV. using photoelectron spectroscopy, and a value of 11.40 eV. was obtained by Lossing, Tickner and Bryce (69) using the electron impact method.

After the threshold energy, there are many peaks on the photoionization efficiency curve for acetylene as illustrated in Figure 24. The energies corresponding to the tops of each peak on the photoionization efficiency curve are recorded in Table XIII.

Table XIII

Peaks due to Vibrational Structure of Acetylene

Transitions	E (eV.)	ν (cm^{-1})	$\Delta \nu$ (cm^{-1})
0-0	11.40	91952	
0-1	11.63	93808	1856
0-2	11.86	95662	1854
0-3	12.09	97492	1830
0-4	12.28	99050	1858
0-5	12.48	100663	1613
0-6	12.70	102437	1774
0-7	12.96	104535	2098
0-8	13.19	106389	1754
0-9	13.40	108084	1659
0-10	13.58	109634	1550
0-11	13.83	111552	1918
0-12	14.06	113407	1855

Average $\Delta \nu$
= 1780 cm^{-1}

From Table XIII, the energy separation between two

adjacent peaks, (Δv), differs by the order of 100 cm^{-1} which corresponds to only 0.008 eV. It is reasonable to say that each peak is separated from one another by an equal amount of energy, and the average energy separation between two adjacent peaks is 1780 cm^{-1} . The value of 1780 cm^{-1} is very close to the carbon-carbon stretching frequencies of 1849 cm^{-1} for the 3R states of acetylene reported by Wilkinson (149).

The photon energy for the first four peaks as shown in the photoionization efficiency curve for acetylene (Figure 24) are in excellent agreement with the four peaks in the photoionization efficiency curve obtained by Dibeler and Reese (18), who termed them vibrational transitions, 0-0, 0-1, 0-2, and 0-3, of the ($^1\Pi_u$) state. Turner (129) in a study of the photoelectron spectrum of acetylene, also reported vibrational structure for acetylene, but he showed only two peaks at almost the same energy as the first two peaks in the curve reported here.

From the evidence of Wilkinson, Dibeler and Reese, and Turner, the peaks observed from the photoionization efficiency curve for acetylene are most probably due to the vibrational transitions of the ($^1\Pi_u$) state.

Dissociation of Acetylene

The photoionization efficiency curve for the C_2H^+ fragment ion is illustrated in Figure 25. The appearance potential of this ion is obtained from the point of initial onset at $17.76 \pm 0.05 \text{ eV}$. This value agrees well with that at 17.8 eV. by Coats and Anderson (7) and Tate, Smith and Vaughan (121), and at 17.9 eV. by Kusch, Hustrulid and Tate

(65), all using the electron impact method. There were no photoionization and spectroscopic data for comparison.

The bond dissociation energy $D(\text{HC}_2\text{-H})$ can be obtained from the following equation:-

$$D(\text{HC}_2\text{-H}) = V(\text{C}_2\text{H}^+) - I(\text{C}_2\text{H}) - \text{K.E.} - \text{E.E.} \dots 6.22$$

The appearance potential, $V(\text{C}_2\text{H}^+)$, is found to be 17.76 eV., and the ionization potential of the C_2H radical is 11.3 eV. obtained by Elenton (23). If the kinetic and excitation energies are small and can be neglected, the bond dissociation energy $D(\text{HC}_2\text{-H})$ is equal to or less than 6.46 eV. in good agreement with the value of 6.5 eV. found by Coats and Anderson (7).

The photoionization efficiency curve for the C_2H^+ ion remains fairly constant between 18.4 and 18.7 eV. as shown in Figure 25. An inner appearance potential of C_2H^+ ion is indicated as the curve starts to rise after the latter energy. The second appearance potential of the C_2H^+ ion is found from the point of steepest ascent to be 18.96 eV. The photoionization efficiency curve remains constant after about 19.2 eV.

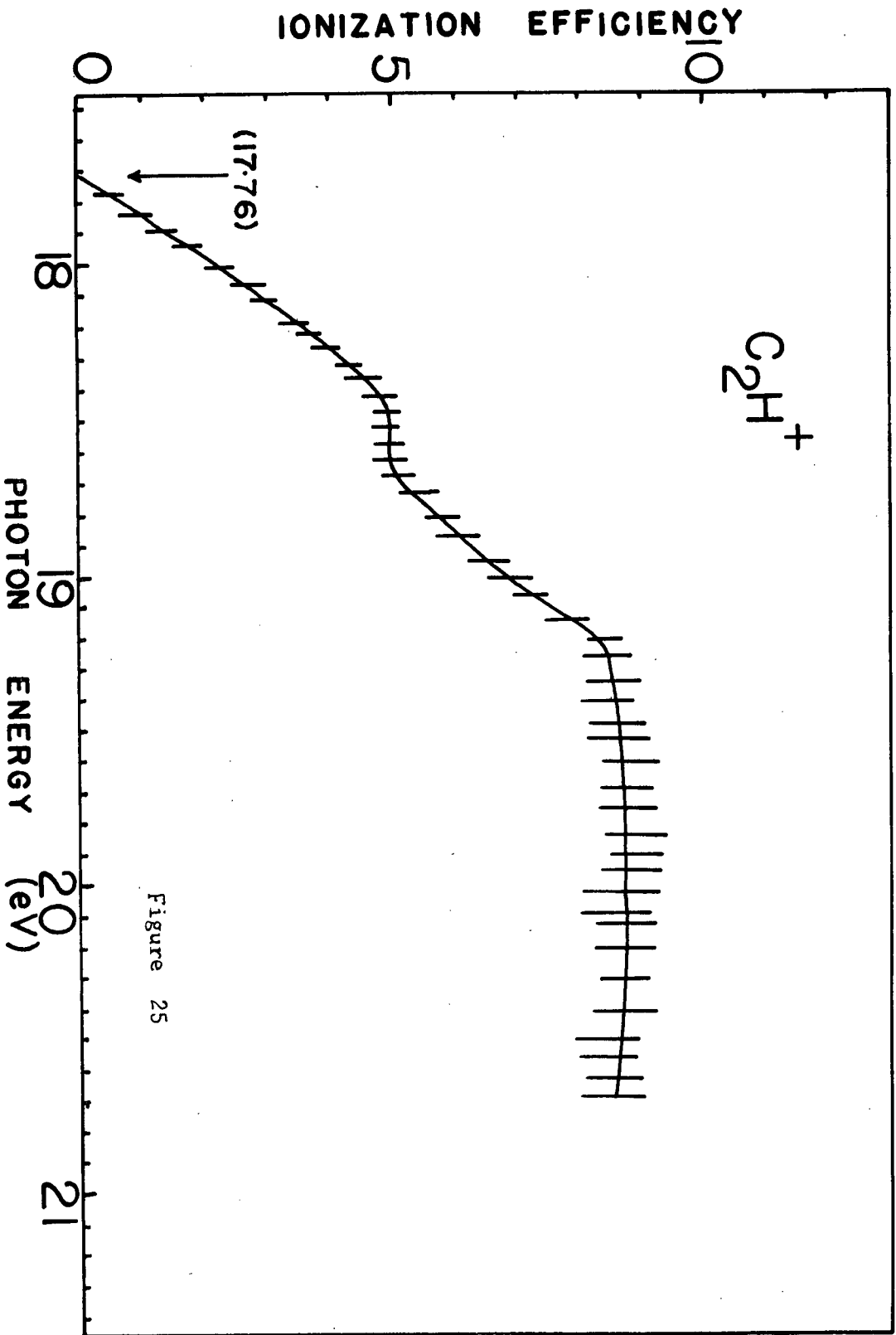


Figure 25

F. Methyl Cyanide

Very little work concerned with the ionization of methyl cyanide has been reported in the literature even though methyl halides and hydrogen cyanide have been studied by many workers. McDowell (74) has described the electronic structure of methyl cyanide as follows:

$$(\sigma_C + \sigma_C, a_1)^2 (\pi_N + \pi_C, e)^4 (\pi e)^4 \dots\dots 6.23$$

with the molecular orbitals listed in the order of decreasing binding energy, omitting the inner orbitals. $(\sigma_C + \sigma_C, a_1)$ is the main bonding C - C orbital, the $(\pi_N + \pi_C, e)$ represents the two mutually perpendicular degenerate bonding orbitals of the CN group, and the (πe) orbitals are largely localised in the CH_3 group.

The photoionization efficiency curve of methyl cyanide is shown in Figure 26. The threshold ionization potential of methyl cyanide measured from the point of initial onset of the curve is 12.33 eV. which is in good agreement with the electron impact data of 12.39 eV. by Morrison (82) and 12.52 eV. by McDowell and Warren (73). After the threshold energy, the photoionization efficiency shows three distinct steps.

The second and third ionization potentials measured at the points of steepest ascent of the curve are 13.01 eV. and 13.80 eV. respectively as indicated in Figure 26 by arrows.

The ionization efficiency curves of methyl cyanide and krypton by electron impact are shown in Fig.27(40). Three distinct breaks are observed on the methyl cyanide curve, and the energies of these breaks correspond to the energies for three processes responsible for the CH_3CN^+ ion formation. These values are

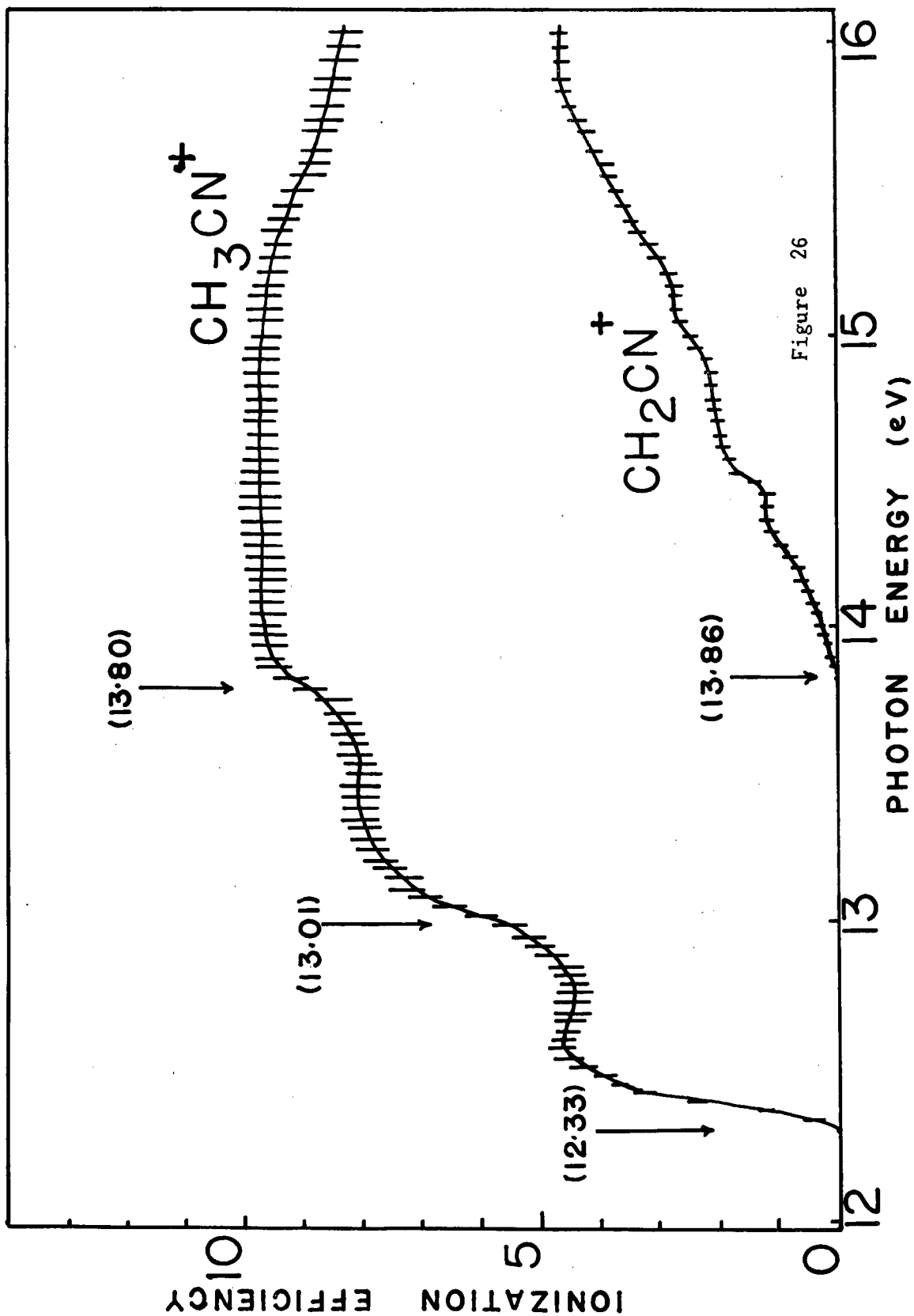


Figure 26

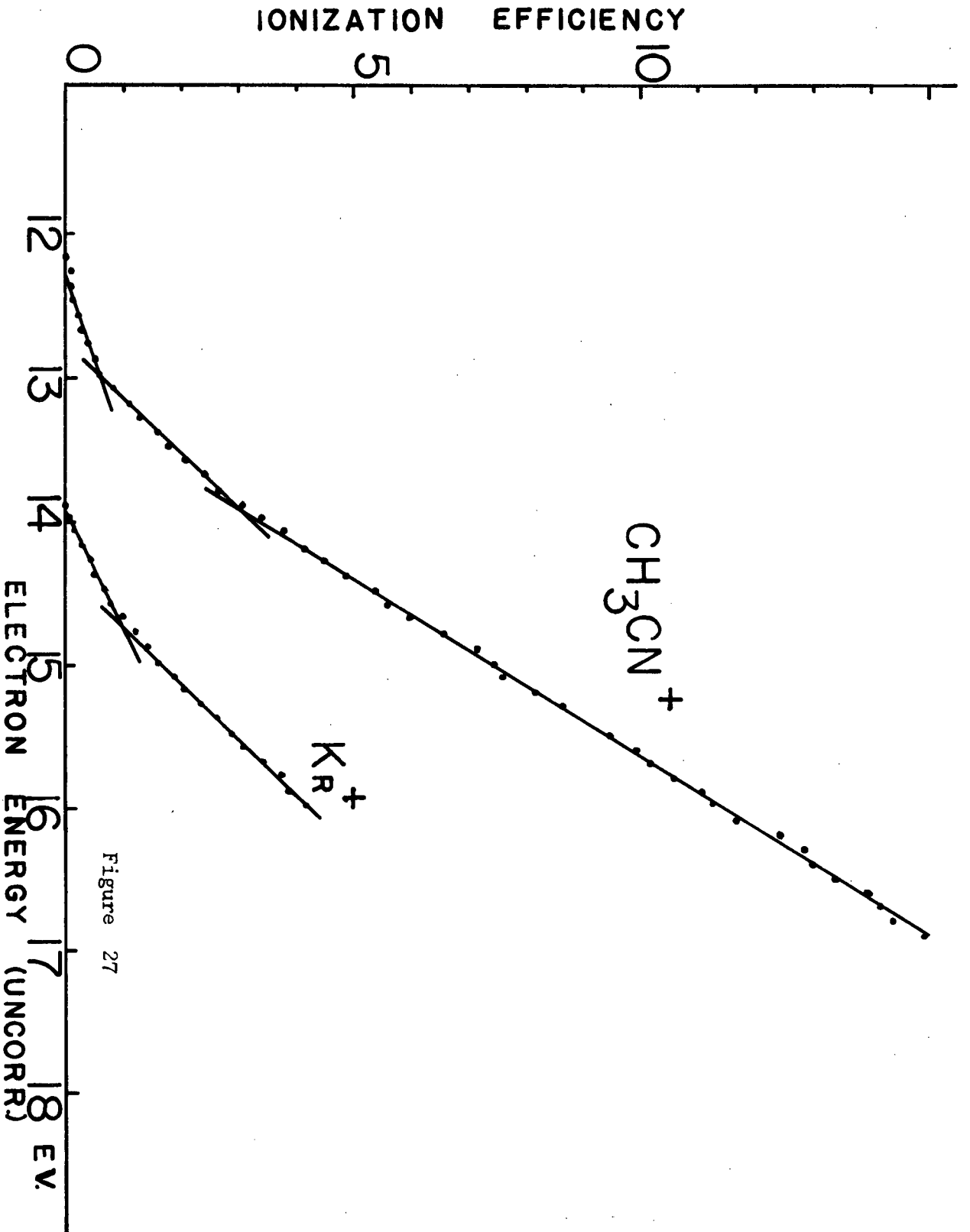


Figure 27

12.34 \pm 0.1 eV., 12.96 \pm 0.1 eV. and 13.92 \pm 0.1 eV. which are in good agreement with the values obtained by photoionization.

The three ionization potentials from photoionization and electron impact studies should be related to the outer three orbitals, since the next innermost orbital is largely localised in the CH₃ group, and the similar orbitals in methane and the methyl halides are bound by about 19 eV.

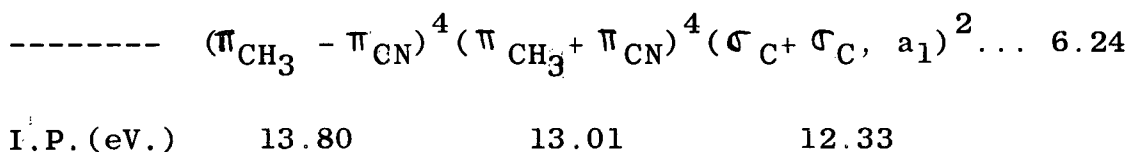
The energy required for the removal of an electron from the (π e) orbital of the methyl cyanide should be close to that from the similar orbital of methane, which is 12.87 eV., and one would expect to require about 13.7 eV. (ionization potential of hydrogen cyanide) in order to remove an electron from the CH($\pi_{\text{N}} + \pi_{\text{C}}$, e) orbital of the methyl cyanide.

Interaction between the π orbitals of the CH₃ and CN groups will produce two new orbitals of the type ($\pi_{\text{CH}_3} + \pi_{\text{CN}}$) and ($\pi_{\text{CH}_3} - \pi_{\text{CN}}$), and so it is suggested here that the second ionization potential at 13.01 eV. refers to the removal of an electron from the ($\pi_{\text{CH}_3} + \pi_{\text{CN}}$) orbital, and the third ionization potential at 13.80 eV. arises from the removal of a ($\pi_{\text{CH}_3} - \pi_{\text{CN}}$) predominantly bonding electron. The methyl cyanide ion will be formed in a ²E state in each case.

The threshold ionization potential of methyl cyanide at 12.33 eV. apparently refers to the removal of a ($\sigma_{\text{C}} + \sigma_{\text{C}}$, a₁) bonding electron, as the slight curvature near the onset of the photoionization efficiency curve of methyl cyanide indicates that the bonding electron may be involved in the threshold ionization. The ionization potential of ethane, C₂H₆, is 11.8 eV., and this refers to the removal of an electron from the C-C bonding (σ a₁) orbital. The dissociation energy of ethane, D(H₃C-CH₃), is

3.68 eV., and the dissociation of methyl cyanide, $D(\text{H}_3\text{C-CN})$, is 5.8 eV. (40). Since dissociation energy may be considered to give a fair indication of the firmness with which electrons are held in bonding orbitals, we expect to find the ionization potential for methyl cyanide somewhat higher than 11.8 eV. This threshold ionization potential of methyl cyanide could well lie at 12.33 eV., which is the energy at the initial onset in the methyl cyanide photoionization efficiency curve. Furthermore, if the assignments regarding the two higher ionization potentials of methyl cyanide are correct, the remaining one - the lowest of all - should be associated with the σ bonding orbital since the next higher unassigned orbital should have an energy of about 19 eV. as mentioned above.

Thus, the electronic structure of methyl cyanide should be written as follows:



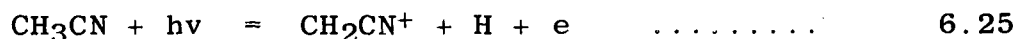
Dissociation of Methyl Cyanide

The photoionization efficiency of the CH_2CN^+ fragment ion is shown in Figure 26. The appearance potential of CH_2CN^+ ion as measured from the point of initial onset of the curve is 13.86 eV. which is lower than the electron impact data at 14.30 eV. by McDowell and Warren (73).

For the first half of a volt after the threshold energy, the ion intensity increases fairly constantly, and a change of slope is observed at 14.25 eV. which may correspond to the vertical transition of the electron impact data at

14.30 eV. Three steps are not so well defined as those in the parent ion curve because of the smaller ionization probability.

The process observed here for the formation of the CH_2CN^+ fragment ion at 13.86 eV. can be represented as follows:



and the energetics of the fragment ion formation are given by:

$$V(\text{CH}_2\text{CN}^+) = D(\text{H}-\text{CH}_2\text{CN}) + I(\text{CH}_2\text{CN}) \quad \dots\dots\dots 6.26$$

Since $I(\text{CH}_2\text{CN})$, the ionization potential of the fragment ion, is unknown, $D(\text{H}-\text{CH}_2\text{CN})$, the dissociation energy of the $(\text{H}-\text{CH}_2\text{CN})$ bond cannot be obtained. If we assume $D(\text{H}-\text{CH}_2\text{CN}) = D(\text{H}-\text{CH}_3)$, i.e. 4.41 eV., the ionization potential of the CH_2CN fragment ion is approximately 9.4 eV.

Table XIV

Relative Ionization Probabilities of Methyl Cyanide

<u>Ion</u>	<u>This work</u>	<u>McDowell(73) (at 50V.)</u>
CH_3CN^+	100	100
CH_2CN	71.5	50.0
CHCN^+	20.0	14.7
CH_2^+	6.5	8.6

The mass spectrum of methyl cyanide is shown in Figure 28. Table XIV shows the relative ionization probabilities of the parent and fragment ions at a photon energy of 16.66 eV. obtained in this work, and those of McDowell's (73) at an electron energy of 50 V.

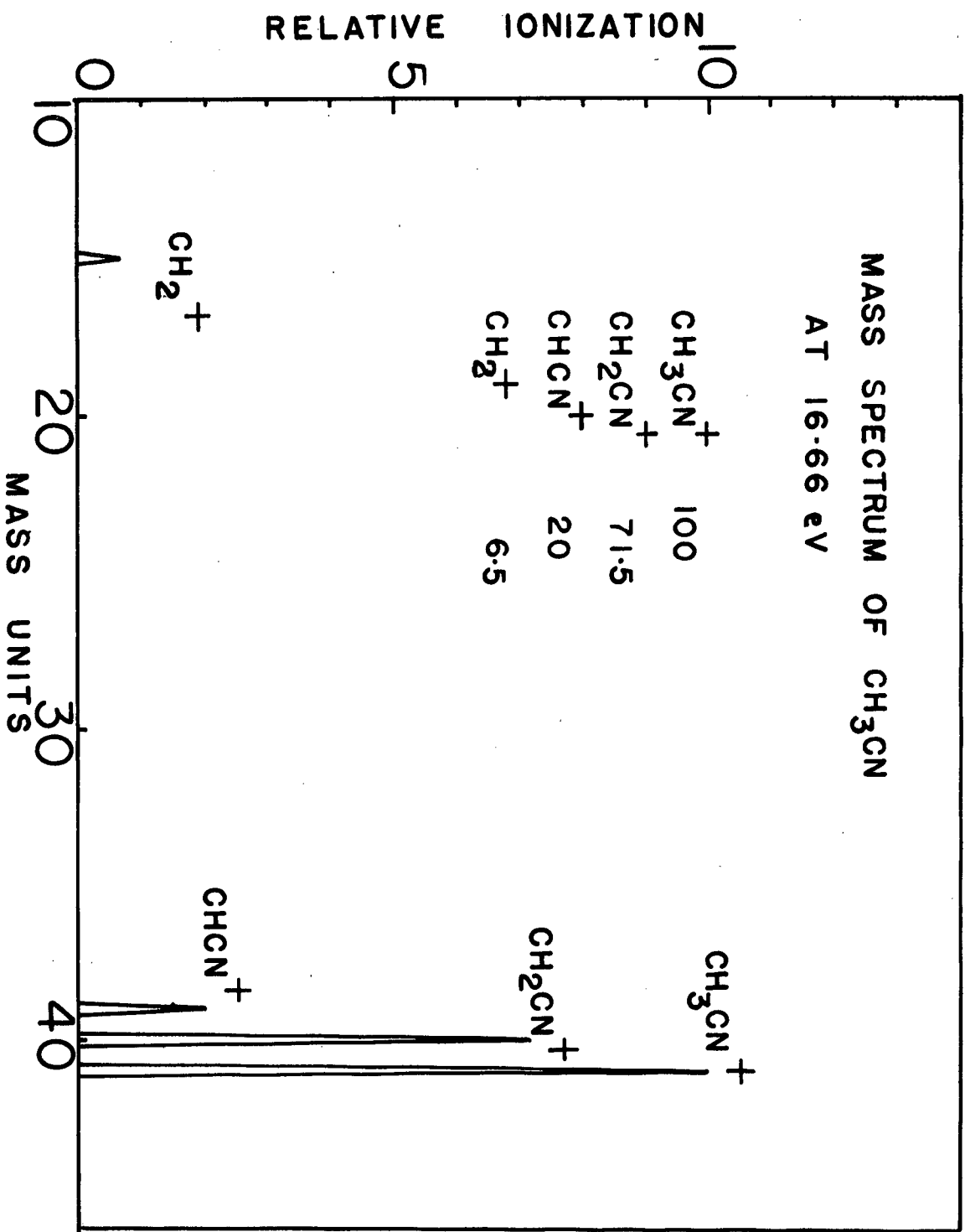
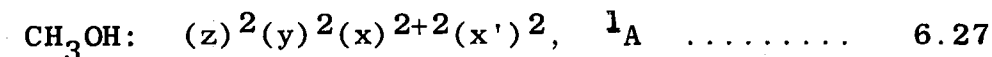


Figure 28

G. Methyl Alcohol

There are no spectroscopic ionization potential values for this molecule, because the vacuum ultraviolet spectrum of methanol does not exhibit well defined Rydberg series. Photoionization of this molecule has been studied by Inn (60) and Watanabe (135). Using the electron impact method, Morrison and Nicholson (82), Stevenson (112), Cummings and Bleakney (16), Cox (15), Omura, Baba and Higasi (96) and Friedman, Long and Wolfsberg (34), were able to obtain an approximation to the vertical ionization potential.

According to Mulliken (87), the ground state of methanol should be 1A state, and this has the following electronic configuration:-



with the molecular orbitals listed in order of decreasing binding energy, omitting the inner orbitals. The electrons in the (x') orbital are localized in the oxygen atom, and are practically free from mixing. They have the lowest energy of any electron in the molecule. The (x) orbital is split into two orbitals differing slightly in energy, belonging essentially to the CH_3 group. The (z) and (y) orbitals together give the O-H and O-C bonding respectively, but the actual orbitals must, however, be mixtures of these extreme forms.

The photoionization efficiency curve for methanol is shown in Figure 29. The threshold ionization potential, at the point of initial onset of ionization, is 10.53 eV. which refers to the removal of an electron from a non-bonding orbital (x') localized mainly on the oxygen atom. This value

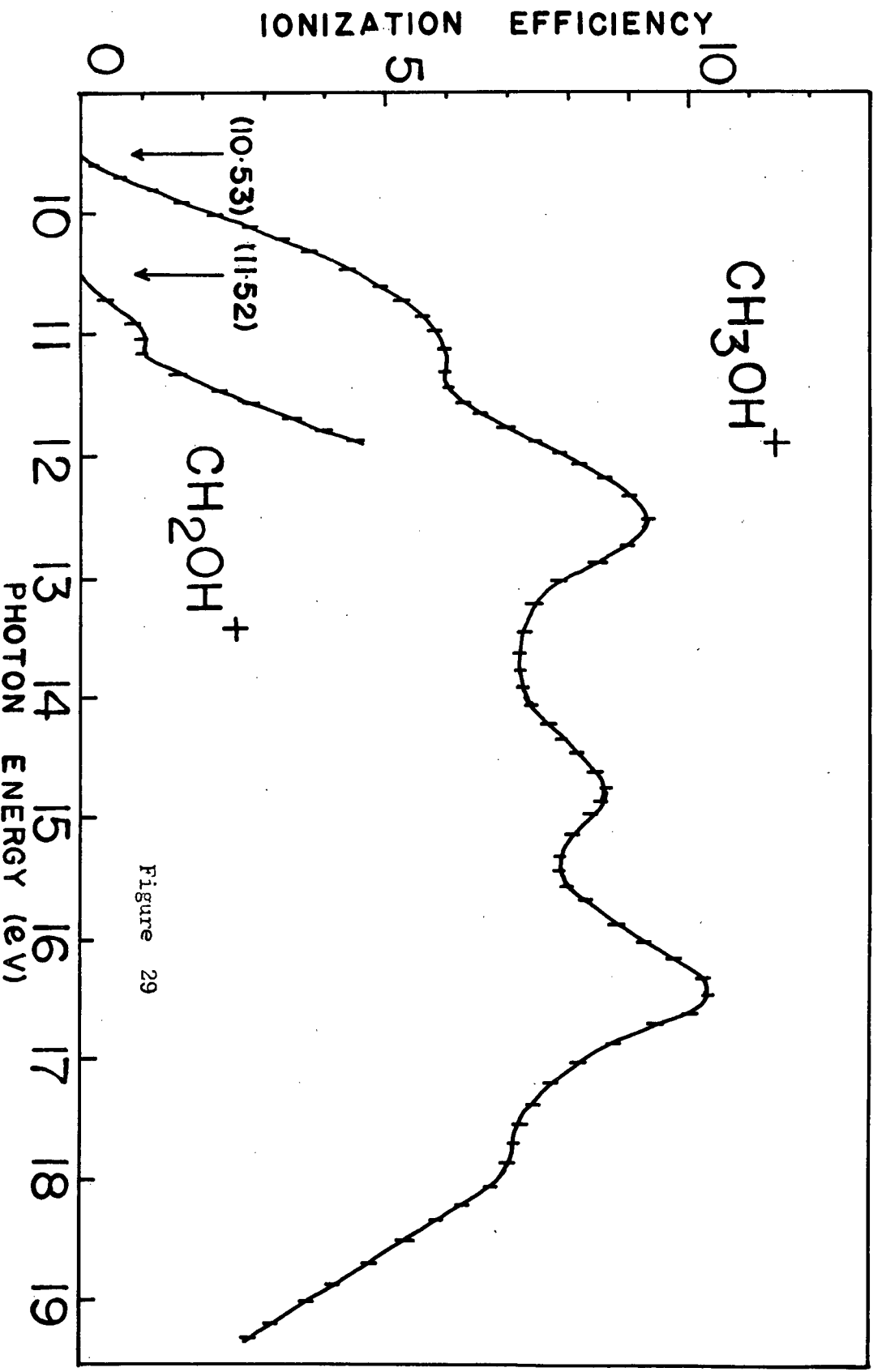


Figure 29

is in excellent agreement with the photoionization value at 10.52 eV. by Inn (60). However, Watanabe (135) obtained a higher value at 10.85 eV. The curve given by Watanabe does not show a distinct break near the ionization threshold, but a weak, long tail in the yield curve which was ascribed to impurity.

The photoionization efficiency curve in Figure 29 shows a slight curvature near the threshold energy, and this indicates that the equilibrium internuclear distances of the molecule (neutral) and ion are different. This might be one of the reasons that no well-defined Rydberg series are obtained from the absorption spectra of methanol. The electron impact data for the ionization potential range from 10.8 to 10.97 eV. and these are supposed to represent the vertical ionization potential.

Table XV summarizes the threshold ionization potentials of methanol:

Table XV

Threshold Ionization Potential of Methanol

I.P. (eV.)	Workers	Method	Year
10.53 ± 0.05	Present work	Photoionization	1966
10.52 ± 0.03	Inn (61)	Photoionization	1953
10.85 ± 0.05	Watanabe (142)	Photoionization	1954
10.8 ± 0.2	Bleakney (15)	Electron Impact	1940
10.95 ± 0.1	Morrison (84)	Electron Impact	1952
10.86 ± 0.05	Cox (14)	Electron Impact	1954
10.97 ± 0.05	Omura (100)	Electron Impact	1956
10.9 ± 0.1	Friedman (34)	Electron Impact	1957

The second ionization potential of methanol (obtained from the point of steepest ascent of the curve), is found to be

12.90 eV. and refers to the removal of an electron from the (x) orbital, belonging essentially to the CH₃ group. Three maxima were observed from the photoionization efficiency curve at 13.5, 15.75 and 17.4 eV., and the reason for those maxima is not clear. Harrison (45) has also reported two maxima in his absorption spectra of methanol.

Dissociation of Methanol

The photoionization efficiency curve for the CH₂OH⁺ fragment ion is illustrated in Figure 29. The appearance potential of this ion is obtained from the point of initial onset of the curve at 11.52 ± 0.05 eV. which is slightly lower than the value at 11.8 eV. obtained by Cummings and Bleakney (16).

The dissociation of the methanol molecule involves the breaking of a C-H bond, and CH₃-O-H can become CH₂=O⁺-H after dissociation. Furthermore, the change from single to double bond 'gives back' some of the energy ordinarily required to break a C-H bond.

The bond dissociation energy D(H-CH₂OH) can be obtained from the appearance potential of the CH₂OH⁺ ion by the following equation:-

$$D(\text{H-CH}_2\text{OH}) = V(\text{CH}_2\text{OH}^+) + \Delta E - I(\text{CH}_3\text{O}) - \text{K.E.} - \text{E.E.} \quad \dots\dots\dots 6.28$$

where the appearance potential, V(CH₂OH⁺), is 11.52 eV., ΔE is the energy difference between C-O and C=O bonds which is equal to 3.65 eV. (16), and the ionization potential of the (CH₃O) radical, I(CH₃O), is 10.7 eV. (63). If the kinetic and excitation energies are small and can be neglected, the bond dissociation energy D(H-CH₃) is 4.41 eV.

CHAPTER SEVEN

Conclusion

In the present work, we have been concerned with the results of ionization and dissociation of various species produced by photoionization in a mass spectrometer. We have discussed in some detail the interpretation of the photoionization efficiency curves and the measurement of ionization and appearance potentials, and the use of such data in the evaluation of bond-dissociation energies and zero-point energy differences between isotopic ions. We have also attempted to understand the nature of the threshold ionization law for photoionization and the mechanisms for different types of processes such as excitation, autoionization and photodissociation. In addition, we have been concerned with the insight which these studies can provide on problems concerning the electronic structures of molecules and ions.

Photoionization measurements with mass analysis provide a powerful method for the determination of ionization and appearance potentials. This method (together with the less accurate electron impact one) is often the only available method of studying those molecules for which the Rydberg series near the ionization potential is complex, and for which the ionization limit is not available. In favorable cases, this method can also detect vibrational structures such as those found in acetylene and hydrogen chloride.

Previous work on photoionization in this laboratory utilized a many-line light source, and this limited the number of data points on the photoionization efficiency curves. The

gap between two data points was often large and this prevented certain fine features from being observed. In this work, a McPherson spark source produced a hydrogen or helium continuum of fairly strong intensity, and a continuous photoionization efficiency curve could be obtained.

Reproducible results on the photoionization of Ar, Kr, Xe, O₂, N₂, CO, Cl₂, HCl, NH₃, NO₂, H₂O, CH₄, CD₄, C₃H₆, C₂H₂, CH₃CN and CH₃OH have been obtained in the energy region between 8 and 21 eV. The accuracy of ionization and appearance potential in this work is comparable to that of the spectroscopic method, and superior to that of the electron impact method.

The atoms and molecules investigated are of considerable importance in many fields. They are rather simple molecules. The electronic structures and the fine features of the photoionization efficiency curves of these molecules seem comparatively easy to explain. Also, the ionization and appearance potentials of both the parent and fragment ions of these molecules are within our working range of 8 to 21 electron volts.

Some of these molecules have been studied by many workers using different approaches, however the reported literature values were often inconsistent. The wish was to present new photoionization measurements, and try to explain the earlier inconsistencies.

The main difficulty in this work is that the photon flux is quite low, and the ionization cross section is much smaller than that obtained by the electron impact method. In

order to secure workable photo-ion currents, the mass spectrometer and monochromator slit widths have to increase at the expense of resolution. This affects the accuracy of the numerical values obtained from the efficiency curves, and also prevents certain fine structure from being resolved.

Watanabe has reported the accidental discovery that a small amount of platinum vapor deposited on the surface of a grating has an effect that greatly increases the light intensity, and he gives convincing evidence for this in later experiments. Thus, further research pointing in this direction should not be delayed. However, a grating usually contains about 30,000 lines per inch, and the space between two adjacent lines is exceedingly small. The method of coating a thin layer of platinum without affecting the functioning of the grating is another problem one will have to face.

The other difficulty is that for some molecules such as nitrogen, carbon monoxide, and oxygen, the photoionization probabilities leading to higher ionization potentials are small in comparison with the competition of those processes such as autoionization. The photoionization efficiency curve often exhibits strong autoionized peaks, and the inner ionization continua of those molecules cannot be clearly seen.

Photoionization is a powerful method for studying the electronic structure of molecules, and in recent years it has been extended to free radical studies. The reactions of atoms and free radicals in the gas phase are of considerable importance in chemistry, and they have provided subject matter for a great many investigations. Most of the data

concerning the ionization of free radicals are given by the spectroscopic and electron impact method in the past, and photoionization of free radicals has shown significant progress in recent years (59).

BIBLIOGRAPHY

1. Becker E. W., and Goudsmit S. A., "Atomic Energy States", McGraw Hill, New York (1932).
2. Berry C. E., Phys. Rev. 78, 597 (1950).
3. Beutler H., Z. Phys. 93, 177 (1935).
4. Brion C. E., J. Chem. Phys. 40, 2995 (1964).
5. Clarke E. M., Can. J. Phys. 32, 764 (1954).
6. Cloutier G. G. and Schiff H. I., "Advances in Mass Spectrometry" ed. Waldron J. D., Pergamon Press, New York (1959).
7. Coats F. H. and Anderson R. C., J. Am. Chem. Soc. 77, 895 (1955).
8. Comes F. J. and Lessman W., Z. Naturforsch. 16a, 1038 (1961).
9. Comes F. J. and Lessman W., Z. Naturforsch. 16a, 1396 (1961).
10. Comes F. J. and Lessman W., Z. Naturforsch. 19a, 1230 (1964).
11. Cook G. R. and Metzger P. H., J. Chem. Phys. 41, 321 (1964).
12. Cook G. R. and Metzger P. H., J. Chem. Phys. 41, 642 (1964).
13. Cook G. R. and Metzger P. H., J. Opt. Soc. Am. 54, 968 (1964).
14. Cook G. R., Metzger P. H., Ogawa M., Becker R. A. and Ching B. K., "Absorption, Photoionization and Fluorescence of Some Gases of Importance in the Study of the Upper Atmosphere", Aerospace Corporation, (1965).
15. Cox B. G., Ph. D. Thesis, U.B.C., (1954).
16. Cummings C. S. and Bleakney W., Phys. Rev. 58, 787 (1940).
17. Dibeler V. H., Mohler F. L. and Reese R. M., J. Res. Natl. Bur. Stand. 38, 617 (1947).
18. Dibeler V. H. and Reese R. M., J. Chem. Phys. 40, 2034 (1964).

19. Dibeler V. H., Krauss M., Reese R. M. and Hartlee,
J. Chem. Phys. 42, 3791 (1965).
20. Dibeler V. H., Reese R. M. and Krauss M.,
J. Chem. Phys. 42, 2045 (1965).
21. Dixon, Phys. Rev. 43, 711 (1933).
22. Duncan H. B.F, J. Chem. Phys. 27, 423 (1957).
23. Elenton G. C., J. Chem. Phys. 15, 455 (1947).
24. Ellison F. O. and Shull H., J. Chem. Phys.
23, 2348 (1955).
25. Elliott A., "Mass Spectrometry" ed. McDowell C. A.
McGraw-Hill. New York (1963).
26. Erying H., Technical Report V-1. Univ. of Utah, 1954.
27. Fano U., Phys. Rev. 124, 1866 (1961).
28. Foner S. N. and Hudson R. L., J. Chem. Phys.
25, 602 (1956).
29. Foner S. N. and Nall B. H., Phys. Rev.
122, 512 (1961)
30. Fox R. E. and Hickam W. M., J. Chem. Phys.
22, 2059 (1954).
31. Fox R. E., J. Chem. Phys. 30, 385 (1960).
32. Fox R. E., J. Chem. Phys. 35, 1379 (1961).
33. Franklin J. L. and Field F. H., "Electron Impact
Phenomena and the Properties of Gaseous Ions",
Academic Press, New York, (1957).
34. Friedman L., Long F. A. and Wolfsberg M.
J. Chem. Phys. 27, 613 (1957).
35. Frost D. C. and McDowell C. A., Proc. Roy. Soc.
(London) A232, 227 (1955).
36. Frost D. C., Ph. D. Thesis, U.B.C. 1956.
37. Frost D. C., and McDowell C. A., Can J. Chem.
36, 39 (1958).
38. Frost D. C. and McDowell C. A., J. Am. Chem. Soc.
80, 6183 (1958).
39. Frost D. C. and McDowell C. A., Can. J. Chem.
38, 407 (1959).

40. Frost D. C. and McDowell C. A., Unpublished Results.
41. Frost D. C., McDowell C. A. and Vroom D. A.,
Phys. Rev. Letters, 15, 612 (1965).
42. Gaydon A. G. "Dissociation Energy" Dove Publication
New York (1950).
43. Geltman S., Phys. Rev. 171, 102 (1956).
44. Hagstrum H. D., Rev. Mod. Phys. 23, 185 (1951).
45. Harrison A. J., Cederholm B. J. and Terwilliger M. A.
J. Chem. Phys. 30, 355 (1959).
46. Hertz, Wied. Ann. 31, 983 (1887).
47. Herzberg G., "Infrared and Raman Spectra"
van Nostrand, New York, (1945).
48. Herzberg G., "Molecular Spectra and Molecular
Structure, I. Spectra of Diatomic Molecules"
van Nostrand, New York (1950).
49. Herzberg G. and Shoosmith J., Can. J. Phys.
34, 523 (1956).
50. Herzberg G., Proc. Roy. Soc. (London) A262, 291 (1961).
51. Hickam W. M., Fox R. E. and Kjeldaas T., Phys. Rev.,
96, 63 (1954).
52. Honig R. E., J. Chem. Phys. 16, 105 (1948).
53. Huffman R. E., Tanaka Y. and Larrabee J. C.
Appl. Optics. 2, 947 (1963).
54. Huffman R. E., Tanaka Y. and Larrabee J. C.
J. Chem. Phys. 39, 902 (1963).
55. Huffman R. E., Tanaka Y. and Larrabee J. C.
J. Chem. Phys. 40, 356 (1964).
56. Huffman R. E., Tanaka Y. and Larrabee J. C.
J. Chem. Phys. 40, 2261 (1964).
57. Hughes A. L. and DuBridge L. A., "Photoelectric Phenomena"
McGraw-Hill, New York (1932).
58. Hurzeler H., Inghram M. G. and Morrison J. D.,
J. Chem. Phys. 27, 313 (1957).
59. Inghram M. G., Elder F. A., Giese C. and Steiner B.
J. Chem. Phys. 36, 3292 (1962).
60. Inn E. C. Y., Phys. Rev. 91, 1194 (1953).

61. Itamoto F. K. and McAllister H. C., "Sci. Report No. 4" Hawaii Inst. Geophys. (1961).
62. Johnson F. S., Watanabe K. and Tousey R. J. Opt. Soc. Am. 41, 702 (1951).
63. Kiser R. W. "Introduction to Mass Spectrometry and its Applications" Prentice-Hall, New Jersey (1965).
64. Koffel M. B. and Lad R. A., J. Chem. Phys. 16, 420 (1948).
65. Kusch P., Smith P. T. and Tate J. T., Phys. Rev. 48, 525 (1936).
66. Kurbatov B. I., Vilesor F. I. and Terenin A. N., Soviet Phys. - Dokl. 6, 490, 883 (1961).
67. Lenard P., Ann. Physik, 1, 488 (1900).
68. Lossing F. P., Tickner A. W. and Bryce W. A., J. Chem. Phys. 19, 1254 (1951).
69. Lossing F. P., Tickner A. W. and Bryce W. A., J. Chem. Phys. 19, 1254 (1951).
70. Lossing F. P. and Tanaka Y., J. Chem. Phys. 25, 1031 (1956).
71. McDowell C. A. and Warren J. W., Disc. Fara. Soc. 10, 53 (1951).
72. McDowell C. A. "Applied Mass Spectrometry" Institute of Petroleum, London (1954).
73. McDowell C. A. and Warren J. W., Trans. Fara. Soc. 48, 1084 (1952).
74. McDowell C. A., Trans. Fara. Soc. 50, 423 (1954).
75. McDowell C. A., Lossing F. P., Henderson I. H. S. and Farmer J. B., Can. J. Chem. 34, 345 (1956).
76. Mann M. M., Hustrulid A. and Tate J. T., Phys. Rev. 58, 340 (1940).
77. Marmet P. and Kerwin L., Can. J. Phys. 38, 787 (1960).
78. Massey H. S. W., New Scientist (1965).
79. Matsunaga F. M., Jackson R. S. and Watanabe K. J. Quant. Spectrosc. Radiat. Transfer, 5, 329 (1965).
80. Mitchell J. J. and Coleman F. F., J. Chem. Phys. 17, 44 (1949).
81. Morrison J. D., J. Chem. Phys. 19, 1305 (1951).

82. Morrison J. D., J. Chem. Phys. 20, 1021 (1952).
83. Morrison J. D., Hurzeler H., Inghram M. G. and Stanton H.E., J. Chem. Phys. 33, 821 (1960).
84. Mulliken R. S. and Stevens D. S., Phys. Rev. 44, 720 (1933).
85. Mulliken R. S., J. Chem. Phys. 1, 492 (1933).
86. Mulliken R. S., Phys. Rev. 46, 549 (1934).
87. Mulliken R. S., J. Chem. Phys. 3, 506 (1935).
88. Mulliken R. S., J. Chem. Phys. 3, 514 (1935).
89. Namioka T., Sci. of Light (Tokyo), 3, 15 (1954).
90. Nicholson A. J. C. and Morrison J. D., J. Chem. Phys. 20, 1021 (1952).
91. Nicholson A. J. C., J. Chem. Phys. 39, 954 (1963).
92. Nicholson A. J. C., J. Chem. Phys. 43, 1171 (1965).
93. Nier A. O., Rev. Sci. Instr. 18, 398 (1947).
94. Norling F., Z. Physik, 104, 638 (1936).
95. Ogawa M. and Tanaka Y., Can. J. Phys. 40, 1593 (1962).
96. Omura I., Baba H. and Higasi K., Bull. Chem. Soc. (Japan) 29, 501 (1956).
97. Page T. L., Monthly Notices Roy. Astron. Soc. (London) 99, 385 (1939).
98. Price W. C., Phys. Rev. 47, 444 (1935).
99. Price W. C. and Collins G., Phys. Rev. 48, 714 (1935).
100. Price W. C., J. Chem. Phys. 4, 437, 539 (1936).
101. Price W. C. and Tuttle W. T., Proc. Roy. Soc. (London) A174, 207 (1940).
102. Price W. C., Teegen J. P. and Walsh A. D., Proc. Roy. Soc. (London) A201, 600 (1950).
103. Samson J. A. R. and Cairns R. B., J. Geophys. Res. 69, 4588 (1964).
104. Samson J. A. R., J. Opt. Soc. Am. 54, 420 (1964).
105. Samson J. A. R. and Cairns R. B., "GCA Technical Report" 1965.

106. Samson J. A. R. "Conversion Table" GCA Report 61-5-N, 1961.
107. Schoen R. I., J. Chem. Phys. 40, 1830 (1964).
108. Seya M., Sci. of Light (Tokyo) 2, 8 (1952).
109. Smith L. G., Phys. Rev. 51, 263 (1937).
110. Stark, Z. Phys. 9, 15 (1909).
111. Stevenson D. P. and Hipple J. A., J. Am. Chem. Soc. 64, 2769 (1942).
112. Stevenson D. P., J. Chem. Phys. 22, 1564 (1942).
113. Stevenson D. P., Disc. Fara. Soc. 10, 35 (1951).
114. Steiner B., Giese C. F. and Inghram M G., J. Chem. Phys. 34, 189 (1961).
115. Sugden T. M., Walsh A. D. and Price W. C., Nature, 148, 373 (1941).
116. Sugden T. M. and Price W. C., Trans. Fara. Soc. 44, 108 (1948).
117. Szwarc M., Proc. Roy. Soc. A198, 267 (1949).
118. Takamine T. and Tanaka Y., Inst. Phys. Chem. Research (Tokyo) 40, 371 (1943).
119. Tanaka Y., Inst. Phys. Chem. Research (Tokyo) 39, 447 (1942).
120. Tanaka Y., Jursa A.S. and LeBlanc F. J., J. Chem. Phys. 26, 862 (1957).
121. Tate J. T., Smith P. T. and Vaughan A. L., Phys. Rev. 48, 525 (1936).
122. Tate J. T. and Smith P. T., Phys. Rev. 59, 354 (1941).
123. Tanaka Y., Jursa A. S. and LeBlanc F. J., J. Opt. Soc. Am. 48, 304 (1958).
124. Terenin A. N. and Popov B., Z. Sowjetunion, 2, 229 (1932).
125. Terenin A. N. and Vilessov, "Advances in Photochemistry" Vol. 2, ed. Noyes W. A., Interscience Publishers, New York (1964).
126. Thorburn R., Proc. Phys. Soc. 123, 122 (1959).
127. Turner D. W. and Al-Joboury M. I., J. Chem. Phys. 37, 3007 (1962).

128. Turner D. W. and Al-Joboury M. I., J. Chem. Soc. 5141 (1963).
129. Turner D. W. and Al-Joboury M. I., J. Chem. Soc. 616, (1965).
130. Wallace, Astrophys. J. Suppl. Ser. VII, 165 (1962).
131. Wannier G. H., Phys. Rev. 100, 1180 (1955).
132. Watanabe K., Zelikoff M. and Inn E. C. Y., AFCRC Tech. Report No. 53, Geophysical Research Paper No. 21 (1953).
133. Watanabe K., Marmo F. F. and Inn E. C. Y., Phys. Rev. 91, 1155 (1953).
134. Watanabe K. and Inn E. C. Y., J. Opt. Soc. Am. 43, 32 (1953).
135. Watanabe K., J. Chem. Phys. 22, 1564 (1954).
136. Watanabe K. and Marmo F. F., J. Chem. Phys. 25, 965 (1956).
137. Watanabe K. and Mottl J., J. Chem. Phys. 26, 1773 (1957).
138. Watanabe K., J. Chem. Phys. 26, 542 (1957).
139. Watanabe K., Nakayama T. and Mottl J., "Final Report on Ionization Potential of Molecules" Hawaii (1959).
140. Watanabe K., Nakayama T. and Mottl J., J. Quant. Spectry. Radiat. Transfer, 2, 369 (1962).
141. Weissler G. L., Wainfan N. and Walker W. C., J. Appl. Phys. 24, 1318 (1953).
142. Weissler G. L., and Lee P., Phys. Rev. 99, 540 (1955).
143. Weissler G. L., Wainfan N. and Walker W.C., Phys. Rev. 99, 542 (1955).
144. Weissler G. L. and Walker W. C., J. Chem. Phys. 23, 1540 (1955).
145. Weissler G. L. and Sun H., J. Chem. Phys. 23, 1625 (1955).
146. Weissler G. L., Samson J. A. R., Ogawa M. and Cook G. R., J. Opt. Soc. Am. 49, 338 (1959).
147. Wigner E. P., Phys. Rev. 73, 1002 (1948).
148. Wilkinson P. G. and Johnson H. L., J. Chem. Phys. 18, 190 (1950).
149. Wilkinson P. G., J. Mol. Spectry. 2, 387 (1958).